


Politecnico di Torino

Department of Electronics and Telecommunications
Master of Science in Nanotechnologies for ICTs

Master Thesis

DESIGN AND MODELING OF AN OXYGEN-RELEASING HYDROGEL FOR MYOCARDIAL INFARCTION TREATMENT

Thesis advisor:
Prof. Danilo Demarchi

Research supervisor:
Dr. Yu Shrike Zhang

Candidate:
Marisa Mangiatordi

October 2020

"Non il possesso della
conoscenza,
della verità irrefutabile,
fa l'uomo di scienza,
ma la ricerca critica,
persistente e inquieta,
della verità".

Karl Popper

Acknowledgements

Firstly, I would like to thank my Master thesis advisor, Prof. Danilo Demarchi, who supported my ideas and choices in such a tough historical moment. He has always promoted the project I have been working on, following it from the early stages with precious advice and continuous availability. WIth his lectures during the first semester of my Master program, I acquired notions and practical experience that proved to be particularly useful for the turn that my project took as well as for my future career.

I would like to express sincere gratitude to Prof. Yu Shrike Zhang, who offered me the chance to join his HMS-affiliated Lab in Boston, US, making one of my biggest dream come true. He has incited me to share opinions and collaborate with other researchers and then he has welcomed all my suggestions in a constructive way. Prof. Zhang has guided me throughout the entire project, offering valuable mentorship and inspiring insights, even though the work has been carried out remotely.
During these six months, I have also enjoyed the tutorship of Sushila who has introduced me to this pioneering project. Discussing with her on both academic and personal topics has been fruitful and supportive and for those reasons I thank her with all of my heart.
I am deeply indebited to my PhD advisor Valerio, who has always been a friend to me. He has taken care of my work with selfless commitment, infinite patience and full dedication. He helped me more than I could expect, encouranging me to get new ideas and turn them into something real.

Con queste pagine si conclude il mio percorso universitario che ha seguito strade dritte lungo le quali ho deciso di correre per spingermi oltre la linea dell'orizzonte, strade sterrate sulle quali ho fatto incontri imprevisti e inaspettati con le mie paure e i miei limiti, sentieri di montagna che ho percorso in salita, affannosamente, ma, al termine dei quali, ho provato un brivido, una forte emozione che mi ha fatto sentire di essere viva.
Tra queste pagine si concludono i progetti che ho iniziato ad immaginare cinque anni fa e che ho costruito, mattoncino dopo mattoncino, imparando nuove tecniche di stabilità. Queste pagine, però, sono anche un punto di inizio per tutti i progetti che non smetto mai di comporre dentro di me e che sono certa si modificheranno e cresceranno.
Perciò, in questo punto di mezzo, che è fine ed inizio, vorrei ringraziare profondamente la Marisa tenace, energica, socievole, curiosa, sempre desiderosa di cambiare e

sperimentare ma anche la Marisa giovane-vecchia, che non si accontenta e non si sente all'altezza perchè, se non coesistessero, adesso non sarei qui a raccontare questi viaggi, queste scoperte e queste conquiste.
Ad appoggiarmi costantemente, senza mai smettere di credere in me, c'è la mia famiglia a cui sono grata dal profondo del cuore. ll loro supporto è indefesso perchè fondato sul vero amore che si percepisce dallo sguardo anche quando a separare gli occhi ci sono degli schermi. Il sostegno, i consigli e i pareri dei miei genitori, Stella e Nico, sono linfa vitale per me così come lo è la tacita solidarietà di mia sorella Francesca, complice e amica. Grazie a voi per aver sempre rispettato le mie scelte.
Sono grata alla mia famiglia tutta: ai miei nonni e alle mie nonne che seguono ancora e sempre i miei passi nel mondo; a zia Angela per la sua dolcezza e la sua capacità di comprendermi anche quando dice di vedermi diversa; a zio Ettore e zia Luisa, preziosi mentori che mi ispirano gioia di scoprire e intraprendenza. Dai miei genitori a loro, tutti mi hanno insegnato l'importanza dell'indipendenza e della libertà.

Parlando di amore vero e sincero, vorrei dedicare questi miei traguardi anche a Marco, stella polare che illumina le notti più buie, mio riparo e sostegno. Gli sono grata perchè mi sprona a migliorare, a non arrendermi, perchè non si stanca di spiegarmi ciò che non conosco, perchè ridimensiona e razionalizza le mie paure, perchè fa sempre il tifo per me, perchè mi rispetta, perchè si prende cura delle mie debolezze affinchè io impari a trasformarle in virtù.

Si concludono tra queste pagine due anni particolarmente intensi, ricchi di sfide che ho affrontato anche grazie al mio collega Michele che è (stato) per me una spalla, un insegnante, un complice, un supporter. Mi ha ascoltata sempre sia quando sono stata in crisi nera con l'elettronica sia quando non riuscivo a trovare degli stivali "per polpacci grossi" e mi intristivo. Abbiamo condiviso progetti, pettegolezzi, crostate e panzerotti, gioie e dolori universitari. La sua bontà e la sua gentilezza sono peculiari ed io non avrò mai abbastanza voce per ringraziarlo di ciò che ha fatto per me durante questo faticoso ma appagante percorso.

In queste righe, vorrei ringraziare Martina, amica di sempre, anima empatica dalla quale imparo a lasciar andare, ad accettare ciò che accade senza affanni perché il nostro daìmon conosce la strada. Confrontarsi con lei così come con Francesco e Michela mi arricchisce, permettendomi di considerare punti di vista sempre nuovi. Dagli anni del liceo stiamo crescendo insieme e questo mi riempie il cuore.
Guardando il tramonto, il mio grazie va anche a Raffa con la quale condivido traguardi e sconfitte, canzoni e giornate al mare, progetti per il futuro e innamoramenti. La ringrazio perché con lei non ho tabù e la schiettezza che c'è tra noi è un genuino segno di fiducia e sincerità.
Gli anni torinesi, invece, mi hanno regalato la compagnia di Fabiana che ha saputo

offrirmi diversivi quando i pensieri negativi prendevano il sopravvento e che mi ha fatto sentire a casa quando ne sentivo più nostalgia, accogliendomi anche quando l'esperienza di collegio si è conclusa.

Insomma, io sono grata alla Vita per avermi permesso di incontrare queste persone (e molte altre), di fare mille esperienze, di mettermi in gioco e di guardare sempre oltre la punta del mio naso. Sono certa che continueremo a collaborare molto proficuamente.

Si ringraziano per la partecipazione: SARS-CoV-2, il canile di via Amendola, l'ubriaco di Lione, Éliane e la sua potente voce che annuncia la fine di un esame, Numana Blu e Riva d'Ugento, il cioccolato, Ghemon e Marracash per le colonne sonore motivanti pre-esami, il mare sia calmo che mosso, gli ulivi, lo sport, lo yoga, la pizza, tutte le forme di telecomunicazione esistenti ad oggi, gli Intercity notte 754 e 757, Flixbus e Blablacar, la clean room, le smart lenses, lo sci, il barbecue di fine Grenoble, il tramonto, i concerti, il vino rosato, la Cala dell'Acquaviva, la Val Gardena, le orchidee e i bonsai, la Svizzera, i mandala, il tonno Callipo e Propaganda Live.

Summary

Oxygen represents the fuel of life. It is essential for the survival of the entire human organism, from the small cellular compartments to the wide organs. Hence, if absent, it can undermine the physiological behavior of the body.
One of the districts that is mainly affected by lack of oxygen is the cardiovascular one where the heart muscle, without O_2 supplied by the coronary arteries, hardly contracts and pumps blood to feed the organism. This can occur as a consequence of a coronary heart disease (CHD), namely a myocardial infarction (MI), during which the blood flow headed to the heart is stopped, altering cardiomyocytes functions and eventually leading to their necrosis.
Current clinical treatments for MI reintroduce oxygen in the infarcted region with a systemic approach that may not be efficient since the blood flow in that area is reduced and, hence, may not correctly transport its payload. Conversely, our project wants to design an oxygen-releasing biomaterial for the treatment of myocardial infarction through a topical approach that will oxygenate the damaged area without affecting healthy tissues.
This study proposes an adhesive hydrogel that embeds an oxygen-delivering system made up of perfluorocarbon (PFC) and hemoglobin (Hb). Those molecules, separately, have been already employed in the fabrication of synthetic oxygen carriers thanks to their peculiar oxygen-delivery characteristics. This work, instead, analyzes their combination that is meant to promote an efficient oxygenation of the myocardium, consistently with its needs.
The proposed framework presents the FEM modeling of this novel biomaterial, moving from the biochemical properties of its components. In particular, specific functions are designed to simulate the kinetics of oxygen delivery from both hemoglobin and perfluorocarbon molecules and their interactions. Then, the oxygen-releasing behavior of the hydrogel is simulated and analyzed taking into account its proximity to the infarcted area in hypoxic conditions ($\sim$1% O_2 level). Results show that, after release from Hb and PFC carriers, the oxygen concentration inside the myocardial damaged portion is at physiological levels, suggesting that cardiomyocytes can carry out their metabolic activities since no harmful consequences related to oxidative stress should occur. The hydrogel guarantees tissue oxygenation for a period of time that is comparable to similar biomaterials found in literature.

Turin, October 2020 *Marisa Mangiatordi*

Contents

List of Tables

List of Figures

List of Abbreviations

Symbol	Meaning
2D	Two-dimensional
2,3 BPG	2,3-bisphosphoglycerate
3D	Three-dimensional
ABG	Arterial Blood Gas
ADP	Adenosine DIphosphate
ATP	Adenosine Triphosphate
CHD	Coronary Heart Disease
CT	Computer tomography
CVD	CardioVascular Disease
DOF	Degree of freddom
DMSO	Dimethyl sulfoxide
ECM	Extracellular matrix
ELP	Elastin-like polypeptides
ESR	Equilibrium swelling ratio
FDA	U.S. Food and Drug Administration
FEM	Finite Element Method
GMV	Gas molar volume
Hb	Hemoglobin
HbOCs	Hemoglobin-based oxygen carriers
HEMA	hydroxyethyl methacrylate
IRI	Ischemia Reperfusion Injury
LCST	Lower critical solution temperature
MA	Methacrylic anhydride
MAC	Methacrylamide chitosan
MACF	Fluorinated methacrylamide chitosan
MI	Myocardial Infarction
MMP	Matrix metalloproteinase

Symbol	Meaning
MRI	Magnetic resonance imaging
NIPAAm	N-isopropylacrylammide
OCC	Oxygen carrying capacity
PAA	Polyacrylic acid
PBD	Polybutadiene
PCI	Percutaneous Coronary Intervention
PCL	Poly-ϵ-caprolactone
PDE	Partial differential equations
PDMS	Polydimethylsiloxane
PEG	Polyethylene glycol
PEO	Polyethylene oxide
PFC	Perfluorocarbon
PFOB	Perfluorooctylbromide
PLA	Polylactide
PLGA	Poly(D, L-lactide- coglycolide)
PLL	Poly(L-lysine)
PVP	Poly(N-vinylpyrrolidone)
RBC	Red blood cell
RBCM	Red blood cell mimics
RES	Reticulo-endothelial system
RGD	Arginine-glycine-aspartic acid
ROS	Reactive Oxygen Species
SPO	Sodium Percarbonate
SSAD	Skin secretion of *Andrias davidianus*
STP	Standard temperature and tressure
UCST	Upper critical solution temperature

Chapter 1

Introduction

During the 20th century, industrialization and lifestyle changes pushed the epidemiologic transition further, modifying mortality causes. Among them the one that stands out is related to cardiovascular diseases (CVDs) which led to 17.8 million deaths worldwide in 2017 [1].

CVDs include stroke, hypertension, rheumatic valvular disease and coronary heart disease (CHD). This latter accounts for 80% of CVD-related deaths [2] and occurs when the heart muscle suffers from a blood flow reduction due to plaques formation in the arteries. Although those kinds of deaths among men and women in most developed countries are diminuishing, in the United States, for instance, they still give rise to 1 every 4 deaths [3].

Myocardial infarction (MI) occurs as a consequence of a coronary heart disease. The myocardium is a striated muscle tissue which forms 90% of the heart muscle and, contracting, pumps blood to the rest of the body. To accomplish its task, the myocardium needs oxygen, provided by coronary arteries located on the outermost surface of the heart.
Due to different risk factors such as smoking habits, incorrect diet and high blood pressure, atherosclerotic plaques (mainly made up of fat) may form inside coronary arteries, reducing their lumen. Exposed to arterial pressure, these plaques can undergo rupture, exposing their content to the blood and triggering thrombus formation. If abrupt and substantial, this process stops the blood flow headed to the heart, producing necrosis of myocytes in the downstream region with respect to the artery [4] (Figure 1.1).

Cells which first suffer from lack of oxygen are subendocardial cells, positioned below the endocardium, the inner heart surface. Here, first reversible alterations occur $\sim$20 minutes after blood flow stop [6]. Then, the wavefront movement of an irreversible myocardial injury proceeds towards the subepicardium, the region underneath the outer heart surface. The event is usually concluded after 3-4 hours, triggering cardiac function decrease. Thus, time is crucial when treating myocardial infarction (Figure 1.2): the effectiveness of therapeutic strategies aimed at reducing the damaged area and promoting cardiac repair is directly proportional to their promptness [7].

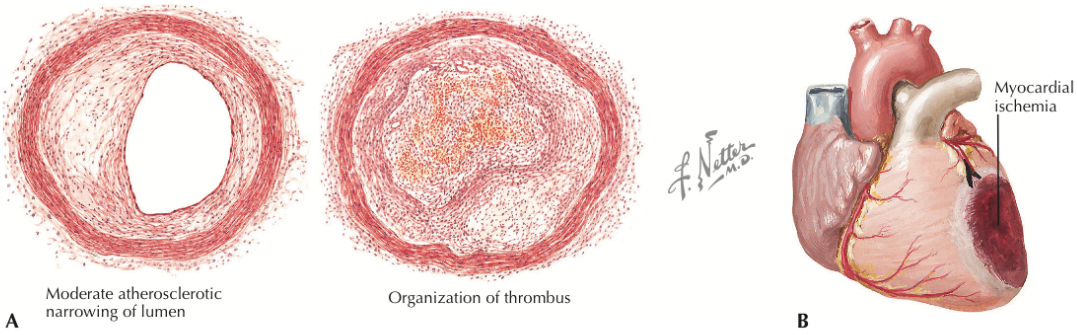

Figure 1.1. **A**. Pathophysiology of myocardial infarction: the atherosclerotic plaque narrows the lumen of a coronary artery and, when in rupture, release its thrombogenic content that triggers platelet activation and then thrombus formation. This thrombus occludes the related artery. **B**. Myocardial ischemia occurs because cells supplied by that occluded artery cannot anymore perform their contractile work. From Netter's cardiology [5].

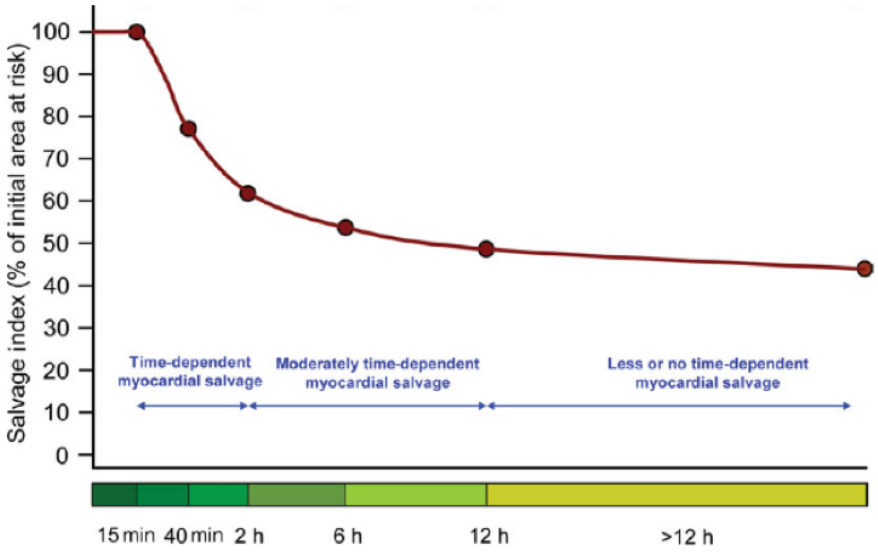

Figure 1.2. Myocardial salvage expressed as percentage of initial area at risk varies with respect to time. After 15 min from the coronary occlusion, cardiomyocytes necrosis is not yet observed. After 40 min, cell death develops consistently. From Shuvy et al. [8].

1.1 Current clinical treatments

As soon as a patient with suspected myocardial infarction is diagnosed primarily by means of 12-lead electrocardiography (ECG), drug therapy is set in order to control the

pain and reduce oxygen demand. In this case, aspirin or beta-blockers are administered.

If persistent, MI leads to a time-dependent loss of myocardial tissue. Thus, it is essential to restore myocardial blood flow as soon as possible in order to stop necrosis progression towards the so-called ischemic penumbra. Hence, pharmacological or mechanical clinical reperfusion is carried out.
Pharmacological reperfusion is performed within 30 minutes of presentation to the hospital through the intravenous administration of fibrinolytic agents. These are able to lyse the fibrin thrombus and restore full perfusion of the infarcted vessel. Unfortunately, evident contraindications are shown for patients who have experienced cerebrovascular events, for those with marked hypertension, in case of pregnancy or of recent surgical procedure. Furthermore, fibrinolitic agents can remove not only pathological blood clots but also physiological ones, exposing patients to risk of haemorrhage [9].

Mechanical reperfusion, also known as percutaneous coronary intervention (PCI) is preferred when treating MI if patients arre not eligible for pharmacotherapy or when symptoms have been present for 2-5 hours. With PCI it is possible to open a blocked vessel and restore its blood flow, without an open-heart surgery.
First PCIs involved semi-compliant or non-compliant baloon catheters. By means of a guidewire, those catheters are inserted at the origins of the coronary artery to reach the stenosis. Once there, they are inflated in order to push the plaque against the artery's wall. Nowadays, wire meshes, called stents, are implanted on-site to eliminate vessel recoil and reduce risk of restenosis (vessel reclosing) (Figure 1.3).
Stents can be of bare-metal (stainless steel, cobalt, platinum chromium alloys etc.) or polymer-coated with biocompatible polymeric coatings containing antiproliferative drugs aimed at preventing newborn vascular cells from blocking the artery [10].
Although it appears more effective than fibrinolyisis, PCI is expensive in terms of qualified personnel and its availability is limited to a small number of hospitals. Moreover, a relevant issue related to this technique is the so-called ischemia reperfusion injury (IRI), a process that is estimated to cause 50% of the final infarcted area. The absence of oxygen during MI creates a pathophysiological condition conducive to the formation of reactive oxygen species (ROS) as soon as the blood flow is restored. An increase in the generation rate of two major ROS, superoxide anion (O_2^-) and hydrogen peroxide (H_2O_2), during reperfusion cause tissue and cellular oxidative stress. This let inflammatory cells accumulate at the injury site triggering a damage extension not related to oxygen starvation. Despite the restoration of coronary flow, IRI extends myocardial dysfunction that usually improves after few weeks from MI event [11]. There are strategies to reduce the effects of IRI but they have not yet been recognized in clinical pratice.

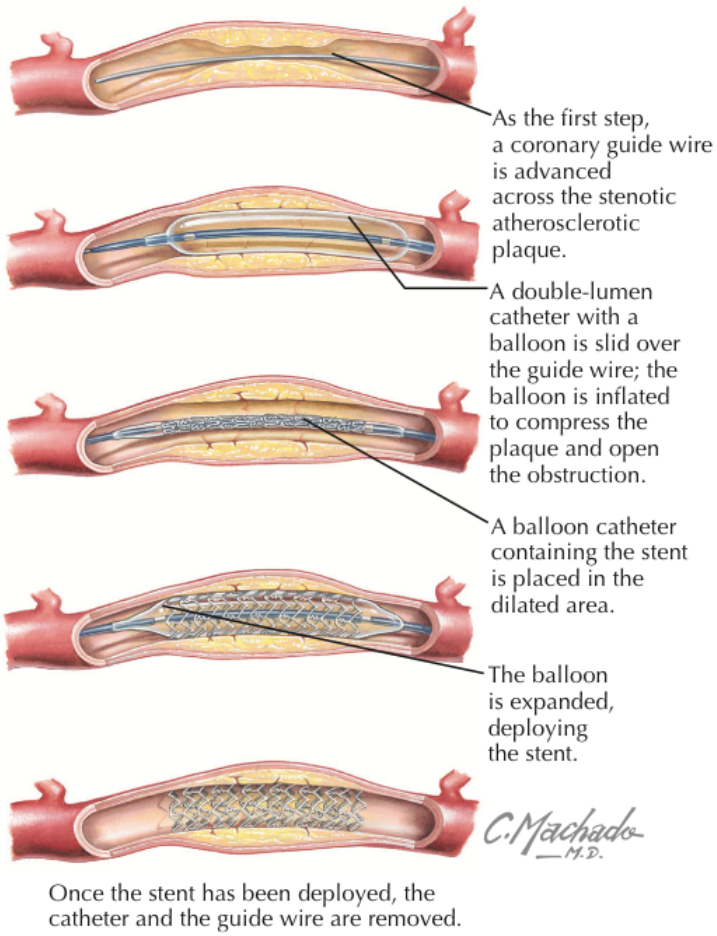

Figure 1.3. Mechanism of mechanical reperfusion involving stents to open the occlusion caused by the atherosclerotic plaque. From Netter's cardiology [5].

PCI is the gold standard for acute MI treatment but other therapies such as oxygen supplementation join the group of MI medical care strategies. In presence of MI, myocardium lacks oxygen and this may lead the body to hypoxic conditions in which oxygenation is not enough to carry out metabolic functions. The goal of oxygen therapy is to provide a great amount of oxygen to hypoxic patients by let them breathe, through a nasal cannula or a face mask, the gas at a specific partial pressure and flow controlled by a flowmeter. Increasing the blood oxygen level, this approach is believed to reverse systemic hypoxic effects [12].
Nevertheless, if oxygen saturation level in ischemic patients are not those of hypoxia, oxygen supplementation can produce irrelevant effects. In 2016, a Cochrane report showed that there is no benefit associated with oxygen therapy in patients with acute MI. Morevover, according to a meta-analysis of 7 studies, for acute MI patients with

no hypoxemia, routine oxygen supplementation does not reduce short-term mortality [13]. Further issues are similar to those of PCI, since the abrupt restoration of oxygen flow in the myocardium can lead to ROS formation and, thus, to oxidative stress which may eventually extend the damage.

1.2 New therapeutic strategies

Current clinical treatments can effectively mitigate MI effects but they are not able to regenerate the damaged myocardium. Thus, cardiac function remains altered and this represents an issue for the quality of life of recovered patients. Moving from this, in recent years, research has focused on strategies for myocardial regeneration to guarantee a satisfactory post-ischemic repair.

Among those strategies, cardiac cell therapy is a new potential approach. Although there is evidence of the ability of the heart to regenerate through stem cells activity, after MI, the muscle is not enough capable of compensating for a so-wide tissue loss. So, cells are transplated to the infarcted region to promote cardiac tissue regeneration. At the moment, there are two strategies for cell transplantation: in situ cardiomyoplasty and cardiac tissue engineering.
The first relies on direct distribution into the damaged area of cells like fetal or neonatal cardiomyocytes, skeletal myoblasts or bone marrow, embryonic or cardiac stem cells (Figure 1.4). The rationale behind this approach is that transplanted stem cells can differentiate in cardiomyocytes, promoting myogenesis, or integrate in the myocardium and participate in angiogenesis. In situ cardiomyoplasty limitations are related to finite retention of injected cells, poor nutrition supply from the infarcted tissue and host immune rejection [14].

Cardiac tissue engineering combines cell types eligible for cardiac therapy with biomaterials such as hydrogels or 3D scaffolds. The in-situ approach delivers to the myocardium cells embedded in an injectable biomaterial, on which they can adhere and better survive. Fibrin, collagen, matrigel, self-assembling peptides and chitosan are the typical biomaterials employed. This technique has been proved to significantly enhance cell survival and reduce infarct scar during animal tests but its main issue lays behind the mismatch in biomechanical characteristics between injectable biomaterials and heart tissue. Indeed, up-to-date biomaterials are not enough flexible to sustain myocardial contraction [14].
An alternative approach seeds cardiomyocytes into 3D tissue constructs to recreate myocardial mechanical and electrical functions and be implanted into the infarcted heart. This provides mechanical support to the myocardium, reducing its wall stress, and immediately restores its contractile function because the scaffold enable cells to propagate the electrical pulses and communicate to each other. Scaffolding materials can be natural (collagen, gelatin, fibrin) or synthetic polymers such as poly(lactide-co-glycolide) (PLGA), polycaprolactone (PCL), poly(glycerol–sebacate)

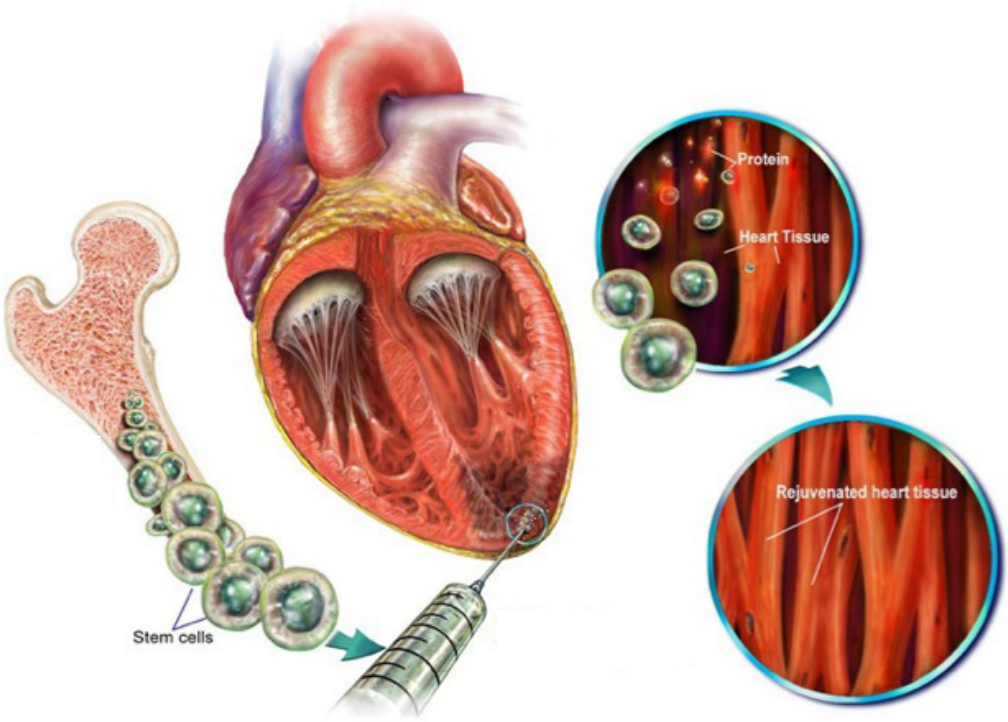

Figure 1.4. Cardiac stem cell therapy through in situ cardiomyoplasty. Stem cells extracted from human bone marrow are injected into the infarcted area. Here, they differentiate in cardiomyocytes and promote myocardial regeneration. Adapted from [15].

(PGS) and polyurethane. To better control pore size and structure, nanofibrous scaffolds are designed.
Current limitations to cardiac tissue engineering strategies are related to the fact that those 3D tissue constructs do not possess neither exactly the same stiffness of the myocardium nor the same structural properties of the myocardial ECM. Thus, present research goals in this field aim at creating biomimetic tissues able to mimic cardiac features [14].

1.3 Thesis objectives

Current clinical treatments for myocardial infarction, like oxygen supplementation, aim at reducing the area that can be damaged by the absence of oxygen and nutrients, re-establishing adequate blood oxygen levels. Nevertheless, these approaches are systemic, as they inject relevant amount of O_2 in the entire circulation through breathing. This increases the risk of hyperoxia and oxidative stress. Moreover, the

blood flow inside the infarcted area is extremely low and, hence, circulating oxygen may not diffuse towards the region that needs it the most.
On the other hand, newer MI therapeutic approaches target cardiac tissue regeneration by means of stem cells direct distribution inside the infarcted area (cardiac cell therapy) or by substituting part of the myocardium with biomimetic cell-based scaffolds. Unfortunately, those strategies present limitations on both material and biological integration aspects. Indeed, scaffolds appear to have different mechanical and structural properties with respect to myocardium and cells embedded inside those scaffolds are not enough oxygenated and fed in order to reduce the infarct scar.

It is against this background that the project idea has grown. With this novel oxygen-releasing biomaterial we would like to target the treatment of myocardial infarction with a topical approach that acts specifically on the damaged area.
As will be described in Chapter 4, oxygen-delivering biomaterials, exploiting various oxygen sources, already represent a well-established technique to provide oxygen to ischemic tissues as well as to cell-based scaffolds. Actually, very few of them entered *in vivo* studies because of issues related to biocompatibility as well as to biological retention. Additionally, when designing those carriers, it is fundamental to analyze the real needs of the target tissue and to avoid burst release of oxygen inside the area in need. This, in fact, can produce cytotoxic effects.

This project designs an oxygen-releasing system, based on perfluorocarbon (PFC) and hemoglobin (Hb) molecules, embedded into a bioadhesive hydrogel made up of gelatin methacryloyl (GelMA) and skin secretion of *Andrias davidianus* (SSAD). The interplay of the two oxygen sources should slow the release of oxygen, thanks to their different behavior. On one hand, PFCs particles are able to carry large amount of O_2 and deliver great part of it in a short time window, regardless of the oxygen partial pressure (pO_2) levels in the surroundings. Oppositely, Hb binds oxygen cooperatively and, hence, its release is more efficient and sensitive with respect to tissue conditions: Hb molecules act as oxygen reservoirs if the surrounding tissue is not in hypoxemic conditions (low pO_2).
Being bioadhesive, the hydrogel is ment to be directly printed on the infarcted area by means of a handheld skin printer that is able to deposit biomaterials *in-situ* in a conformal way.

In the next chapters, after some notion of physiology and material science useful to depict a clear background, current solutions of oxygen-delivering systems will be described. Afterwards, our biomaterial will be described in details together with its computational modeling built with Comsol Multiphyisics 4.2a.

Chapter 2

Physiology background

The objective of this chapter is to describe the primary heart metabolic function that underlies all the other biological functions. Another highlight refers to the role of oxygen in the aforementioned functions as well as to the importance of its physiological and pathological levels.

2.1 Myocardium energy metabolism

At the center of our circulatory system there is the heart muscle whose main function consists in pumping blood towards tissues and periferal body districts providing them with oxygen and nutrients. This is accomplished through periods of muscular relaxation (diastole), during which the myocardium is at rest and blood spontaneously fills atria and ventricles, and periods of contraction (sistole), during which first atria and then ventricles are emptied because the heart muscle pumps the blood in both arterial and venous circulations. Both diastole and sistole occur spontaneously and rithmically.
From a metabolic point of view, this pump works thanks to the production of energy in the form of adenosine triphosphate (ATP).
Under normal cardiac function, in aerobic conditions, fatty acids produce about 50%-70% of ATP which is broken down to release energy for the myocardial work and then it is resynthesized from adenosine diphosphate (ADP) during mithocondrial oxidative phosphorilation, a biochemical process that occurs at the end of the cellular respiration.
Another approach is represented by glycolysis. In this case, in the cell cytosol, pyruvate is derived from both reduction of glucose, uptaken by the myocardium, and conversion of lactate, extracted from the blood. In mithocondria, pyruvate is oxidized to acetil-coenzyme A which is then employed in cellular respiration mechanisms.
Even in presence of a cardiac output increase, those mechanisms of ATP production and breakdown are balanced enough to avoid a fall in ATP concentrations [16].

Under ischemic conditions, this methabolic energy production is altered because cardiomyocytes do not receive enough oxygen to produce ATP in mithocondria. Consequently, cell homeostasis changes in a significant way and pyruvate is not immediately oxidized but rather transformed into lactate. So, instead of consuming blood-derived

lactate, myocardium starts producing it, increasing its levels and reducing contraction power.
Indeed, drugs chosen for MI treatment aim at reducing arterial blood pressure and heart rate in order to reduce the need for mithocondrial ATP synthesis.

2.2 Myocardial oxygen tension and concentration

As already stated, during myocardial infarction, the coronary blood flow headed to the heart can be blocked, interrupting tissue oxygenation and producing unwanted metabolic and systemic consequences.
Since oxygen is poorly soluble in blood, in the arterial circulation, it is carried through dissolution in the plasma as well as by means of a protein, hemoglobin (Hb). Thus, blood oxygen concentration depends on various factors such as hemoglobin concentration, its level of saturation, oxygen partial pressure in the arteries and so on. Although it is nearly impossible to exactly know the amount of blood oxygen content, in clinical practice it is possible to understand its trend in order to recognize pathological changes and avoid the consequences of oxidative stress. This analysis is carried out through the measurement of the oxygen partial pressure (pO_2), during the arterial blood gas (ABG) test.
Oxygen tension represents the quantity of oxygen dissolved in the plasma and in the international system, it is defined by the Pascal (Pa) unit. Nevertheless, in medicine the unit largely employed to describe oxygen tension is millimeter of mercury (1 mmHg=133.322 Pa).
In normal conditions, at sea level, arterial oxygen partial pressure (PaO_2) is enough to satisfy the needs of the entire organism and its value ranges between 75 and 100 mmHg (Figure 2.1) [17]. This value varies according to the altitude to which the subject is exposed. In particular, if the barometric pressures diminuishes, PaO_2 is reduced, too.

The arterial oxygen tension differs from the pO_2 inside tissues. Here, O_2 arrives by diffusing across capillaries and other barriers, like the mithocondrial membrane, and, then, it is consumed by cells at a certain rate. So, tissue oxygen tension (PtO_2) depends both on blood flow and on cellular consumption rate, resulting in values smaller than those of PaO_2. In physiologic conditions, larger amount of O_2 are delivered to highly aerobic cells like cardiomyocytes in order to sustain their metabolic and contractile activities. This guarantees normoxic conditions under which oxygen concentrations range between 4% and 13%.

When oxygen concentration drops below tissue physiological levels (<0.5-3%), hypoxia occurs. This condition can be caused by low PaO_2 (hypoxemia), reduced blood oxygen-carrying ability or reduced O_2 perfusion of the tissue in case of ischemia. If tissues have not enough oxygen to produce energy in form of ATP, their survival depends on their glycogen content, that is to say on their ability to support anaerobic energy production. Heart cells are known for having a very low tolerance threshold for

hypoxia that produces irreversible changes in few minutes. Indeed, when the carotid bodies sense this lack of oxygen, some physiological responses, such as vasodilatation to increase perfusion to the O_2-lacking tissues, and metabolic responses, such as increase in anaerobic glycolysis and reduction of energy-demanding processes, take place. One of the most important mechanism that uses up a great amount of energy is ATPase ionic pumping which regulates electrical activities of excitable cells like cardiomyocytes. Thus, for the heart, hypoxia corresponds to reduced contractile activity. In the end, cell death can follow because ATP supply is not enough to sustain ionic and osmotic equilibrium, leading to events that produce cell swelling and hydrolysis of main cellular components [18].

The opposite condition of hypoxia is hyperoxia that occurs when there is an excessive O_2 supply to the tissue and the PaO_2 grows far beyond the levels of normal condition breathing (> 100 mmHg). This condition is a consequence of supplemental oxygen administration and produces an increase of cellular ROS and, consequently, oxidative stress [19].

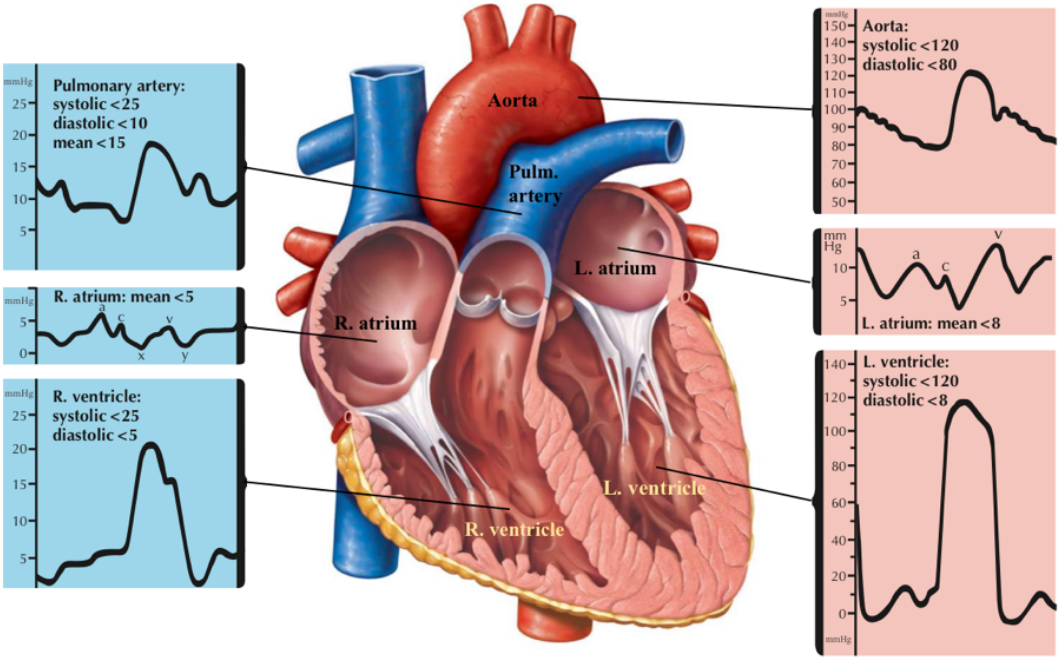

Figure 2.1. Intracardiac pressure waveforms expressed in mmHg and measured by means of a pulmonary artery catether. Adapted from Netter's cardiology [5].

Chapter 3

Material science background

The aim of this chapter is to provide knowledge about polymeric materials known as hydrogels, analyzing their composition, synthesis and principal characteristics that let them be so widely employed in tissue engineering applications.

3.1 Hydrogels

In 1960, Wichterle and Lim [20] studied various types of plastic that had been proposed for biological use and turned out to have physiologically toxic effects. They highlighted the demands that those bio-plastics should meet: permeability to metabolites, biological inertness and a structure able to guarantee the desired water content. To address those requirements, materials must have hydrophilic groups and enough crosslinks to inhibit absorption. So, for the first time in literature, they studied crosslinked HEMA (hydroxyethyl methacrylate) hydrogels. After this pioneering work, hydrogels gained the attention of many biomedical researchers worldwide.

Hydrogels are three-dimensional networks formed from the crosslinking of hydrophilic polymeric chains inside an aqueous environment. In presence of external stimuli, hydrogels can swell and change their volume by retaining large amount of water.
During swelling, the inner glassy phase of the hydrogel is separated from the rubbery one by a moving boundary that favor the presence of water inside the polymer network and the diffusion of molecules. For instance, in pH-dependent hydrogels it seems that the transition to swelling state occurs at pH values close to the apparent dissociation constant (pKa) because, in correspondence of pKa, polymers ionization occurs and electrostatic repulsions between backbone chains let water permeate inside the hydrogel matrix [21].
The swelling process may deform the hydrogel but this does not happen thanks to the equilibrium between the osmotic forces, that promotes water penetration, and elastic forces, that balance the structural stretching.
The equilibrium swelling ratio (ESR) of a hydrogel can be calculated as described in Equation 3.1 [22]:

$$ESR = \frac{W_t - W_i}{W_i} \cdot 100 \tag{3.1}$$

where W_i is the initial weight of the dry hydrogel while W_t is the weight of the same hydrogel swollen in distilled water.

Various natural and synthetic polymers can be transformed into hydrogels by means of several gelation mechanisms mainly divided between physical and chemical ones and shown in Figure 3.1.
Thermal condensation is one physical approach typical of thermo-responsive polymers that, following a temperature change, turn into gel because of a change in their solubility that creates rigid packed polymer backbones. Gelatin, for instance, starts its gelation when the temperature drops below its upper critical solution temperature (UCST) while for poly(N-isopropylacrylamide) (PNIPAAm) the transition temperature is a lower critical solution temperature (LCST). Molecular weight, co-polymers ratio and balance between hydrophobic and hydophilic segments can be adjusted to tune these critical temperatures [23]. Those hydrogels swell because of the presence of hydrogen bonds between hydrophobic groups of the polymer backbone and water molecules.

The method used to fabricate protein-based hydrogels, such as collagen-based hydrogels, is the noncovalent molecular self-assembly, a physical method. This is a natural process that, by means of weak noncovalent interactions (e.g. van der Waals forces, hydrogen bonds, etc.) that act collectively, let molecules organize into well-ordered structures with precise functionalities. Nowadays, this approach is used to create biomimetic scaffolds [23].

Physical gelation may occur spontaneously in presence of chelation or electrostatic interactions. For example, hydrogels based on alginates, naturally derived polysaccharides, are formed from chelation. Alginate is made up of α-L-guluronic acid (G) and β-D-mannuronic acid (M) residues. In presence of some divalent cations like Ca^{2+}, alginate G-blocks gel in pairs that pack helical chains and surround the ions.
Conversely, electrostatic interactions form between two opposite electrostatic charges along the polymer backbone. Among natural polymers, those rich of carbossilic groups are negatively charged oppositely from those with predominant amine groups. On the other hand, synthetic polymers possess more tunable electrostatic properties like in the case of poly(L-lysine) (PLL)/polyacrylic acid (PAA) pair. Those are two oppositely charged polyelectrolytes that, when mixed, create insoluble complexes [23].

Differently from physical gelation mechanisms which primarily rely on polymers' physical properties, chemical crosslinking is more controllable providing enhanced flexibility and structural precision to the hydrogel. When in contact with water, chemically active molecules on the side chains of the polymer backbone, in presence of specific conditions, create covalent bonds, forming the hydrogel. Condensation reactions, radical polymerization, aldehyde complementation, high-energy irradiation and enzyme-enabled biochemistry are the standard crosslinking methods [23]. Different components and mechanisms have been mixed during chemical crosslinking to achieve

the best hydrogel formulation with the finest mechanical characteristics.

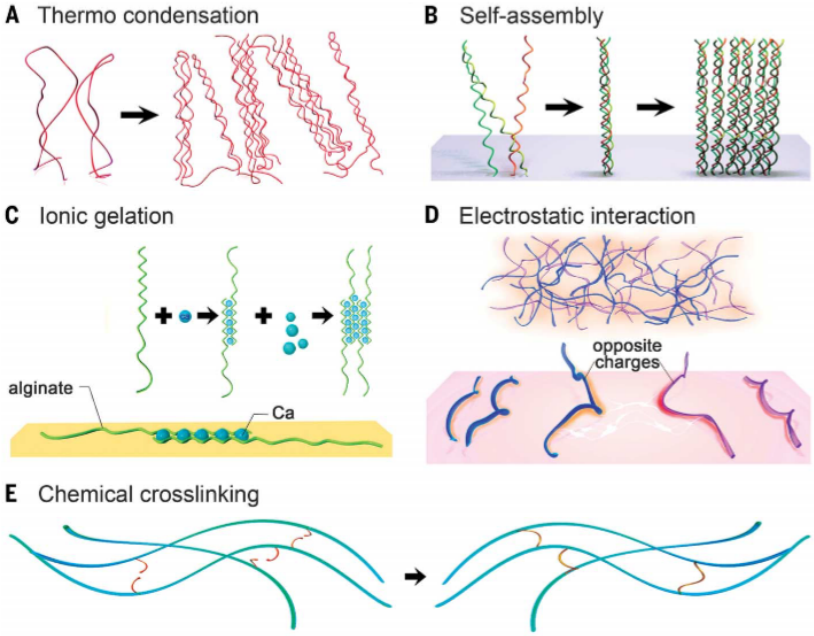

Figure 3.1. Hydrogel crosslinking mechanisms. From A to D, sketches describe physical gelation methods. Chemical crosslinking is depicted in part E. From Zhang et al. [23].

3.2 Hydrogel properties

Applications like soft robotics and wearables pushed the research towards the development of tough and stretchable hydrogels. Nevertheless, hydrogels can be typically stretched up to few times their starting length and their fracture energies are smaller than 100 $\mathrm{J\,m^{-2}}$. Hence, some strategies have been adopted.
Natural hydrogels are the first to be targeted because of their exceptional elasticity. For instance, elastin, a structural protein that gives elasticity to human tissues and blood vessels, has been engineered into enzimatically crosslinked versions, called elastin-like polypeptides (ELPs) that can be stretched up to 5 times their original length. However, in this case costs are really high and this represents a disadvantage for applications that require large hydrogel quantities [23].
An alternative to improve hydrogels mechanical properties is their hybridization with nanomaterials, like carbon nanotubes and inorganic particles, that possess tunable surface characteristics and relevant strength. Making those materials interact with hydrogel polymer chains means reducing the issues related to the presence of dense crosslinkers that can limit hydrogel final stretchability.

Porosity, too, influences hydrogels mechanical properties, since their stiffness decrease is inversely proportional to their porosity increase. This occurs because, combined together, the microscale pores features constitute the hydrogel microarchitecture. Moreover, pore distribution is relevant when targeting angiogenesis or cell survival in tissue engineering, because interconnections between pores favor nutrients and oxygen transport that mainly happens through diffusion. So, it is crucial to fabricate 3D porous hydrogels that facilitate those processes. It has been demonstrated that hydrogels with larger pores let oxygen diffuse faster [24]. Other research studies demonstrated the average pore size required for neovascularization (5 μm), for skin regeneration (20-125 μm) and osteoid growth (40-100 μm) [25].
Hydrogel porosity can be estimated with the solvent replacement method [22], according to which dried hydrogels are immersed in ethanol and, then, weighed after elimination of excess ethanol. Equation 3.2 describes the calculation.

$$Porosity = \frac{M_2 - M_1}{\rho V} \cdot 100 \tag{3.2}$$

where M_1 and M_2 are, respectively, the hysrogel mass before and after immersion in ethanol, ρ is the ethanol density and V is the hydrogel volume.

Hydrogel porosity can be engineered through various techniques, which can also be combined together (Table 3.1). Recently, to achieve a more accurate control of single and group pores microfeatures and geometries, micromolding and micropatterning are employed, too.

Technique	*Description*
Particle leaching	Dissolution of porogen with controlled particle size into a polymer solution; solidification; solute particles leaching and porous network formation [25].
Freeze-drying	System rapid cooling to crease phase instability; sublimation under vacuum to remove solvent and create void regions in the network [25] (Figure 3.2).
Gas foaming	Nucleation and growth of gas bubbles inside the polymer network to create pores [25]

Table 3.1. Techniques for control of hydrogel porosity.

Together with porosity, application fields like tissue engineering require hydrogels able to heal from damage because, in this way, they can be, for instance, injected by means of a syringe.

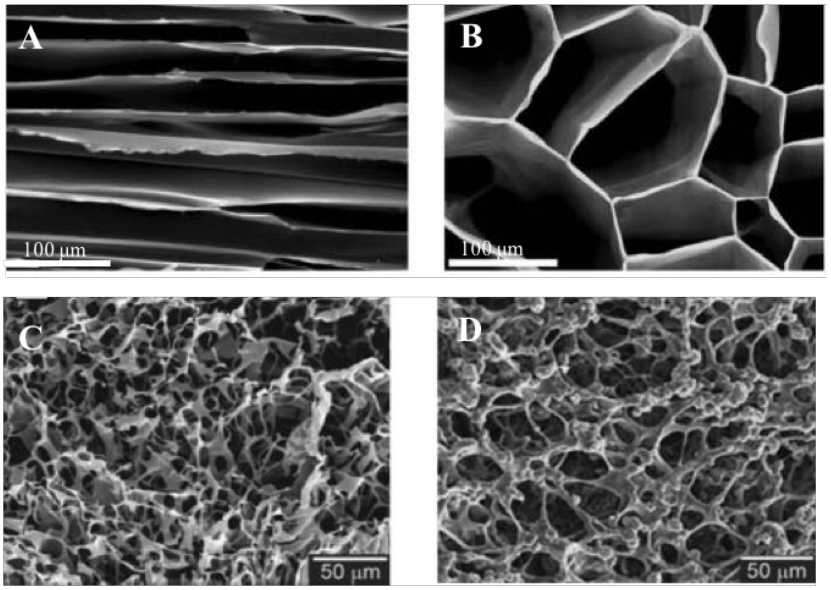

Figure 3.2. SEM images of pores in freeze-dried agarose hydrogel (longitudinal (**A**) and cross-sectional (**B**) orientation) and in freeze-dried chitosan-poly(ϵ-caprolactone) hydrogel (pure chitosan (**C**) and chitosan blended with 50% poly-ϵ-caprolactone (**D**)). From Annabi et al. [25].

This characteristic is achieved by inserting, inside the polymer network, reversible but strong interactions (e.g. electrostatic or hydrophobic interactions, hydrogen bonds, etc.) thus creating shear-thinning hydrogels. An example consists in adding charged nanoparticles to a pre-formed hydrogel in order to generate electrostatic interactions between the polymer chain and the nanomaterial. Thanks to these interactions, in presence of shear stress, the hydrogel reduces its viscosity, setting in a more stretched conformation due to a shear-induced rearrengement of polymeric chains. This favors hydrogel injectability through a plug flow mechanism. Then, when the stress source is eliminated, the material regains its original viscosity [23].
By adding amine or carboxyl side groups to the hydrogel polymeric backbone it is possible to create hydrogen bonds that promote self-healing of the biomaterial. This approach leads also to pH-dependent healing.
All those mechanisms that produce hydrogels able to self-recover from damage rely on physical or chemical principles. Nowadays, research efforts aim at mimicking the self-healing abilities of biological tissues in order to establish a new approach that involves biologically active molecules, too.

Hydrogels are relevant materials in a variety of applications ranging from biomedicine to soft electronics to robotics since their physicochemical characteristics

can be easily tuned.
The complexity of the biological environment and of its components made up of hierarchically architectures of various dimensions represent the challenge that bioengineers and material scientists face when designing hydrogels. Micro and nanoengineering help them to program the assembly of gel building blocks in order to synthesize biomimetic tissues.
Although recent advances in technology and research, some issues remain to be solved. Only few hydrogels received approval from U.S. Food and Drug Administration (FDA) in order to enter clinical trials [26] and processes that embed hydrogels into biofabrication techniques should be optimized in order to obtain the best outcomes. In addition, swelling, too, can cause adverse effects because when hydrogels are immersed into aqueous environments with low osmolarity, the equilibrium between osmotic forces that prevent gel deformation is broken. If this occurs for a relatively long period, the hydrogel matrix can be weakened and the material can loose its mechanical and structural characteristics. For this reason, "non-swellable" hydrogels or hydrogels with controlled swelling are being studied.

Chapter 4

Oxygen delivering biomaterials

One of the new therapeutic approach to treat myocardial infarction and promote tissue repair is that of tissue engineering which combines biomaterials and cells to create living tissue constructs *in vitro*. Together with those presented in Chapter 1, another limitation of this method is the failure in vascularization that occurs when the scaffold enters the body. Indeed, embedded cells should be fed and oxygenated by diffusion from surrounding capillaries that are located too far away: oxygen can diffuse only 100-200 μm and scaffolds have usually thickness of few millimeters. Thus, trying to solve this issue, research in the field has started to deal with a way to deliver oxygen continuously and consistently through a biomaterial [27].
Nevertheless, this is not the only goal of this approach. Oxygen-delivering biomaterials can be useful to treat O_2-demanding tissue, such as ischemic or infarcted ones.
Before designing those biomaterials, it is fundamental to study the oxygen requirements of the target tissue in order to guarantee a stable and congruent delivery. Indeed, as explained In Chapter 2, hyperoxia can cause cellular oxidative damage because of reactive oxygen species production. Moreover, ROS species are known to be mediator in the inflammatory process and to negatively affect cell differentiation [28].

4.1 Oxygen sources

4.1.1 Solid and liquid peroxides

A subclass of oxygen-releasing biomaterials is that of oxygen-generating biomaterials. In this group, largely investigated oxygen sources are solid peroxides. Most popular peroxides are sodium percarbonate (SPO), calcium peroxide (CaO_2) and magnesium peroxide (MgO_2). Those compounds, in presence of water, dissociate and release hydrogen peroxide, H_2O_2 from which oxygen can be produced (Figure 4.1). However, H_2O_2 is one of the major reactive oxygen species and, if not correctly decomposed in oxygen and water, it produces hydroxyl radicals which alter metabolic cellular functions and may lead to cell damage. For this reason, to safely deliver oxygen *in vivo*, scaffolds with solid peroxides must contain catalase, an enzyme found in mammalian blood and liver, able to convert H_2O_2 into oxygen and water with high

efficiency [29].

The oxygen release rate of solid peroxides is influenced by their solubility coefficient in water. This is the main reason why calcium peroxide happens to produce the largest O_2 amount with the longest release time. CaO_2 is frequently chosen for its promising release features and also because of its high purity (60-80% vs 15-25% of MgO_2 [27]), another element that improves oxygen release.
Furthermore, when targeting tissue oxygenation, the effect should not be abrupt but rather smooth and prolonged in time in order to avoid hyperoxia and its consequences. To reduce hydrolysis rate, solid peroxides are typically encapsulated in hydrophobic polymers, such as poly(D, L-lactide- coglycolide) (PLGA) and polydimethylsiloxane (PDMS). Unfortunately, some of these encapsulation materials are not biocompatible. Moreover, despite of this solution, studies show that solid peroxides are dissolved much before that sufficient tissue vascularization takes place [28].

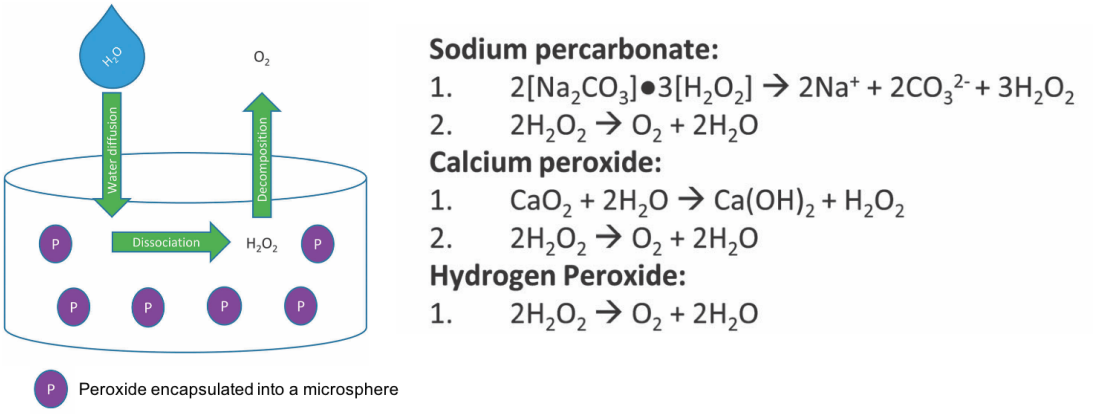

Figure 4.1. Mechanism and reaction for oxygen release from peroxide compounds encapsulated into microspheres within hydrogels. Adapted from Farris et al. [28].

To increase the release time, solid peroxides can be substituted by liquid peroxides (e.g. hydrogen peroxide) that have a higher solubility coefficient in water. Those compounds are typically encapsulated into microspheres and embedded inside alginate or polymeric matrices. With liquid peroxide, an oxygen release over a period of two weeks has been demonstrated, guaranteeing cellular differentiation [29]. Nevertheless, even in this case, in absence of enzymatic support, the reaction that decompose H_2O_2 into oxygen and water produces cytotoxic byproducts that induce oxidative stress into the host body.

4.1.2 Hemoglobin-based oxygen carriers

Hemoglobin is the protein which stores and transports oxygen across the blood, binding it in the lungs and releasing it into tissue districts in the body. For this reason, the most popular blood substitutes are based on hemoglobin extracted from human or mammalian red blood cells.

Hemoglobin

Oxygen molecules have poor solubility in water and blood and the amount of oxygen dissolved in plasma is not enough to satisfy metabolic needs of the human body. Thus, oxygen needs to be carried through the bloods by a protein, called hemoglobin (Hb). This is an iron-containing protein which forms an unstable and reversible chemical bond with oxygen molecules.

Hemoglobin molecules have a tetrahedral structure with four monomeric units, namely 2 α units and 2 β units. The structure that enables oxygen binding is the heme group composed by a ringlike organic compound, protoporphyrin. This ring is made up of four pyrrol rings and it is surrounded by four methyl groups. The iron atom is placed at the center (Figure 4.2). Each hemoglobin molecule possesses four heme groups and thus four iron atoms each of which binds one O_2 molecule. Hence, each Hb molecule binds 4 O_2 molecules [30].

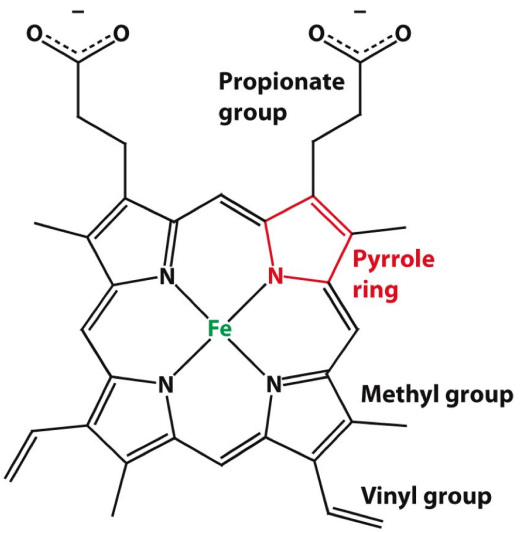

Figure 4.2. Heme group structure (Fe-protoporphyrin IX). From [30].

The iron atom is in its ferrous oxidation state (Fe^{2+}) and it is able to create two additional links in its 5th, occupied by a residue of histidine, and 6th coordination sites. In the deoxyhemoglobin (deoxyHb) which is a taut molecule (T state), this

latter site is available for binding. As soon as O_2 binds to this coordination site, electrons around the Fe atom rearrange so that the Fe ion (Fe^{3+}) becomes smaller and moves into the heme plane shifting the histidine residue upwards (Figure 4.3). This amminoacidic residue is part of a α-elix whose C-terminus is linked to the other Hb subunit. Hence, the structural modification of the iron atom due to oxygen binding produces structural changes in the entire tetrahedral structure that moves from the taut state (T) of deoxyHb (low affinity) to the relaxed state (R) (high affinity) of the oxyhemoglobin (oxyHb), increasing the oxygen affinity of all the heme groups. Due to this modification, hemoglobin is an allosteric protein and its binding to oxygen is defined as cooperative [30].

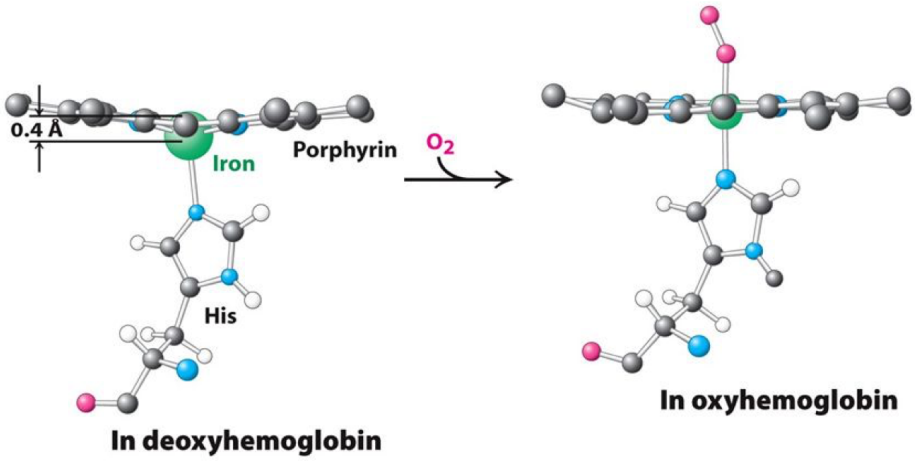

Figure 4.3. Structural modification from deoxyhemoglobin (taut, low affinity state) to oxyhemoglobin (relaxed, high affinity state). In deoxyHb, the iron atom is slightly below the heme plane. As soon as it binds O_2, Fe ion gets smaller and shifts into the plane of the porphyrin ring. From [30].

Hemoglobin cooperativity is perfectly described in Figure 4.4 where the binding of oxygen to isolated Hb follows a sigmoidal behavior that reaches a plateau when all iron atoms are fully bound to oxygen. Actually, the optimal hemohlobin saturation for an adult subject is approximately 95-95%.
In physiologic conditions, oxygen needs to be transported from the lungs, where pO_2 is equal to 100 mmHg, to tissues, where pO_2 is almost equal to 40 mmHg. Following the sigmoid, the 98% saturation that hemoglobin exhibits in the lungs diminishes to 32% when hemoglobin moves into tissues, Thus, 66% of hemoglobin binding sites participate to oxygen delivery. This means that, with respect to a protein with no cooperativity, hemoglobin is able to transport an amount of oxygen 1.7 times larger. So, cooperativity enhances hemoglobin transport efficacy which is, in turn, extremely sensitive to variations in the environmental oxygen partial pressure [30]. Indeed, when Hb saturation is above 90%, a pO_2 increase does not produce any effect on the relative

oxygen content. On the other hand, when pO_2 drops below ∼60 mmHg, the curve in Figure 4.4 presents a "slippery slope" that describes a notable increase in the amount of oxygen delivered to tissues, for small variations in pO_2.

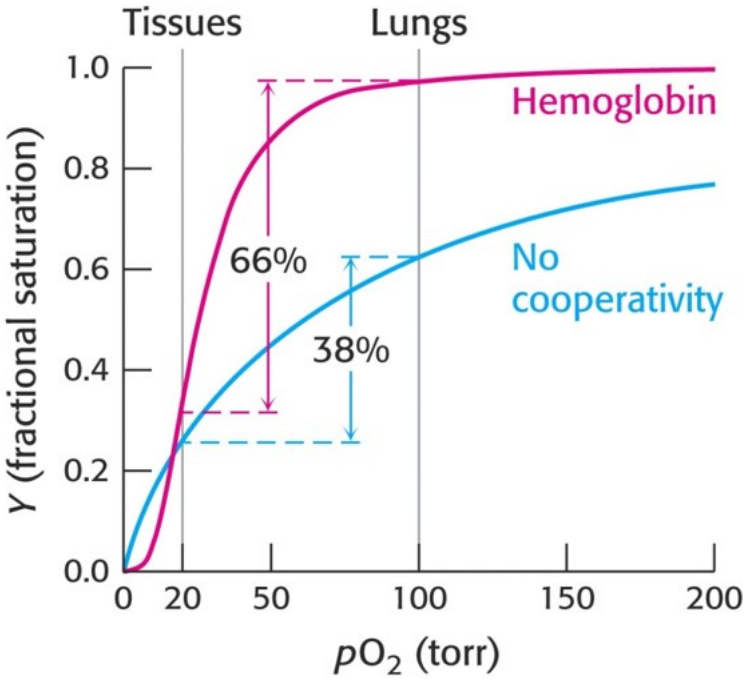

Figure 4.4. Oxygen saturation curve of hemoglobin. Oxygen binding to hemoglobin follows a sigmoidal behavior which reflects the cooperativity between those molecule. This increases the efficacy and sensitivity of oxygen delivery to tissues with respect to a non-cooperative protein. From [30].

In 1910, Hill described the cooperative behavior of allosteric proteins through the Hill equation. For a protein with n binding sites, the reaction between protein and ligand is described as follows:

$$P + nL \rightleftharpoons PL_n \tag{4.1}$$

The association or equilibrium constant (K_a) of this reaction, expressed in M^{-1}, describes the affinity that a ligand has for a certain protein. In this case, K_a is defined as:

$$K_a = \frac{PL_n}{[P][L]^n} \tag{4.2}$$

Now, it is possible to define the ratio between occupied binding sites and total

amount of binding sites (θ) which, in other words, is the fraction of link sites occupied by the ligand (S_{O2}).

$$\theta = \frac{[L]^n}{L^n + K_d} \tag{4.3}$$

In equation 4.3, K_d is the dissociation constant, the reciprocal of the association constant, expressed in M. It is most commonly used to express the affinity of the protein to the ligand: lower K_d means higher affinity. In other words, K_d represents the ligand molar concentration at which 50% of total protein binding sites are occupied. Indeed, if the protein has a high affinity for the ligand, it takes less ligand concentration to reach half saturation between protein's link sites [31].

Applying the logarithm to both terms of equation 4.3, it leads to:

$$\frac{\theta}{1-\theta} = \frac{[L]^n}{K_d} \tag{4.4}$$

$$\log\left(\frac{\theta}{1-\theta}\right) = n\log[L] - \log K_d \tag{4.5}$$

Equation 4.5 is the Hill equation where n or n_H is the Hill coefficient which measures the degree of cooperativity between protein and ligand: if $n_H<1$, there is no cooperativity; if $n_H>1$, cooperativity occurs. The maximum cooperativity degree in the hemoglobin is present when $n_H=3$, but for human hemoglobin $n_H=2.7$.

In order to adapt the Hill equation to the cooperative binding between oxygen and hemoglobin, in the expression of θ (Equation 4.3), L, the ligand, should be susbstituted with the partial pressure of oxygen, pO_2, and K_d with ${P_{50}}^n$.

$$S_{O_2} = \frac{\left(\frac{pO_2}{P_{50}}\right)^n}{1 + \left(\frac{pO_2}{P_{50}}\right)^n} \tag{4.6}$$

P_{50} is the value of oxygen partial pressure at which half of the hemoglobin binding sites are occupied. For human Hb, P_{50} is approximately 26 mmHg. Increasing P_{50} by shifting the oxyhemoglobin dissociation curve to the right, means decreasing Hb oxygen affinity and favor O_2 release. The contrary happens if the curve is shifted to left and consequently P_{50} is reduced [31].

Some studies revealed that purified hemoglobin has a higher affinity for oxygen with respect to intraerithrocytic hemoglobin because inside red blood cells there is 2,3-bisphosphoglycerate (2,3 BPG) at a concentration approximately equal to Hb's

one. This anionic compound binds deoxyHb in a folder at the center of the tetramer making the taut state (T) more stable and thus reducing oxygen affinity. In order to make the transition T to R favorable, the links between 2,3 BPG and deoxyHb should be broken and this requires a certain amount of energy: this is why the binding of the first oxygen molecule is energetically less favorable [30].

Oxygen release mechanism of hemoglobin perform at its best in working tissues because it is promoted by hydrogen ions (H^+) and carbon dioxide (CO_2), metabolic byproducts. Hemoglobin affinity to oxygen decreases in presence of low pH or of high CO_2 concentrations so that the transition from R to T state is favored. Both H^+ and carbon dioxide help form interactions, namely salt bridges, between amminoacidic residues at the interface between the four subunits. These interactions make the structure of deoxyHb more stable and thus promote O_2 release in tissues. In this way, H^+ and CO_2 are bound to Hb molecules and they can be transported towards the lungs where pH increases and the inverse process occurs: this heterotropic regulation is called the Bohr effect [31].

Temperature too may affect the binding affinity of hemoglobin to oxygen. During exercise, body temperature increases and oxygen demand from muscle tissues raises. For this reason, high temperature decreases Hb affinity to oxygen and promotes its release to the tissues.

To summarize, the mechanisms which cause a right shift of the oxyHb dissociation curve, and thus a decrease in affinity for oxygen, involve an increase in either temperature or $[H^+]$ or $[CO_2]$ or [2,3 BPG]. Figure 4.5 shows the effect of two of those mechanisms.

In human blood, hemoglobin is the physiological mean of transport for oxygen and for this reason it has been largely employed as a blood substitute for intravenous administration in order to exploit its efficient and sensitive oxygen delivering kinetics. Solution of hemoglobin-based oxygen carriers (HbOCs) are made up of native, free human or mammalian Hb and they can be stored for periods up to 2 years without concerns about compatibility [33].

Although those advantages, some issues arise. When Hb is removed from red blood cells, its behavior is no more affected by the presence of 2,3-bisphosphoglycerate and hence the O_2-Hb dissociation curve is shifted to the left, leading to a decrease in P_{50} and to a reduction of tissue oxygenation capabilities. In pure Hb, P_{50} can reach the

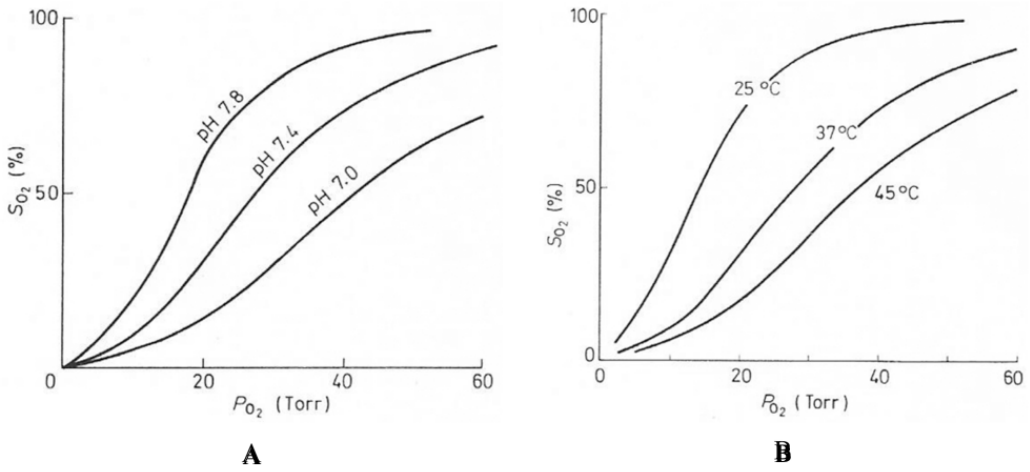

Figure 4.5. A decrease in pH (**A**) or in temperature (**B**) shifts the oxygen-hemoglobin dissociation curve to the right, increasing P_{50} and promoting oxygen release to the tissues. Adapted from [32].

value of 10 mmHg. Usually, bovine Hb is preferred to human Hb because bovine plasma does not contain 2,3-bisphosphoglycerate and so P_{50} is always around 50 mmHg both inside and outside red blood cells [34].
Another relevant issue occurs because the Hb tetramer ($\alpha_2\beta_2$) tends to dissociate into dimers ($\alpha\beta$) when the molecule is freed from the red blood cells. Those dimers are immediately cleared by the kidneys and this can cause renal toxicity together with a short circulation lifetime [33].

Cell-free hemoglobin modification techniques have been developed since 1980s to solve those problems. These techniques are cross-linking, polymerization, conjugation and recombination.
In cross-linked hemoglobin, the tetrameric structure is stabilized by the covalent binding of cross-linkers like bis-(3,5-dibromosalicyl) fumarate that links lysine residues in two α chains, creating $\alpha\alpha$-hemoglobin [33].
Polymerization involves cross-linking agents, like glutaraldehyde or raffinose, to create polymers of Hb tetramers of different molecular weights. PolyHb has greater stability, longer intravascular half-life ($\sim$12-48 hrs) and a P_{50} closer to that of human blood that prevents the release of excessive amounts of oxygen. Hence, HbOCs made up of polymerized hemoglobin have passed clinical trials.
Another technique used to improve Hb retention in plasma by increasing Hb molecular size is conjugation. It links cell-free hemoglobin with soluble polymers like polyethylene glycol (PEG) [35].
The last approach based on recombinant technology produces human hemoglobin from the engineering of E.coli. The target is still that of avoiding tetramer dissociation

into dimers. Therefore, α chains are linked together increasing Hb structure stability. Unfortunately, contamination risks are present when manufacturing recombinant hemoglobin.
Figure 4.6 shows the oxygen-hemoglobin dissociation curves of different types of modified hemoglobin.

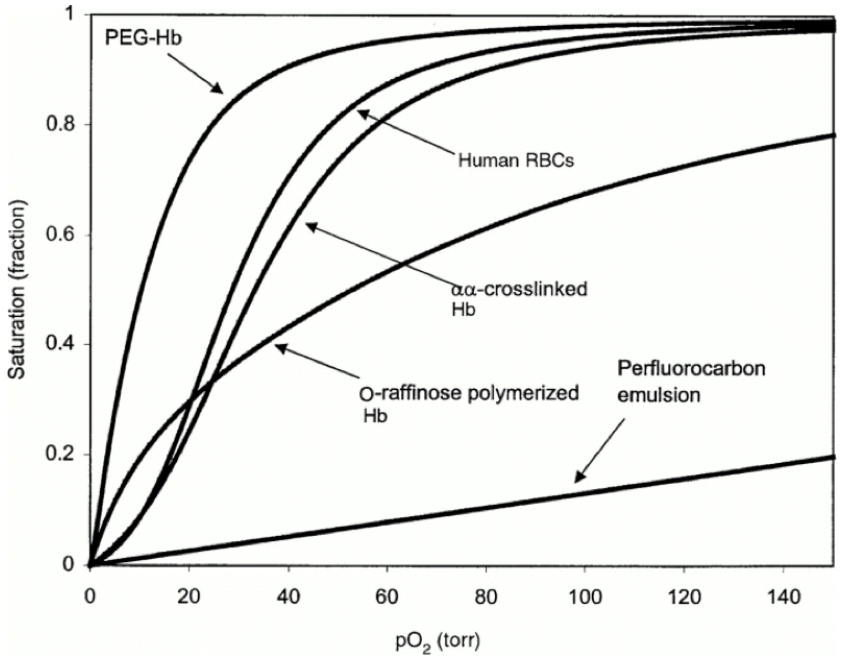

Figure 4.6. Fractional saturation of various hemoglobin solutions versus environmental partial pressure of oxygen. Polymerized and cross-linked Hb are those that better resemble the characteristics of human RBCs hemoglobin. From Stowell et al. [33].

The research into these first-generation HbOCs did not get too far because of adverse effects encountered during experiments.
The first of these effects is vasoconstriction which leads to hypertension. It is common opinion that this drawback arises from nitric oxide (NO) scavenging by hemoglobin. Nitric oxide is a gas that biologically works as a signaling molecule. It has been identified as an endothelium-derived relaxing factor that promotes vasodilatation and it also acts as an inhibitor of platelet activation. NO is widely distributed in tissues and when it diffuses into blood (extravasation), it gets in contact with oxygenated hemoglobin, which is its principal scavenger. NO has an intravascular half-life of approximately 2 ms which is reduced 500 times when NO is scavenged by oxyHb. This action is lowered in presence of red blood cells that contain hemoglobin [36].

Another adverse effect found experimentally and related to first-generation HbOCs is due to rapid autoxidation of cell-free hemoglobin. According to the hypothesis of

Weiss [37], in blood, a part of oxygenated hemoglobin ($HbFe^{2+}O_2$) is in the form $HbFe^{3+}O_2{}^-$ where the iron atom is in its ferric state. The autoxidation starts with the simple dissociation of $HbFe^{3+}O_2{}^-$ into methemoglobin (metHb), $HbFe^{3+}$, and superoxide anion ($O_2{}^-$). In presence of H^+, $O_2{}^-$ attacks other oxyHb molecules producing metHb, hydrogen peroxide and oxygen. Hydrogen peroxide, then, continues to amplify this reaction producing biologically highly reactive hydroxil radicals and metHb which has a stable tetrameric structure but it is not able to bind oxygen.
In human blood, in presence of RBCs, metHb represents no more than 1% of total Hb concentration and specific enzymes are present to eliminate hazardous reactive species from the circulation. When hemoglobin is extracted from RBCs those prevention mechanisms are lacking. Therefore, now, research aims at overcoming those toxicity issues, for instance, modiying Hb with endogenous antioxidants that mitigate autoxidation consequences or changing heme pocket reactivity towards NO [35].

Nevertheless, those approaches still lack of the protective function that RBCs membrane carries out and they do not possess a long circulation time.
So, third-generation of HbOCs aims at creating artificial red blood cells encapsulating hemoglobin molecules with RBC enzymes. Doing so, no modification is needed since the toxicity issues, that characterize cell-free Hb, are avoided.
One technology employs bilayer lipid membranes that include not only Hb but also molecules (e.g. cholesterol) to increase mechanical stability and 2,3-bisphosphoglycerate to match oxygen-carrying characteristics of blood. Hb lipid vescicles are in the early stage of development and further deepening is needed to study the uptake of liposomes from RES.
Other encapsulation materials that recently gained attention are biodegradable polymers which are cheaper and more widely available. With them it is possible to create Hb nanocapsules of smaller diameter (0.15 μm) with respect to lipid-based Hb vescicles (1 μm) [35]. Polymeric nanoRBCs have better permeability with respect to liposome-encapsulated Hb since lipid membranes appear to be impermeable to some reducing agents that prevent Hb to oxidize into metHb [38].
Chang [39] developed biodegradable nanopolymeric artificial red blood cells where hemoglobin is encapsulated together with other biologically active molecules. Here, the shell is made up of polylactides since they are easily degraded inside human body. During *in vitro* experiments, nanoengineered RBCs showed same Hb content, P_{50} and Hill coefficient of human RBCs. The synthesis protocol should be better adjusted to guarantee a high percentage of Hb encapsulation.

Molecular self-assembly mechanism which produces polymersosomes can be exploited to create encapsulation materials for HbOCs. Polymersosomes are nano-microparticles generated in acqueous environment from the spontaneous assembly of amphiphilic block copolymers, such as poly(butadiene-*block*-ethylene oxide) (PBD-PEO) or poly(ethylene oxide-*block*-lactide) (PEO-PLA). Changing molecular weight, composition and concentration of those blocks is possible to adjust capsule size and

protection layer thickness [38].
In the fabrication of those nanoengineered RBCs, hydrogels are taken into consideration in order to reproduce the flexibility of human RBCs which let them easily deform across vessels and capillars. Hence, Desimone et al. [40] developed a technique, called PRINT, based on non-wetting templates to fabricate red blood cells mimics (RBCMs). Figure 4.7 illustrates the PRINT technique. In green, there is the elastomeric fluoropolymer mold whose disc-shaped wells are full of prepolymer mixture (2-hydroxyethyl acrylate and poly(ethylene glycol) diacrylate). A pressure nip passes over the mold eliminating the excess liquid and filling the wells that, once full, are photochemically cured for crosslinking. In order to harvest the hydrogel particles, the mold is freezed onto a thin film of poly(vinyl alcohol) in water (blue).

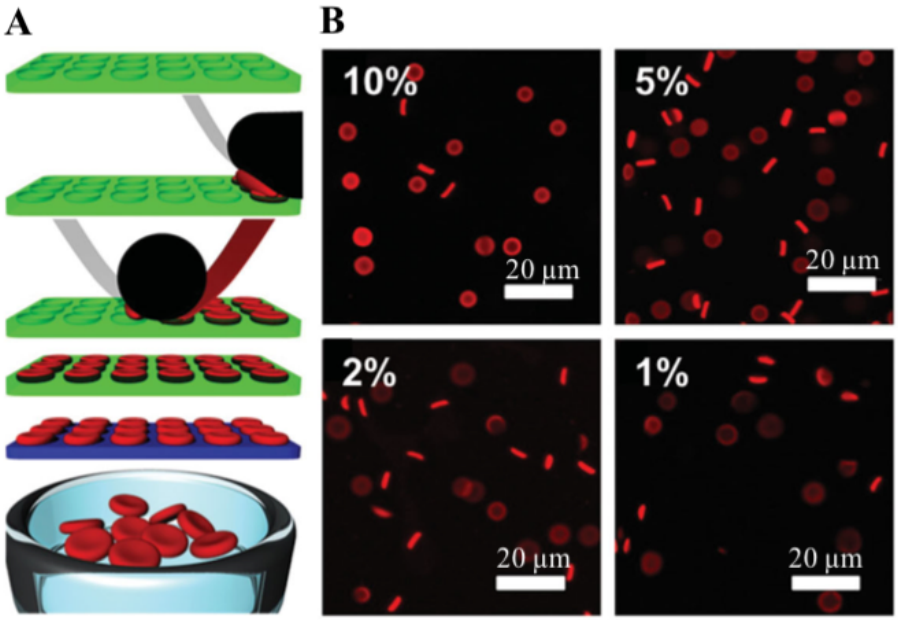

Figure 4.7. **A**. Steps of fabrication of red blood cells mimics with the PRINT technique. **B**. Fluorescent images of hydrated red RBCMs with different crosslinker percentages: lower crosslinker concentration leads to smaller the elastic modulus. Adapted from Desimone et al.[40].

The powerful potential of hemoglobin-based oxygen carriers lies in the cooperative binding between oxygen and hemoglobin that guarantees accuracy and efficacy during uptake and release. This oxygen transport occurs in physiologic conditions thanks to a particular sensitivity to environmental partial pressure that let hemoglobin behave as an oxygen reservoir if in a certain place pO_2 is high enough to guarantee tissue

metabolic functions.
Although HbOCs are not yet widely employed in tissue engineering, they could be essential for some kinds of tissues, like myocardium, that, during hypoxemia, need a life-saving amount of oxygen to avoid necrosis.

4.1.3 Fluorinated compounds

Perfluorocarbon (PFC) molecules are non-polar molecules born from the complete substitution of hydrogen atoms by fluorine atoms (halogenation) inside polar hydrocarbon linear or cyclic chains (Figure 4.8). PFCs are characterized by the strongest single intramolecular bond found in molecular compounds (120 kcal mol^{-1} [41]), because of the great match between carbon and fluorine orbitals. For this reason, PFCs are chemically inert. Moreover, their low polarizability make them hydro- and lipophobic and, above all, it influences PFCs ability to easily dissolve and transport oxygen. Indeed, those non-polar molecules are bond together by Van-der-Waals forces that are weaker (0.5-1 kcal mol^{-1}) than the intramolecular forces. Thus, PFCs act as gas-like fluids and readily dissolve gases like carbon dioxide (CO_2), nitric oxide (NO) and oxygen [42]. For this reason, from 1980s, their potential as blood substitutes has been tested through intravenous administration.

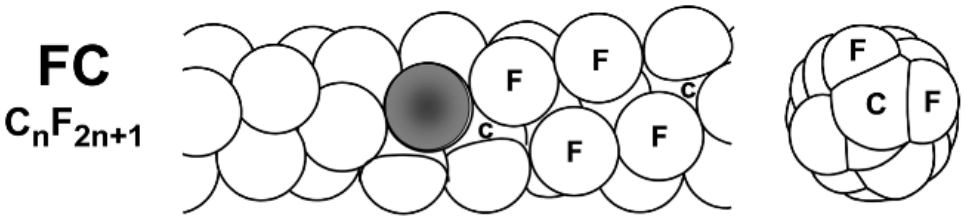

Figure 4.8. Structural composition of fluorocarbon chains with cross-section on the right. Adapted from Riess [42].

Differently from hemoglobin which creates a chemical bond with oxygen molecules, perfluorocarbons dissolve them inside their structure according to gases degree of solubility and proportionally with gases partial pressure (Figure 4.10). This occurs because both PFCs and oxygen are low cohesive compounds.
What governs this transport is the Henry's law according to which, *at a fixed temperature, the amount of gas dissolved in a certain volume of liquid is directly proportional to the partial pressure of that specific gas in equilibrium with that liquid* [41]. The Henry's law is represented by the following equation:

$$C = \alpha \cdot P \tag{4.7}$$

where C is the concentration of the dissolved gas ($\mathrm{mol\,m^{-3}}$), α is the coefficient of solubility expressed in $\mathrm{mol\,m^{-3}\,Pa^{-1}}$ and P represents the partial pressure of the gas in Pa.

Through this mechanism, PFCs are able to dissolve large amount of oxygen that can be double with respect to that dissolved by plasma [41]. This peculiarity is favored also by the fact that, in absence of a chemical bond, PFCs do not reach a saturation condition that limits their oxygen carrying capacity (OCC). Nevertheless, this OCC is limited by the environmental oxygen concentration: the outcome of this oxygen carrier is improved if the fraction of O_2 inspired by the subject to which the PFC emulsion is administered increases.

Being hydrophobic, whether they are to be injected intravenously or embedded into hydrogels, PFCs need to be emulsified with surfactants like phospholipids (Figure 4.9). The resulting stable emulsions are characterized by microdroplets with a diameter of 0.1-0.2 μm [42]. Their surface-to-volume ratio is larger than that of red blood cells so that the gas exchange is more favorable.
One of the best known PFC-based blood substitute is Oxygent (Alliance Pharmaceutical, San Diego, CA) which contains 60% w/v of perflubron (C_8BrF_{17}). Its popularity resides in its characteristics: to achieve good stability, PFC emulsions need to have a relatively high molecular weight which, concurrently, reduces their ease of excretion by the body. Oxygent itself has microdroplets with low molecular weight so that their excretion is rapid and, at the same time, its emulsion is stable because its water solubility is extremely low.

Figure 4.10 shows the oxygen-carrying capacities of Hb and PFC plotted against the environmental oxygen partial pressure (pO_2). Differently from hemoglobin, PFCs do not require any chemical bond as oxygen is simply dissolved inside PFCs particles. This diffusion mechanism leads to faster oxygen exchange and higher oxygen extraction ratio that is approximately 90% of their content when passing across tissues. This value accounts for emulsions containing 60% of perfluorocarbon component: smaller PFC concentration means smaller extraction ratio.
Unfortunately, the velocity at which oxygen exchange between PFC particles and surrounding tissue occurs can trigger adverse effects inducing hyperoxia. Indeed, PFCs do not bind oxygen in a cooperative way and this results in a less efficient transport mechanism because PFC-dissolved O_2 is immediately available to tissues, regardless of pO_2 levels.
Oppositely, the cooperative binding of oxygen to hemoglobin guarantees a more controlled release that happens mainly in presence of hypoxic tissues. Differences between hemoglobin behavior in whole blood and oxygen carriers depend on their P_{50}: modified hemoglobin has a lower affinity for oxygen and, thus, it is more keen to release its payload. For this reason, with Hb-based oxygen carriers it is possible to

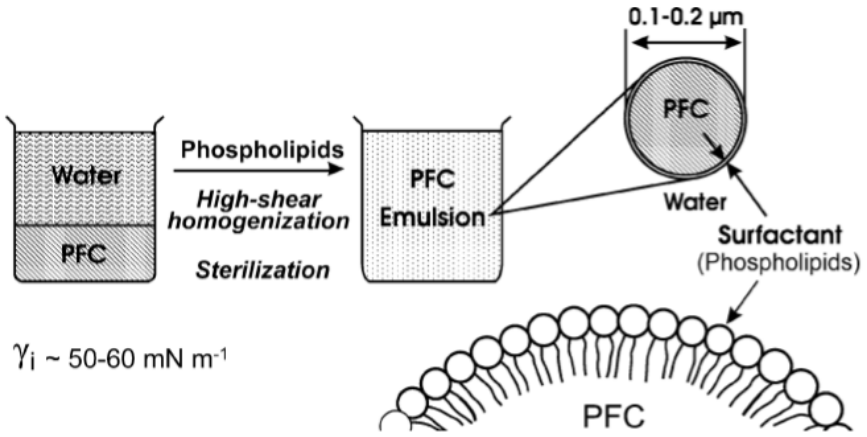

Figure 4.9. Process of production of a PFC emulsion. The emulsifier is typically a phospholipid which creates the emulsion after procedures of homogenization and sterilization. The difficulty of this process resides in the energy level needed to overcome the interfacial tension (γ_i) between PFC and water. From Riess [42].

extract 50% of the O_2 content between 100 and 40 mmHg [35].
Although perfluorocarbons are biologically inert and, thus, they guarantee minimal immunogenicity when they get in contact with biological fluids, their emulsifying agents do not possess this characteristic and can produce toxic effects. This contraindication is enhanced by the fact that, as explained, it is complicated to accurately control PFC particle size or to create a narrow distribution of droplet size around the target one. Hence, bigger droplets are more difficult to be cleared by the reticulo-endothelial system and this still represent the main challenge when dealing with PFC as blood substitutes.

Recently, researchers have been trying to incorporate those perfluorocarbon emulsions into hydrogels and scaffolds for tissue engineering purposes.
White et al. reported an increase in oxygen permeability inside alginate hydrogels by adding 7% perfluorooctylbromide (PFOB) [43]. In this study, PFOB has been emulsified with a non-ionic surfactant, Pluronic F68 (Figure 4.11). Although promising results, the group did not further analyse the effects of PFOB on the mechanical properties of the hydrogel. In fact, they discuss the probability that strain characteristics like fracture stress can be negatively affected by high (>10%) concentrations of PFOB. High concentrations of PFC means high concentrations of surfactanct that can produce harmful cellular consequences.
One way to overcome those issues is to functionalize hydrogels with perfluorocarbon molecules. Indeed, for what concerns White's ([43]) and other works, PFC emulsions are mixed with a polymeric solution which is then crosslinked to obtain the consistency of a gel [28]. On the contrary, Li et al. used the functionalization approach

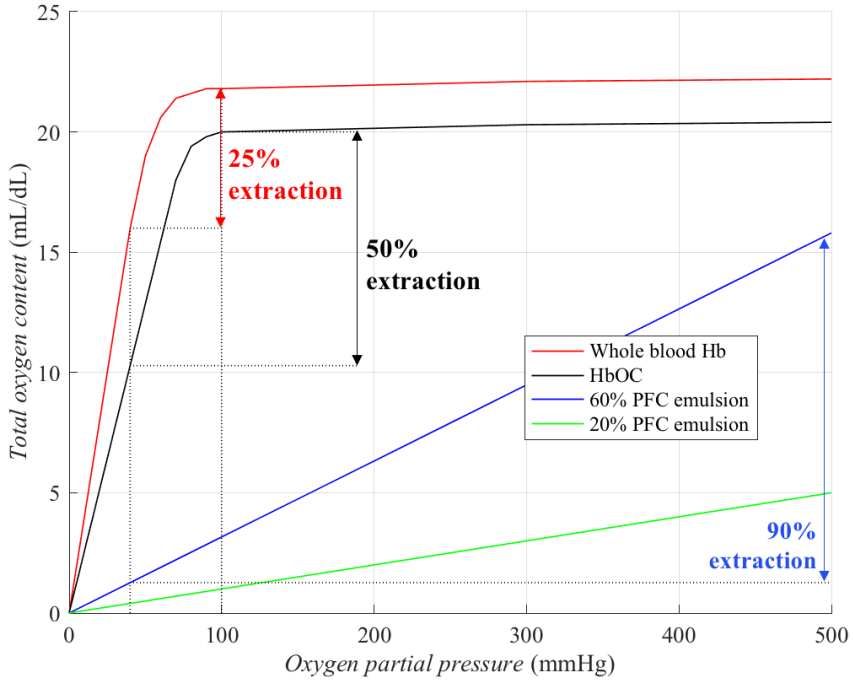

Figure 4.10. Oxygen-carrying capacity (OCC) versus oxygen partial pressure (pO_2) of whole blood, HbOC (soluble unmodified human Hb) and PFC emulsions at 20 and 60%. pvO_2 is the normal venous oxygen partial pressure. Hb extraction percentages are shown for pO_2 varying between 100 mmHg (lungs) and 40 mmHg (tissues). Adapted from Gaudard et al. [35].

to synthesize fluorinated methacrylamide chitosan (MACF) hydrogels for wound healing applications. Here, the free amines of chitosan are conjugated with C_5F_{17} via nucleophilic substitution reaction before gelification [44]. This approach yields high oxygen concentration inside human dermal fibroblasts cultured *in vitro*, guaranteeing their metabolic activity. Moreover, no differences between MAC and MACF elastic modulus have been observed.

The presence of perluorocarbons proved to improve oxygen uptake and release inside biomaterials, to increase cell viability and sustain cellular fundamental metabolism. With respect to other oxygen carriers, PFCs can be produced on a larger scale due to their wide availability and low production costs and they have a prolonged shelf life [33].
Nevertheless, oxygen release from those compounds is not enough prolonged in time for *in vivo* efficacy. It appears that most O_2 release occurs in the first hours of hydrogel implantation while scaffold vascularization occurs within 1-3 weeks from implantation [28]. In this case, a solution to extend O_2 release time could be that of encapsulating

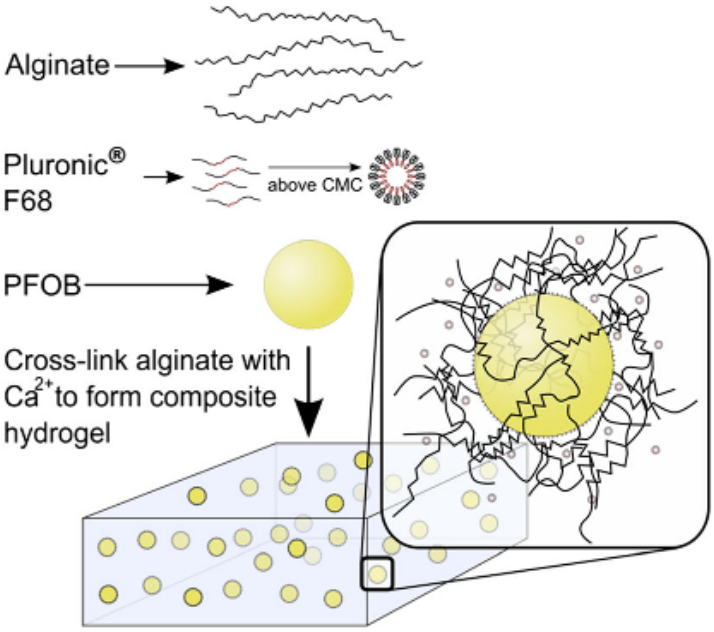

Figure 4.11. Alginate-based hydrogel system described by White et al. The perfluorocarbon component is PFOB emulsified with Pluronic F68, a surfactant whose concentration must be kept low to avoid cytotoxic consequences. From White et al. [43].

perfluorocarbons into materials with low oxygen permeability.

4.2 Carrier biomaterials

A powerful way to overcome the limitations of the oxygen sources just presented is to encapsulate them in specific biomaterials. Those carriers can help promote efficient tissue oxygenation by slowing oxygen release and thus reducing associated cytotoxic effects. Degradation mechanism and release time are key aspects when choosing a carrier biomaterial.
So far, polymers gained the largest success and, among them, particularly poly(lactide-co-glycolide) (PLGA), poly-ϵ-caprolactone (PCL), polyurethane, N-isopropylacrylammide (NIPAAm) and poly(N-vinylpyrrolidone) (PVP). Those materials are biocompatible, they have tunable biodegradability and showed sustained O_2 release for several days.
Hydrogels, too, are investigated to carry out this function. In particular, alginate and gelatin methacyloyl (GelMA) are preferred, being able to encapsulate both oxygen

sources and cells.
More recently, research on stimuli-responsive biomaterials gave promising results opening the possibility to exploit them in order to control oxygen release by means of external triggers like electrical or optical stimuli, temperature or pH [27].

When encapsulating oxygen sources like peroxides, biomaterials should possess a low degree of permeability to water in order to slow the degradation of those solid compounds and thus delay oxygen release. This is the case of hydrophobic PDMS that, by means of the curing method, is mixed with the oxygen source and then heated. When Pedraza and coworkers [45] mixed encapsulated CPO with PDMS through this approach, they demonstrated an oxygen release time greater that 7 weeks. Unfortunately, PDMS is not biocompatible so its application *in vivo* is risky.

The best way to tune biomaterial characteristics and achieve optimum release is to exploit nanotechnology to synthesize different geometries, such as micro- and nanoparticles, nanofibers and 3D scaffolds.
Nanofibers, for instance, can be fabricated through electrospinning during which an electric field is applied to a solution droplet in order to eject it through a syringe. Here, by adjusting solution concentration, electrical field and distance between syringe needle and collector, it is possible to tune fibers' size and uniformity.
Electrospraying is a technology that follows the same principle of electrospinning and it is chosen to fabricate submicron particles. Fan and coworkers [46], for instance, synthesized through electrospraying an O_2-release system with a core-shell structure having PVP/H_2O_2 droplets as core and PVP as shell. Then, this system was embedded into a thermosensitive PNIPAAm hydrogel in order to inject it and immobilize it into the infarcted area of the myocardium. This hydrogel contained the catalase enzyme able to decompose the PVP/H_2O_2 core.
Conversely, hydrogels containing oxygen sources are fabricated via gelation method. According to it, the base gel is synthesized following the standard techniques and, then, molecules or compounds are added into it. In the work of Alemdar et al. [47], for instance, GelMA is synthesized following the protocol which ends with a freeze-drying step that actually creates the porous hydrogel. Then, by magnetic stirring, CPO is added to the the GelMA previously dissolved into dimethyl sulfoxide (DMSO).

Chapter 5

Adhesive oxygen-releasing hydrogel

Oxygen is the fuel of cellular metabolic activities: if absent, it can undermine cell survival and, hence, the physiological behavior of human body. This is what occurs during myocardial infarction when oxygen and nutrients supply to the heart is interrupted and ischemic areas are generated from cell necrosis.
Various srategies have been carried out to stem this adverse effect of MI. Some of these are clinically accepted but research is continuosly in progress in order to improve those approaches by reducing their side effects and boosting their efficacy. Indeed, current therapeutic approaches are systemic and this aspect can reduce their efficacy since the infarcted area has low blood flow and oxygen may not diffuse up to the myocardial region that is most in need.

Hence, our project aims at designing an adhesive hydrogel for site-specific oxygen release in order to directly oxygenate the infarcted portion without affecting healthy tissues. This is achieved by direct bioprinting of the hydrogel on the MI site by means of a handheld printer that will be described in the following.

Up to now, as described in Chapter 4, mainly solid peroxides have been employed as oxygen sources inside oxygen-releasing hydrogels for MI. Unfortunately, the byproducts that those compounds generate during the decomposition that leads to O_2 production possess relevant citotoxicity.
It is against this background that our work stands by engineering a harmless system to provide oxygen to the myocardium. To do so, the adhesive hydrogel hosts perfluorocarbon and hemoglobin molecules that work in synergy to oxygenate the infarcted region in a controlled and efficient manner.
The choice of these two oxygen sources derives from the need to make use of their potential in a combined way. Perfluorocarbons have a large oxygen-carrying capacity (OCC) so that their extraction ratio, when releasing O_2, is particularly high. Nevertheless, since they only dissolve O_2 molecules, this payload, after delivery, is instantly available to the tissue, regardless of its needs expressed by their oxygen partial pressure (pO_2).
On the other hand, hemoglobin binds O_2 molecules through a chemical link in a cooperative way. Hence, oxygen release from hemoglobin is efficient and accurate as it occurs mainly when pO_2 levels drop below $\sim$60 mmHg, in order to correctly sustain tissue oxygenation. Nonetheless, because of this cooperativity, hemoglobin

oxygen-carrying capacity is limited and depends on the number of Hb molecules, as each of them possesses one iron atom that can reversibly bind 4 O_2 molecules.
So, the idea is that of tuning oxygen release from the hydrogel according to the needs of the myocardial portion: as long as its pO_2 is below physiological limits of normoxia, the delivery system carries out its primary function. In this frame, perflubron droplets are expected to easily and rapidly release their large oxygen content, letting it diffuse towards the gel and the tissue. Whenever pO_2 levels get high enough to carry out cellular metabolic functions (>100 mmHg), the release stops and hemoglobin molecules act as oxygen reservoirs that retain their payload.

Property	*Value*
Molecular weight	498.96 $g\,mol^{-1}$ [48]
Density	1.93 $g\,m^{-3}$ [48]
Melting point	6 °C [48]
Oxygen solubility	12 $mol\,m^{-3}\,bar^{-1}$ [49]

Table 5.1. Perfluoro-octyl bromide parameters.

For modeling purposes, perfluoro-octyl bromide (C_8BrF_{17}) is chosen among perfluorocarbons. This is the principal constituent of various biocompatible emulsions employed as synthetic oxygen carriers and its properties are described in Table 5.1. One of these is Oxygent, based on perflubron, a liquid form of perfluoro-octyl bromide and egg yolk phospholipid, that has been presented in Chapter 4. Oxygent is in Phase II and Phase III of clinical trials for the treatment of severe intraoperative blood loss. Its aim is to coadiuvate the blood in its oxygen-carrying function [33].
The hydrogel is designed to be fabricated with gelatin methacryloyl (GelMA) and skin secretion of *Andrias davidianus* (SSAD).

5.1 Gelatin methacryloyl (GelMA)

Peptide and protein-based biomaterials are widely studied in biomedical sciences because they are the most suited to engineer matrices that resemble the native extracellular matrix (ECM). This is the case of gelatin methacryloyl (GelMA): born from the need of stabilizing gelatin hydrogels, it presents some essential characteristics of the ECM and for this reason it is widely employed to fabricate biomimetic tissues.
What is relevant in GelMA chemical structure is the presence of peptide motifs that are cell-attaching (e.g. arginine-glycine-aspartic acid (RGD) sequence) and matrix metalloproteinase (MMP) responsive. Those motifs derive from the chemical architecture of collagen, the most copious ECM structural protein, from which it is possible to derive gelatin by means of partial hydrolysis. Although its solubility in

water occurs at more than 40°C, at room temperature, on cooling, gelatin can form hydrogels that partially keep the triple helical structure of collagen [50]. Unfortunately, those biomaterials showed poor mechanical stability and low transition temperatures that do not guarantee their durability at body temperature. So, methods to crosslink gelatin protein chains have been employed. In particular, in 2000, Van Den Bulcke et al. [51] crosslinked gelatin with methacrylic anhydride (MA), producing GelMA. This hydrogel has gained success in biomedical applications thanks to its easy and versatile fabrication, cost efficiency and compatibility with 2D and 3D cell scaffolding.

GelMA is usually described in a misleading way, being called gelatin methacrylamide or gelatin methacrylate. Actually, the right nomenclature derives from the chemical structure of the material and from the percentage of different functional groups in its backbone.
From a chemical point of view, what happens during gelatin-MA crosslinking is shown in Figure 5.1. In the gelatin backbone, the side groups of amino acid residues host the reactive functional groups, such as hydroxyl groups, amino groups and carboxylic acid substitutes. In particular, hydroxyl and amino groups react with methacrylic anhydride to form methacrylate and methacrylamide groups, respectively.
Yue et al. [50] defined the correct nomenclature of GelMA, analyzing its chemical modification and quantifying the amount of different functional groups in its structure. The results show that, among all MA substitutions, methacrylate groups represent less than 10%. Hence, the amino groups of the gelatin backbone are more reactive and methacrylamide groups are more abundant in GelMA chemical structure, that should be correctly termed as gelatin methacryloyl.

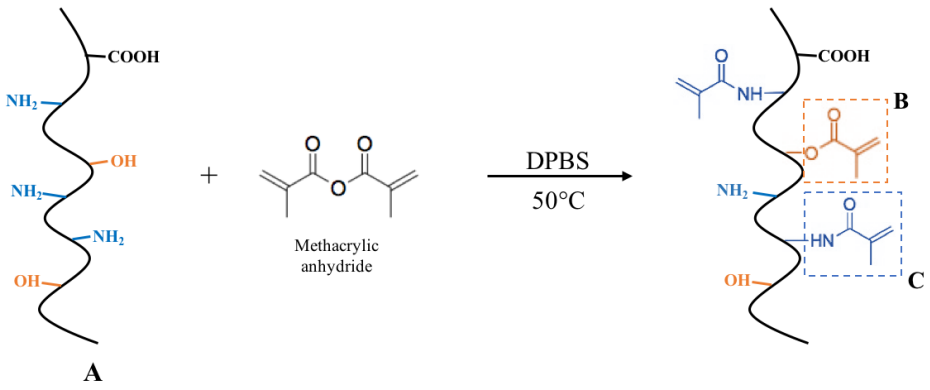

Figure 5.1. Modification of gelatin backbone (**A**) with methacrylic anhydride at 50°C cause hydroxyl and amino groups to react with MA and create methacrylate (**B**) and methacrylamide (**C**) groups.

5.1.1 Synthesis and characterization of GelMA hydrogels

Modification of gelatin with methacrylic anhydride occurs at 50°C. At this temperature, gelatin is dissolved in phosphate buffer (pH 7.5) and then MA is added during intense stirring [51]. If the pH level is kept high during the reaction, the degree of substitution is increased because the reactivity of amino and hydroxyl groups is enhanced. The degree of substitution can be tuned also through the MA amount added to the gelatin solution and it largely influences GelMA physical properties.
To stop the substitution reaction, the mixture is diluted in phosphate buffer and dialyzed against distilled water at 40°C for 5-7 days to remove cytotoxic low-molecular-weight impurities. The products is then freeze-dried producing a white solid that can be stored, preferably under refrigeration [52].

GelMA can form hydrogels through photoinitiated radical polymerization where it is exposed to UV light together with a photoinitiator. UV curing guarantees high polymerization rate, room temperature operation and solvent-free formulations.
Water-soluble photoinitiator like Irgacure 2959 and lithium acylphosphinate salt (LAP) are typically chosen [52] to form a mixture with gelatin methacryloyl at 40°C. This mixture is then exposed to UV light for a given period of time in order to let curing occur.

GelMA hydrogels present high versatility because their physical properties can be finely tuned by adjusting different parameters during synthesis.
For instance, modifying the degree of MA substitution and/or adding organic and inorganic components, it is possible to modify the elastic modulus of the biomaterial ($\sim$ 30 kPa), adapting it to various application requirements and making it particularly suitable for 3D bioprinting. Besides, through freeze-drying, GelMA hydrogel porosity is modulated, considering that average pore size and distribution are inversely proportional to GelMA concentration and process rate [52].
For those reason and also because it showed biocompatibility and biodegradability in *in vivo* myocardial therapy [47], GelMA has been chosen as the principal component of our oxygen-releasing hydrogel. In particular, a 5% GelMA hydrogel will be fabricated to host our novel oxygen-delivery system. Unfortunately, no experimental data are available at the moment in order to characterize this biomaterial and adjust its properties. In particular, oxygen diffusivity inside the gel micronetwork and its pores should be accurately tuned to prevent burst O_2 release inside the myocardium.

5.2 Adhesive biomaterial derived from Skin Secretion of *Andrias Davidianus* (SSAD)

The ultimate goal of this project is to print the oxygen-releasing hydrogel directly onto the myocardium and treat the infarcted area with a topical approach. In order

to facilitate the attachment with the tissue, an adhesive component is added to the GelMA.
Medical adhesives should possess mechanical strength, biocompatibility and simple production processes. Nowadays, materials that fullfil those requirements are natural protein-based ones (collagen, fibrin, albumin, etc) and polysaccharides (chitosan, alginate, hyaluronic acid, etc). Unfortunately, those alternatives present limitations related to cytotoxicity (cyanoacrylate glue), poor elasticity and deceptive adhesion strength (fibrin). So, biomedical research is currently working on finding new reliable biocompatible sealants.

For this project, our choice fell on a naturally-derived adhesive biomaterial synthesized from the skin secretion of *Andrias Davidianus* (SSAD). *Andrias Davidianus* is a Chinese giant salamander, the largest amphibian in the world, whose skin has mucous glands able to secrete, upon irritation, big amount of mucus thanks to which the animal avoids damage and heal. Proteins, amino acids, mucopolysaccharides and antimicrobial peptides are the principal components of this mucus. Recently, its characteristics have been studied and, in 2019, Deng and coworkers [53] presented it as a medical adhesive for sutureless wound closure.

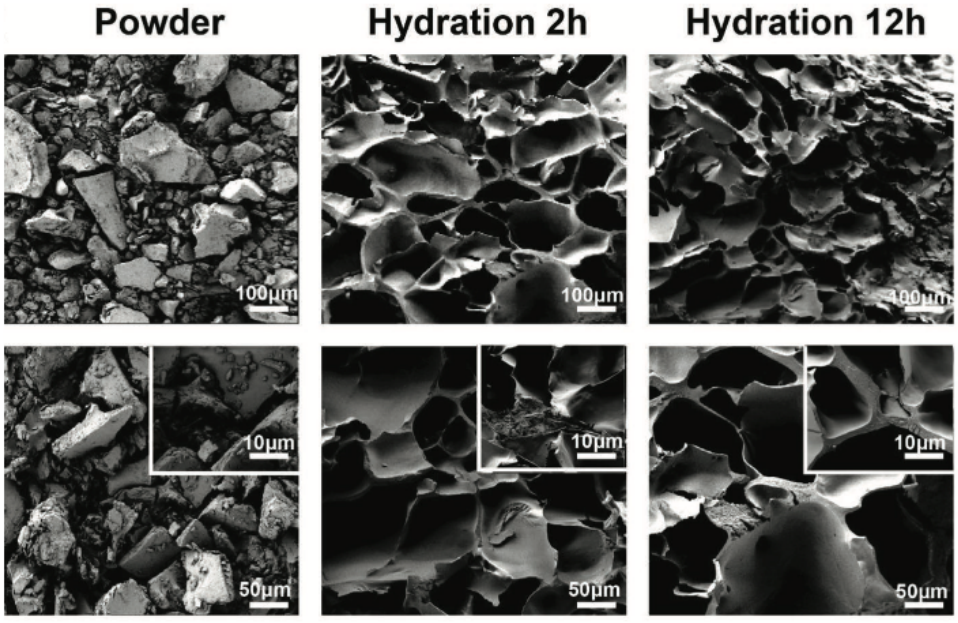

Figure 5.2. SEM images of SSAD powder before and after hydratation at 2h and 12h. From Deng et al. [53].

In this work, it has been demonstrated that 3-5 ml of mucus can be collected from one salamander twice a month and from each ml, after freeze-drying, 200 mg of SSAD powder are extracted. This powder appears in the form of inhomogeneous chunks

containing polypeptide chains that, in contact with water, swell and form a porous hydrogel (Figure 5.2). After 12 hours of hydratation, this hydrogel presents an elastic modulus of 566.86 ± 2.72 Pa.
The functional groups considered to make SSAD adhesive are phenolic hydroxyl groups, amino acids and their benzene rings. During swelling in water, the SSAD protein network expands following the permeation of H_2O molecules and the formation of H-bonds. During this expansion, the amino acid residues inside the backbone undergo a conformational transformation that confers adhesive properties to the hydrogel. Indeed, biological adhesion is favored by van der Waals forces and hydrogen bonds whose donors are the phenolic hydroxyl groups and amino acids [53].
During a pig skin adhesion assessment, the adhesive strength experimentally found by Deng et al. [53] is approximately equal to 30 kPa, a value comparable to that of cyanoacrylate glue (55 kPa) and larger than that of fibrin glue (5 kPa). Elasticity, too, is a relevant requirement for medical adhesive epsecially if they are in contact with contractile tissues. With a three-point bonding test on pig skin with a 2 cm incision, SSAD showed that, with a smaller load, it is able to achieve the same displacement of cyanoacrylate glue. Hence, SSAD provides a more flexible bonding with the tissue.

5.3 Bioprinting

Tissue engineering and regenerative medicine aim at fully restoring damaged or degenerated body portions by means of biomimetic tissues and organ substitutes that should accurately resemble the complexity of their biological counterpart. Indeed, our tissues are composed of many different cell types perfectly organized in three-dimensional complex architectures. So far, various strategies have been studied to engineer functional tissues but none of them has been able to obtain reproducible fabrication of volumetric tissues with high spatial precision [54].
Against this background, three-dimensional bioprinting has been developed. 3D printing was invented in late 80s with the name of stereolithography and with the aim of sequentially print thin layers of a material and form a 3D structure [55]. Being widely employed in industry, researchers in the biomedical field decided to take advantage of this method in tissue engineering. 3D bioprinting represents an additive manufacturing technique thanks to which it is possible to precisely control the positioning of biomaterials, biomolecules and living cells layer by layer, creating 3D functional structures in a reproducible fashion with the support of programmable robotics. 3D bioprinting offers the possibility to recreate engineered constructs with accurate and even personalized features that mimic the fine shape, architecture, and function of targeting tissues and organs [56].

The good outcome of a 3D printing approach mainly relies on the bioink. Hence, bioinks should possess outstanding mechanical properties, biocompatibility and, above all, printability. This characteristic describes the ability to create reliable 3D

structures and keep their stability during time. If a hydrogel is used as bioink, its rheological properties (e.g. viscosity, shear stress, etc) are useful to characterize its printability. In biofabrication, high viscosity limits the collapse of the final construct and increases shape fidelity after deposition. GelMA, for instance, due to its reversible physical crosslinking, appears as a temperature-sensitive material that is more viscous at low temperatures. So, adjusting the temperature during the extrusion process, it is possible to tune its printability [57].

5.3.1 3D Bioprinting strategies

Bioprinting starts with the pre-processing of a computer-assisted design of the configuration in which biomaterials and cells should be deposited to form the desired 3D biological structure. This design is usually developed starting from the information given by imaging and diagnosting technologies, like computer tomography (CT) and magnetic resonance imaging (MRI), about the target tissue. This initial step is followed by the automated deposition of the materials of interest coordinated by an appropriate software. Finally, the post-processing performs the maturation of cell-laden constructs [56].
For the automated deposition step, various strategies have been developed and employed to fabricate 3D biomimetic structures and they are schematically described in Figure 5.3.

Stereolithography (Figure 5.3A) is the first 3D printing technique developed in 1986 and then applied to the bioengineering field. In this approach, the bioink is placed on a stage moveable along the z-axis. By means of photopolymerization, this liquid bioink is selectively solidified layer-by-layer, following a certain 2D pattern that is projected onto it. This projection is carried out by the digital micromirror device (DMD) composed by many microsized mirrors that can be tilted to adjust the light pattern and reproduce the desired geometry, even complex ones, during the phorocrosslinking of different layers [54].
Stereolithography is characterized by a high resolution (~ 1 μm) and a printing speed that is larger than that of nozzle-based strategies. Moreover, no movement in the x and y axes are needed since the crosslinking occurs simultaneously on the entire 2D layer. Unfortunately, this method requires the liquid bioink to be transparent to avoid light scattering and nonuniform crosslinking.

Among nozzle-based bioprinting strategies there is inkjet bioprinting (Figure 5.3B). It relies on a standard inkjet printer containing a bioink deposited on a support moved along x, y and z axes. In this way, droplets of liquid are released on the substrate as a consequence of thermal or piezoelectric actuation following a pattern previously defined on a software. During the process, different layers are build-up in the z direction, creating the desired 3D structure.
Advantages of this approach include low cost, simplicity and the chance to print

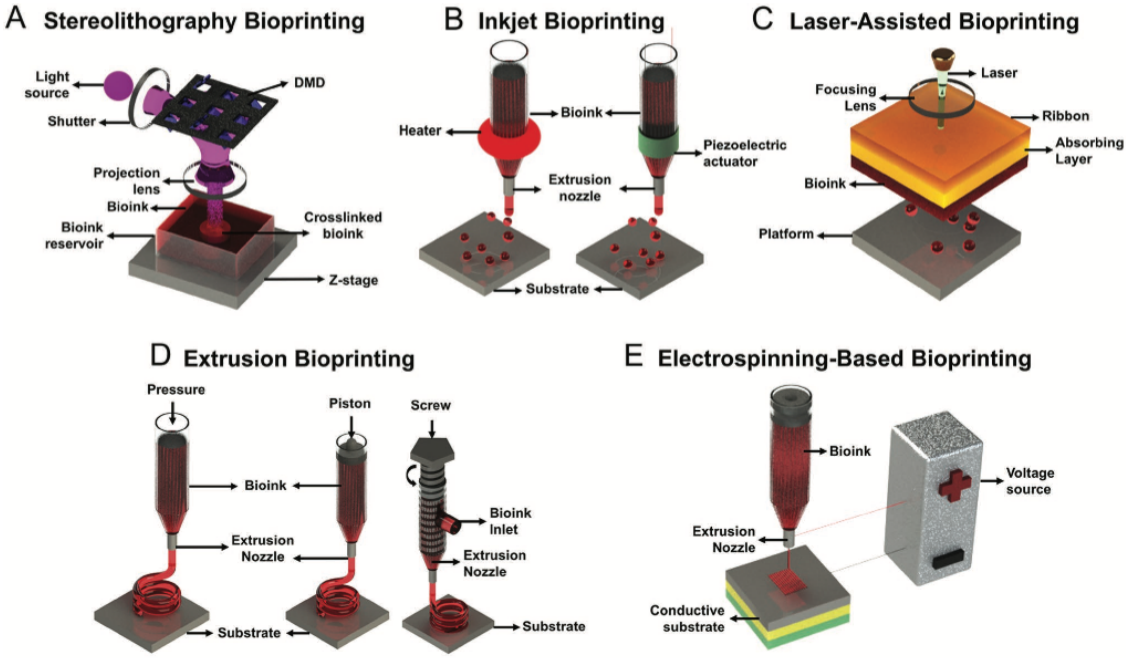

Figure 5.3. Schematic representation of different 3D bioprinting strategies: stereolithography (**A**), inkjet (**B**), laser-assisted (**C**), extrusion (**D**) and electrospinning-based (**E**) bioprinting. From Heinrich et al. [54].

multiple bioinks simultaneously, making multiple printerheads work in parallel and achieving a resolution of ∼30 μm. Nevertheless, a limited range of bioinks can be employed since their viscosities should be in a range of 3.5-12 mPa s [54].

Bioinks with higher viscosities (1-300 mPa s) are the target of laser-assisted bioprinting (Figure 5.3C) since no clogging issues can occur. Here, according to the desired pattern, a laser beam is pointed towards a portion of energy-absorbing layer (e.g. titanium or gold). Behind this target, the corresponding donor layer portion is vaporized creating a bubble pressure at the interface. This pressure produces the ejection of the bioink in form of droplets on the collection layer, that is moved on the z-plane to create tridimensionality [54].
The cost of this technology is high because of the requirements of the laser beam that should possess high resolution and high intensity characteristics.

Figure 5.3D illustrates the extrusion-based bioprinting methods: respectively, pressure-based, piston-based and screw-based. Pressure-based systems can possess a valve, allowing for more precise control over pressure and pulse frequencies and achieving higher resolution, or not if an easier manufacturing process is targeted. In mechanical-driven extrusion bioprinting, the actuator can be a piston or a screw. In

the first case, there is a direct control over the ink deposition while in the other case, the spatial control is more accurate and, hence, it is preferred for high viscosity liquids [54].
Extrusion-based bioprinting methods are the most widely employed in tissue engineering since they guarantee the integrity of the 3D construct because the extrusion is never interrupted. On the other hand, the speed is reduced and the resolution depends on various parameters such as the tip size.

Electrospinning (Figure 5.3E) is used, too, to bioprint 3D structures exploiting its versatility and ability to produce micro- and nanoscale fibers. In this technique, a voltage source applied between the extrusion nozzle and the conductive substrate makes the charged bioink (polymer solution or melt jet) to be stretched and impelled out of the syringe pump in form of fibers. These latter present very small diameters that can also reach 2 nm, reflecting technique high resolution. The deposition can be performed in a continuous or discontinous way [54]. A relevant issue is related to the instability of fibrous structures due to disordered whipping of the charged ink during activation.

5.3.2 Handheld devices for in situ bioprinting

Traditional 3D bioprinting is employed to fabricate biomimetic human tissues and cell-laden scaffolds that, in a second stage, undergo implantation. In our case as well as in all cases in which the tissue defect involves curved surfaces, biomaterial deposition directly onto the damaged area is essential. For this reason, in situ bioprinting has been developed. Nowadays, its popularity resides in the ability to facilitate tissue repair by production of healing structures directly at the defect site.
When this concept was introduced in 2007, clinicians pointed out the need for a less cumbersome apparatus to be used in surgery. From that point on, in situ bioprinting devices have been designed in order to accelerate the translation into the clinics. One of them is the handheld bioprinter thanks to which it is possible to deposit the bioink on-site just by moving the hand.

A low-cost handheld printer (Figure 5.4A) has been outlined at Shrike's Lab by Ying et al. [58]. It is operated by a battery pack so that no external power source is needed and it hosts a motorized extrustion system controlled by various switches: a potentiometer to modify motor rotation speed and hence bioprinting speed, a sensor to turn on/off the apparatus and another one to control the direction. Together with these, a bioink reservoir and a photocrosslinking unit with some ultraviolet light-emitting diodes (LEDs) are embedded.
This handheld printer has been designed to deposit a porous two-phase emulsion bioink made up of GelMA and polyethylene oxide (PEO) for *in situ* medication. The bioink is loaded into a syringe consequently assembled inside the handheld extrusion system.

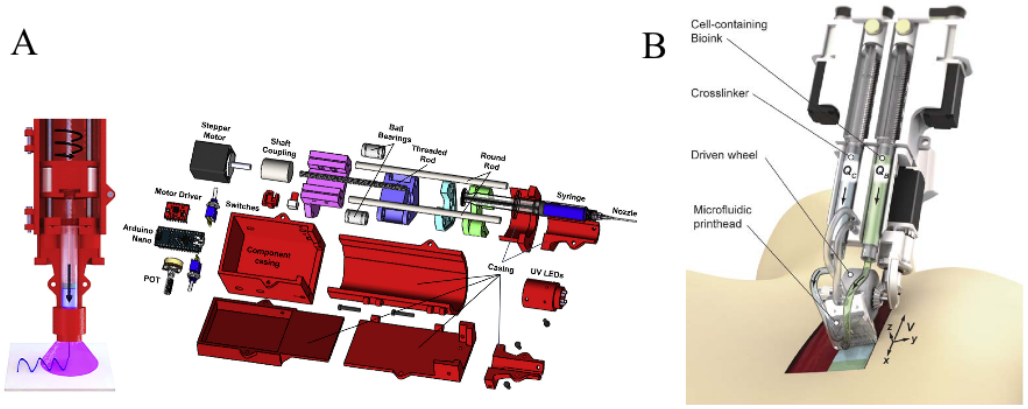

Figure 5.4. **A**. Schematic representation of the handheld bioprinter design with components and assembly. From Ying et al. [58]. **B** Rendered representation of handheld bioprinter for controlled bioink delivery. From Cheng et al. [59].

To avoid potential skin damage caused by the UV light source, another handheld printing system is the one presented by Cheng and coworkers [59] that is, as well, light and manageable (Figure 5.4B). In this device, a toggle switch powers a wheel that guides the deposition process directly on the damaged tissue portion. The microfluidic printhead is positioned downstream of the wheel and it accomodates in two separate inlets the bioink and the crosslinker that, across a parallel arrays of microchannels, are deposited in the form of a sheet.

In situ bioprinting carried out by means of non-cumbersome and light handheld printer is paving the way for a rapid and effective intraoperative wound healing. This is a patient-specific topical approach that guarantees a wound dressing conformal with the physiologic curvature of the damaged area and requires minimal operator training. Hence, for our project, this is the best way to treat the myocardial portion affected by infarction delivering oxygen on-site and preventing cellular necrosis.

Chapter 6

Modeling and simulations

This chapter deals with the modeling of our hydrogel and with the analysis of its oxygen-releasing behavior. The model is created through a finite element method, using Comsol Multiphysics 4.2a.
Starting from this chapter, the terms perfluorocarbon and perflubron will be interchangeable.

Space and time dependent problems of physics and engineering are described through partial differential equations (PDEs) which include governing equations with boundary conditions. In most cases, due to a high level of complexity, those PDEs cannot be solved analytically. Hence, a discretization-based approach is needed since it approximates the problem by means of a set of numerical model equations solved through numerical methods, such as the finite element method (FEM).
This approach divides the original geometry domain into small and simple elements, each with a finite number of degrees-of-freedom (DOFs), connected at nodes. Each element has its own algebraic equation that is easy to solve and, at each node, there is a set of simultaneous algebraic equations that can be interpolated in a piecewise fashion in order to obtain the numerical solution [60].
Meshing is the step in which the starting geometry is divided into small elements. For two-dimensional models, triangular and rectangular elements are preferred. In 3D, mesh elements can be pyramids, prysms, hexahedra or tetrahedra. In principle, a denser mesh leads to more accurate solutions of the PDEs.
The difference between the numerical and the analytical solutions is the error: if the error exceeds the imposed tolerance, the solutions do not converge. This can happen if the mesh size is not appropriate or if the problem is not correctly modeled.
FEM power lies in its ability to solve various physics and engineering intricate problems in complex geometries. Nevertheless, finite element methods give only approximate solutions that are not in closed-form. Thus, it is hard to analyse the system response in order to adjust the model and its parameters [60].

6.1 Model geometry

This adhesive hydrogel is designed as a cube of size 5 mm x 5 mm x 5 mm, containing a certain concentration of hemoglobin (d=5 nm [61]) and perfluorocarbon molecules

(d=0.16 μm [62]) and with a side in direct contact with the myocardium.
Supposing uniform distribution of oxygen sources in the gel, a characteristic portion of the starting volume is considered. Its dimensions are arbitrarily chosen and kept in the micrometers range to speed up the simulation. Then, to translate the problem in 2D and reduce the simulation complexity, this characteristic cube is divided into planes. Since, even at very low concentrations, the number of Hb molecules to be drawn in the characteristic cube is very high and it can limit the mesh quality, those planes are placed 5 nm far from one another so that only one Hb molecule can be accomodated between them.
At this point, given a certain concentration, it is possible to calculate the relative number of Hb molecules in each plane considering Hb molecular weight (64500 $\mathrm{g\,mol^{-1}}$) and the Avogadro number.
Regarding PFC, the number of molecules inside the entire characteristic volume is calculated. Starting from the concentration m/v (e.g. 2 g in 100 ml of hydrogel) and knowing perflubron density (1.93 $\mathrm{g\,cm^{-3}}$), it is possible to calculate the concentration v/v of perflubron in the hydrogel ($C_{v/v_{PFC}}$):

$$C_{v/v_{PFC}} = \frac{V_{PFC}}{V_{hydrogel}} = \frac{\left(\frac{C_{m/v_{PFC}}}{\rho_{PFC}}\right)}{100} \tag{6.1}$$

where ρ_{PFC} is the density of perflubron, $C_{m/v_{PFC}}$ is the perflubron concentration expressed as mass/volume and $V_{hydrogel}$ is the characteristic hydrogel volume equal to 0.512 $\mu\mathrm{m}^3$ because the side of the cube is chosen equal to 0.8 μm.

From Equation 6.1 it is possible to extrapolate the volume occupied by perflubron droplets in the hydrogel (V_{PFC}). This latter is divided by the volume of one droplet, approximated as a sphere (V=2.14e-21 m^3), to obtain the number of perflubron droplets inside the hydrogel characteristic volume.
Finally, a plane that cuts these perflubron molecules exactly in half is taken in consideration so that their larger section is analyzed.
An example of the result of this approach is shown is Figure 6.1 which depicts a characteristic square of side 0.8 μm with 5% PFC and 8% Hb.
All model geometries that will be presented in the following have been designed through the open-source CAD software LibreCAD.

Since a side of the hydrogel is in contact with the myocardium, this proximity is modeled in 2D adding to the characteristic square a small rectangle representing the tissue. The size of this rectangle is defined taking into account a specific ratio between gel and myocardium areas. Indeed, our aim is oxygenating approximately 4 mm^2 of tissue with a gel of 25 mm^2.
This reasoning is detailed in Figure 6.2. In addition, Table 6.1 highlights the parameters used in the modeling of our problem and studied in the following.

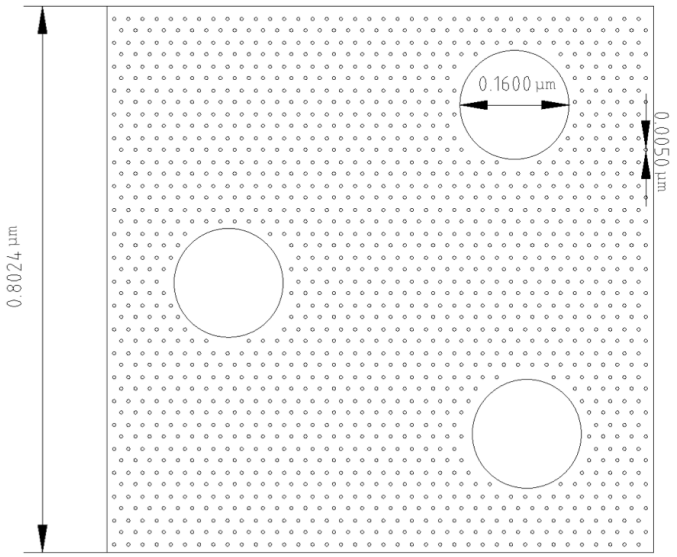

Figure 6.1. Example of characteristic square (l=0.8 μm) geometry with perflubron concentration equal to 2% and Hb concentration equal to 5%. Dimensions expressed in μm.

6.2 Model description and analysis

The physical problem we want to model mainly deals with oxygen diffusion from two different types of oxygen sources towards the myocardium that is in proximity to the gel. Once the geometry is sufficiently simplified, a physics type of Comsol Multiphysics 4.2a that helps design the situation in the best way is selected. In this case, from the module MEMS, the physics "Transport of diluted species" is chosen since it models the transport of chemical species, diluted in the solvent, due to diffusion, convection or external electrical field.

6.2.1 Theory of species diffusion

Diffusion is a phenomenon that involves mass transfer caused by the redistribution of chemical species in a certain space during time. The thermal motion of molecules is the natural propeller for diffusion, since, at temperature above the absolute zero, molecules never stop their movement. Nevertheless, this phenomenon can be due to a concentration, temperature or pressure gradient. For instance, if, at the beginning, the concentration of a species is not uniform, mass transfer due to diffusion creates an even concentration over time.

This mass transfer is defined by a differential equation that considers the reference system as a differential control volume (Δx Δy Δz), with a defined control surface, and applies to it the law of mass conservation. It considers the mass change rate that

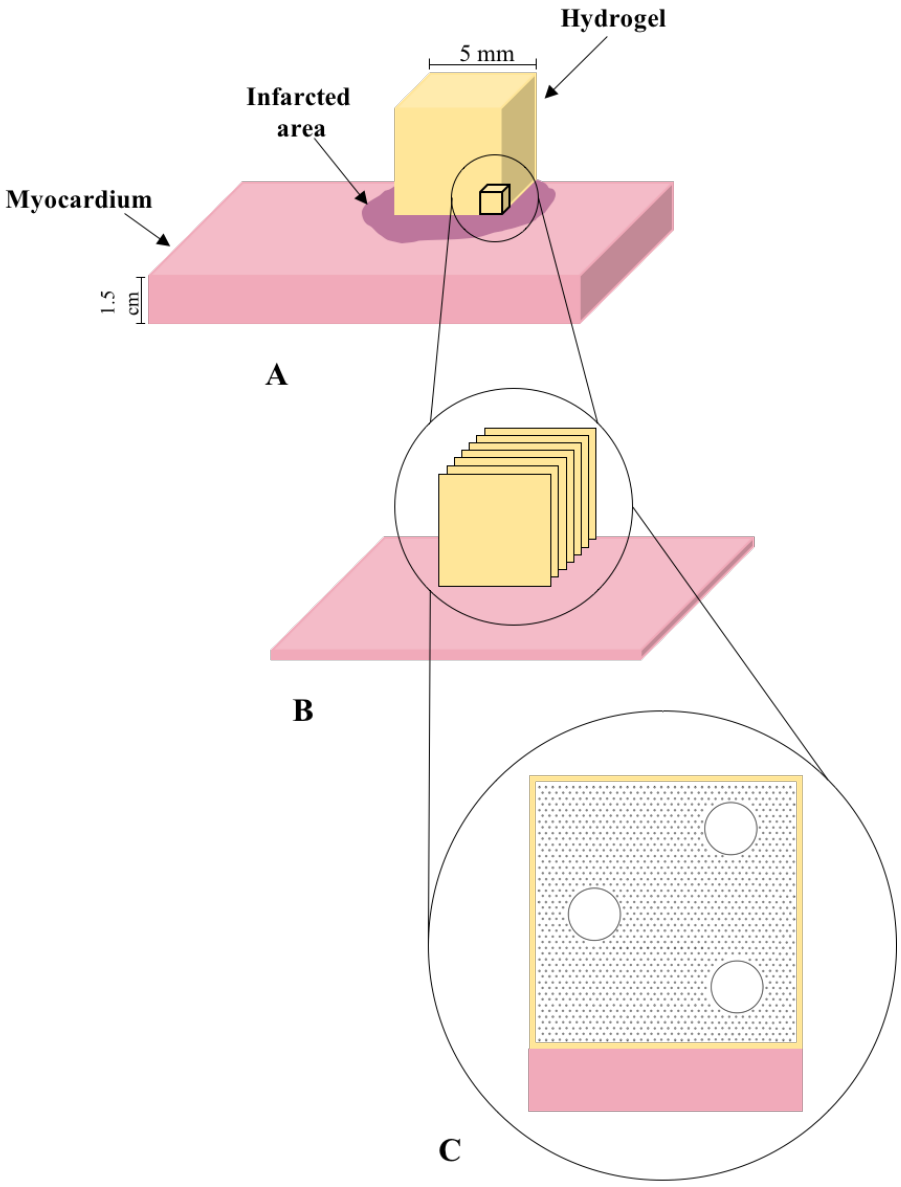

Figure 6.2. **A**. Our piece of hydrogel is printed on the myocardium in correspondence of the infarcted area so that one of its faces is in direct contact with the tissue. Assuming homogeneous distribution of Hb and PFC molecules inside the hydrogel, it is possible to consider one of its characteristic cubes. **B**. The characteristic cube is divided into planes placed 5 nm far from one another. **C**. The plane that cuts PFC molecules exactly in half is chosen for the modeling.

enters the control volume equal to the rate at which mass leaves the control volume, considering the rate at which mass is gained or lost due to sources and sinks inside the control volume (e.g. chemical reactions). The mass conservation law is expressed in

Equation 6.2.

$$\frac{\partial \rho Y_i}{\partial t} + \nabla \cdot \rho Y_i \vec{v_i} = S_i \tag{6.2}$$

where ρY_i represents the mass of species i, $\vec{v_i}$ is the flux vector and S_i is the source/sink term describing the formation/consuming rate of species i inside the control volume.

This flux vector $\vec{v}$ indicates the convection, a phenomenon that involves the movement of the whole solution with all the chemical species inside it. Also diffusion can alter the mass balance inside the control volume and it is described by the Fick's first law. According to it, the diffusive flux vector $\vec{J_i}$ ($\mathrm{g\,m^{-2}\,s^{-1}}$) is proportional to the concentration gradient inside the control surface by a constant called diffusion coefficient ($\mathrm{m^2\,s}$). Fick's first law is expressed in Equation 6.3. The negative sign describes a diffusion movement from a side with higher species concentration to a side with lower concentration.

$$\vec{J_i} = -D \nabla c_i \tag{6.3}$$

Adding the contribution of diffusion to the mass conservation equation, we have:

$$\frac{\partial \rho Y_i}{\partial t} + \nabla \cdot \rho Y_i \vec{v_i} = \nabla \rho D_i \nabla Y_i + S_i \tag{6.4}$$

This latter can be rewritten as follows:

$$\frac{\partial c_i}{\partial t} + \nabla \cdot \vec{J_i} + \vec{u} \cdot \nabla c_i = R_i \tag{6.5}$$

where c_i is the species concentration ($\mathrm{mol\,m^{-3}}$), $\vec{J_i}$ is the diffusive flux vector $\mathrm{mol\,m^{-2}\,s^{-1}}$), R_i is the reaction rate ($\mathrm{mol\,m^{-3}\,s^{-1}}$) that represents the source/sink term and $\vec{u}$ is the mass averaged velocity vector ($\mathrm{m\,s}$) that describes the convective motion.

6.2.2 Model parameters

Our geometry, as described in Figure 6.1, is made up of four different domains, considering hemoglobin molecules to create a single domain. These domains are: hydrogel, tissue, perflubron and Hb molecules. For each of them, the parameters that govern oxygen binding, releasing and diffusion are set and presented in Table 6.1.

Name	*Value*	*Description*
D_{GelMA}	1e-9 $m^2\,s^{-1}$ [63]	Oxygen diffusion coefficient inside the hydrogel.
$D_{myocardium}$	2e-9 $m^2\,s^{-1}$ [64]	Oxygen diffusion coefficient inside myocardium.
α_{PFC}	12 $mol\,m^{-3}\,bar^{-1}$ [49]	Oxygen solubility coefficient inside perflubron emulsion.
$O_{2_{PFC}}$	12 $mol\,m^{-3}$	Initial oxygen concentration inside PFC molecules.
$O_{2_{Hb}}$	101.5 $mol\,m^{-3}$	Initial oxygen concentration inside Hb molecules.
r	20 s^{-1} [65]	Oxygen-hemoglobin dissociation rate constant.
K_{MM,O_2}	6.875e-3 mol^{-3} [64]	Michaelis-Menten constant for cardiomyocytes.

Table 6.1. Modeling parameters.

The goal of the FEM simulation is to calculate the oxygen concentration inside the myocardial portion treated by the hydrogel as well as inside the oxygen sources. In general, the idea is that, according to the oxygen partial pressure of the tissue area, in presence of hypoxia, the oxygen sources release their payload in the gel, following their kinetics. Then, O_2 can diffuse into the tissue, re-establishing physiological levels of pO_2 and reducing the damaged area extension.
To model this condition, two different concentrations are set in Comsol Multiphysics: one is needed to consider oxygen carried by PFC and Hb molecules while the second one refers to the C_{O_2} in tissue domain.

The starting concentration of oxygen inside perflubron emulsion droplets can be calculated referring to the Henry's law described in Equation 4.7. According to it, considering that the emulsion is charged with perfusion of oxygen at a partial pressure equal to ∼750 mmHg, it is possible to calculate perflubron oxygen concentration, finding it equal to 12 $mol\,m^{-3}$.
Regarding hemoglobin, its initial oxygen concentration is calculated knowing that, when fully saturated, each Hb molecule can bind 4 O_2 molecules. Multiplying the Avogadro number by the molecules number, the number of moles is obtained and in this case, it is equal to 6.64e-24 mol. These moles are distributed in the volume of one hemoglobin molecule that has a diameter of 5 nm and that can be approximated as a sphere (V=65e-9 μm^3). Hence, a concentration equal to 101.5 $mol\,m^{-3}$ is found. This value is constant regardless of Hb concentrations, because changing Hb concentration means changing the total amount of oxygen bound to Hb but not its relative O_2 concentration.

6.2.3 Modeling the oxygen-releasing kinetics

The next step of this framework consists in modeling the oxygen-releasing kinetics of our system, considering no flux as a condition imposed on the external boundaries of both gel and tissue. From the mass transfer equation (Equation 6.5), it is possible to calculate the species concentration, considering that, together with diffusion, chemical reactions can also occur. Those reactions are considered through the reaction rate term R, expressed in $\mathrm{mol\,m^{-3}\,s^{-1}}$. By means of the dissociation/association rate constants, this term describes the rate at which, in one domain, the species is produced or consumed.

Concerning hemoglobin, the reaction rate term should refer to the reversible binding of oxygen to the heme group that is perfectly described by the oxyhemoglobin dissociation curve presented and analyzed in Chapter 4.
In this study, the target is the delivery of oxygen, so a dissociation rate constant of 20 $\mathrm{s^{-1}}$ (Table 6.1), is considered. In addition, due to hemoglobin sigmoidal oxygen-delivering kinetics, a function that governs oxygen release from hemoglobin is needed. For this purpose, an activation function (ORH) is set and its behavior with respect to the tissue oxygen partial pressure is described in Figure 6.3. The hemoglobin reaction rate in the model is defined as follows:

$$R_{Hb} = -r \cdot bound \cdot ORH(pO_2) \tag{6.6}$$

where r is the dissociation rate constant equal to 20 $\mathrm{s^{-1}}$ (Table 6.1), *bound* is the oxygen concentration inside hemoglobin molecules and *ORH(pO_2)* is the activation function dependent on the myocardial oxygen partial pressure (pO_2). The minus sign refers to the consumption of the chemical species inside hemoglobin molecules.

The behavior of the piecewise function *ORH(pO_2)* that regulates the O_2 release kinetics in Hb is related to the oxyhemoglobin dissociation curve. As this latter, *ORH(pO_2)* presents a "sleepery slope" when the oxygen partial pressure in the tissue is less than ∼60 mmHg. Hence, in this frame, hemoglobin should deliver a great amount of its payload to rapidly oxygenate the myocardium and this is guaranteed by the activation function. Then, as occurs in the theoretical dissociation curve when saturation approaches, in the model, *ORH(pO_2)* slows down the oxygen release until cancelling it when myocardial pO_2 is ∼100 mmHg.
The estimate done in this framework tells that between 0 and ∼60 mmHg hemoglobin release approximately 80% of its oxygen content. This percentage is then reduced to 17% in the range between 60 and 80 mmHg and to 3% between 80 and 100 mmHg. Around 100 mmHg, the Hb release in the model stops because the environmental pO_2 is high enough to fulfill the metabolic myocardial demands.

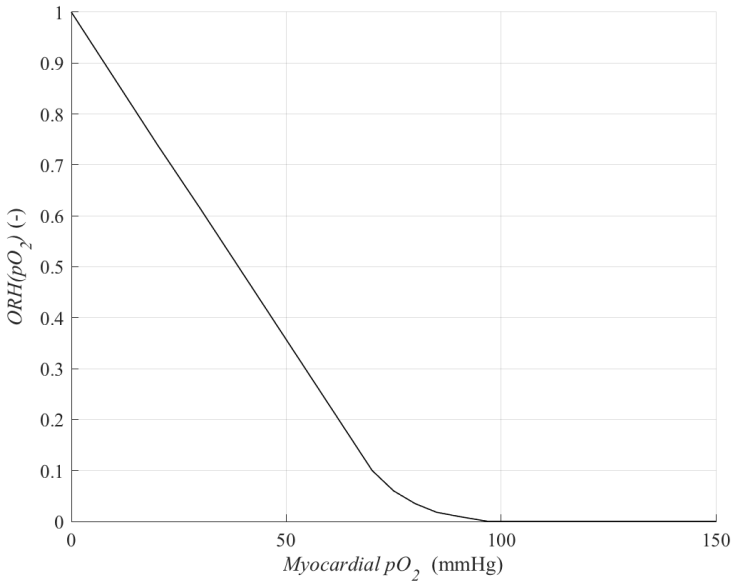

Figure 6.3. Activation function for oxygen release from hemoglobin plotted against the oxygen partial pressure inside the myocardium.

Oppositely with respect to hemoglobin, perfluorocarbons simply dissolve oxygen in their structures without any chemical bond and no dissociation rate constant exists. Nevertheless, for modeling purposes, it is essential to set a reaction rate term in order to accurately describe the release kinetics. So, to avoid reproducing our system in a misleading way, a dissociation rate constant equal to 1 s^{-1} is set.
For the perflubron emulsion, too, an activation function is used to regulate the oxygen release. In reality, this task is carried out by the Henry's law (Equation 4.7) that describes the way in which perfluorocarbons uptake and deliver O_2 according to the environmental pO_2. Plotting the curve of total oxygen content of perflubron emulsion against pO_2, like in Figure 4.10, it is possible to calculate the extraction ratios of the payload between two different environmental O_2 partial pressures. Hence, these percentages are used to build the activation function (ORP(pO_2)) used in the model and shown in Figure 6.4. This function is linear with respect to pO_2 and no particular sensitivity is shown for physiological limits of myocardial pO_2. An extraction ratio of ∼90% is present when perflubron emulsion gets in contact with a tissue pO_2 equal to ∼70 mmHg. Hence, in that frame, the activation function triggers the release of ∼90% of perflubron payload.
The reaction rate term for perflubron emulsion is the following:

$$R_{PFC} = -k \cdot bound \cdot ORP(pO_2) \tag{6.7}$$

where k is the dissociation rate constant equal to 1 s^{-1}, *bound* is the oxygen concentration inside perflubron emulsion droplets and *ORP(pO_2)* is the activation

function dependent on the myocardial oxygen partial pressure (pO_2). The minus sign refers to the consumption of the chemical species inside perflubron molecules.

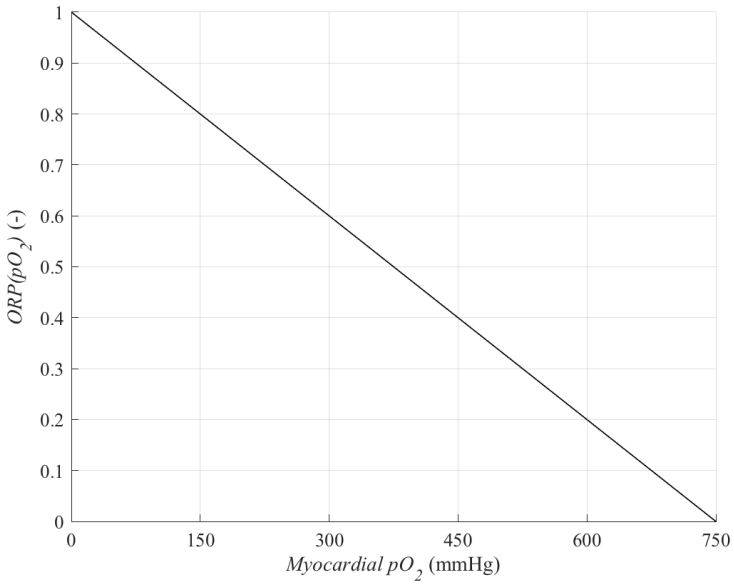

Figure 6.4. Activation function for oxygen release from perflubron emulsion plotted against the oxygen partial pressure inside the myocardium.

As stated in Chapter 5, the principal characteristic of this novel hydrogel is its ability to release oxygen according to the needs of the interested myocardial portion. To this purpose, tissue oxygen partial pressure is continuously monitored in order to tune the delivery profiles of both hemoglobin and perflubron molecules as shown in Figure 6.3 and 6.4.
Myocardial pO_2 is defined in the respective model domain as a variable because its value is determined by the concentration of oxygen inside it. Indeed, as stated in [66], the percentage of oxygen is related to the oxygen partial pressure as follows:

$$1\% = 1013\,Pa \tag{6.8}$$

Comsol solves the mass transfer equation calculating the oxygen concentration inside each domain of the model in $\mathrm{mol\,m^{-3}}$. Multiplying this value by the volume of the tissue portion, it is possible to get the number of O_2 moles inside that portion. Since 22.4 liters is known to be the molar volume of a gas at STP, these O_2 moles occupy a

certain part of the modeled myocardium volume and this part can be expressed as a percentage as follows (Equation 6.9):

$$C_p = \frac{C_m \cdot V_{tissue} \cdot GMV}{V_{tissue}} \cdot 100 \tag{6.9}$$

where C_p is the percentage of oxygen in the modeled tissue portion, C_m is the oxygen concentration calculated by Comsol from the mass transfer equation, V_{tissue} is the volume of the tissue modeled as a rectangle (0.8 μm x 0.128 μm x 1.5 cm) and GMV is the Gas Molar Volume.
Moving from this, the myocardial pO_2 is calculated and used to regulate oxygen release.

Coming back to the mass transfer equation and targeting the myocardial tissue domain, a reaction rate is set here, too, to describe the oxygen consumption rate (OCR) of cardiomyocytes. The volumetric OCR is a function of the local oxygen concentration and it follows the Michaelis-Menten kinetics, according to which:

$$R_{O_2} = R_{max,O_2} \frac{C_{O_2}}{C_{O_2} + K_{MM,O_2}} \tag{6.10}$$

where R_{max,O_2} is the maximum volumetric oxygen consumption rate expressed in $\mathrm{mol\,s^{-1}\,ml^{-1}}$, C_{O_2} is the oxygen concentration inside the tissue and K_{MM,O_2} is the Michaelis-Menten constant, both expressed in $\mathrm{mol\,m^{-3}}$. In particular, the Michaelis-Menten constant corresponds to the C_{O_2} at which consumption drops to half of its maximum [67].
In Equation 6.10, R_{max,O_2} and K_{MM,O_2} are constant values while the oxygen concentration and the volumetric OCR vary in space (lateral and vertical dimensions) and time. For this reason, R_{O_2} in 3D cell cultures is lower than in 2D cell cultures because in *in vivo*-like situations cells closer to capillaries consume oxygen at a higher rate [67].

R_{max,O_2} is calculated starting from the average cellular oxygen consumption rate that is typically expressed in $\mathrm{mol\,s^{-1}\,cells^{-1}}$, In our model, the average OCR of neonatal rat cardiomyocytes in a 2D culture (18 $\mathrm{pmol\,min^{-1}\,10^{-3}cells^{-1}}$) is considered since, *in vitro*, those cells behave similarly to human cardiomyocytes. Then, considering an *in vitro* cell density equal to 1e7 $\mathrm{cells\,ml^{-1}}$, the value of R_{max,O_2} in this model is calculated equal to 3e-10 $\mathrm{mol\,s^{-1}\,ml^{-1}}$.
Additionally, in literature, the Michaelis-Menten constant for cardiomyocytes is found to be equal to 6.875e-3 $\mathrm{mol\,m^{-3}}$ [64].
The reaction rate function for our myocardial portion is depicted in Figure 6.5. According to the Michaelis-Menten kinetics, when the oxygen concentration inside the tissue is low, cells consume it in a fashion that scales with the available C_{O_2} because they struggle to survive. On the other hand, as soon as C_{O_2} levels are sufficiently

high, the OCR gets stable around its maximum and the function shows a plateau.

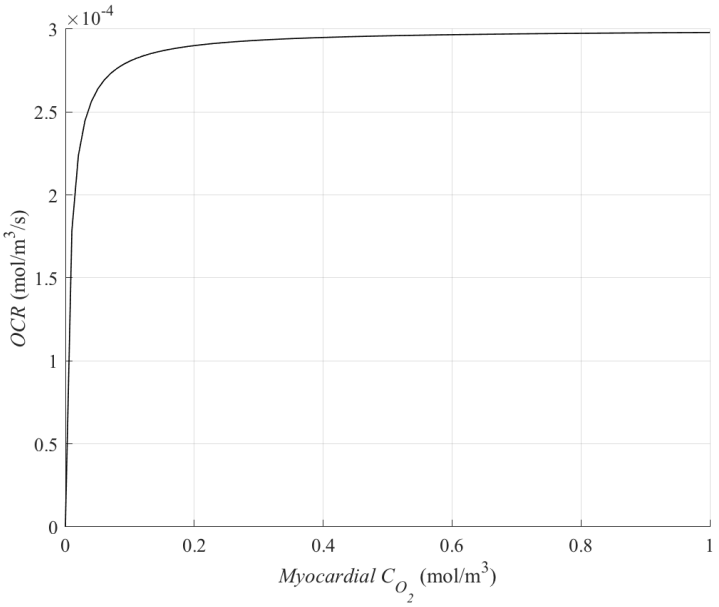

Figure 6.5. Oxygen consumption rate of cardiomyocytes following Michaelis-Menten kinetics.

Together with the reaction rates, diffusion coefficients are needed to model the oxygen-releasing kinetics of our novel system.
Concerning the gel and the tissue, the oxygen diffusion coefficients are cited in Table 6.1. Actually, our hydrogel is a porous material and, hence, its porosity plays a role in O_2 diffusion. Unfortunately, relevant experimental data about gel porosity and density are still not available.
For perflubron and hemoglobin molecules, although their kinetics are mainly described by their reaction rates, oxygen diffusion coefficients are chosen for modeling purposes in order to describe O_2 movement from those molecules to the gel and the tissue districts. For this reason, in both cases, the oxygen diffusion coefficients are the same of hydrogel's one.

6.3 Model mesh

In finite element method analysis, the meshing step is crucial because it divides the starting geometry into simple elements over which the corresponding PDEs are solved. Those elements must accurately approximate the original domains with the goal of

improving convergence and reliability of solutions.
In principle, a denser mesh should be designed for model domains in which the most relevant phenomena are expected to happen, when carrying out a certain study. Hence, a user-defined mesh is tipically chosen.
In this framework, the attention is mostly focused on perflubron and hemoglobin molecules that are the core of our oxygen-delivering system and whose kinetics should behave in a consistent manner with respect to the design. For this reason, finer triangular elements are employed to mesh those two domains. Considering Hb diameter equal to 5 nm and perflubron droplets diameter equal to 0.16 μm, the maximum element size is set to 0.04 μm while the minimum is set to 2.79e-4 μm. The result is shown in Figure 6.6.

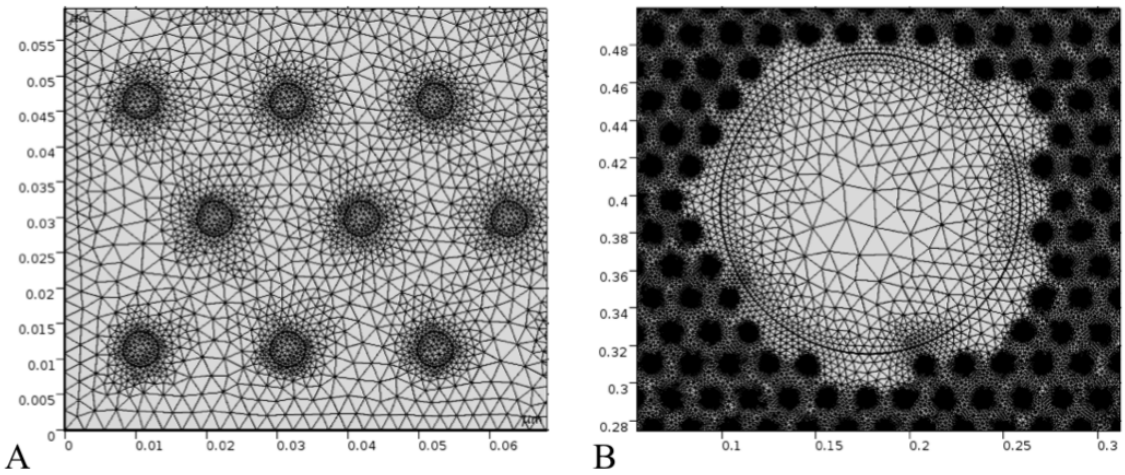

Figure 6.6. Mesh of hemoglobin (**A**) and PFC (**B**) molecules inside the hydrogel.

A similar reasoning is applied to the tissue domain which constitutes the target of the oxygen-releasing system. Creating a denser mesh here helps precisely dealing with the oxygen consumption kinetics of cardiomyocytes which influences the oxygen concentration and, in turn, the relative oxygen partial pressure. In an extra fine mesh, the minimum element size is 1.86 e-5 μm and the maximum is 0.0093 μm. The result can be seen in Figure 6.7 where the tissue represents the rectangle on the leftmost side of the drawing (0.8 μm x 0.128 μm). The boundary between hydrogel and myocardium is finely meshed.

Concerning the hydrogel, a coarser mesh is chosen because it contributes to the oxygen delivery only through the O_2 molecules diffusion across its network. So, a less accurate approximation should not drastically change the final results. Actually, it is worth noticing that the gel mesh strictly depends on the molecules concentration: higher concentration leads to a greater number of molecules in the characteristic square. Indeed, as shown in Figure 6.1, the gel is the space between hemoglobin and perflubron molecules and this space gets smaller if the concentrations increase. For

this reason, although a coarser mesh is set, in the end, the gel domain appears finely meshed around the circles that represent molecules (Figure 6.6) because the software has to average between molecules and gel elements dimensions. So, those dimensions should not differ too much otherwise it would take too long to create the mesh because the complexity would increase.
The mesh of an entire characteristic square of side l=0.8 μm with 2% perflubron and 5% hemoglobin and its relative myocardium portion is depicted in Figure 6.7.
The reasoning just described has been followed also during the upscaling of the characteristic square.

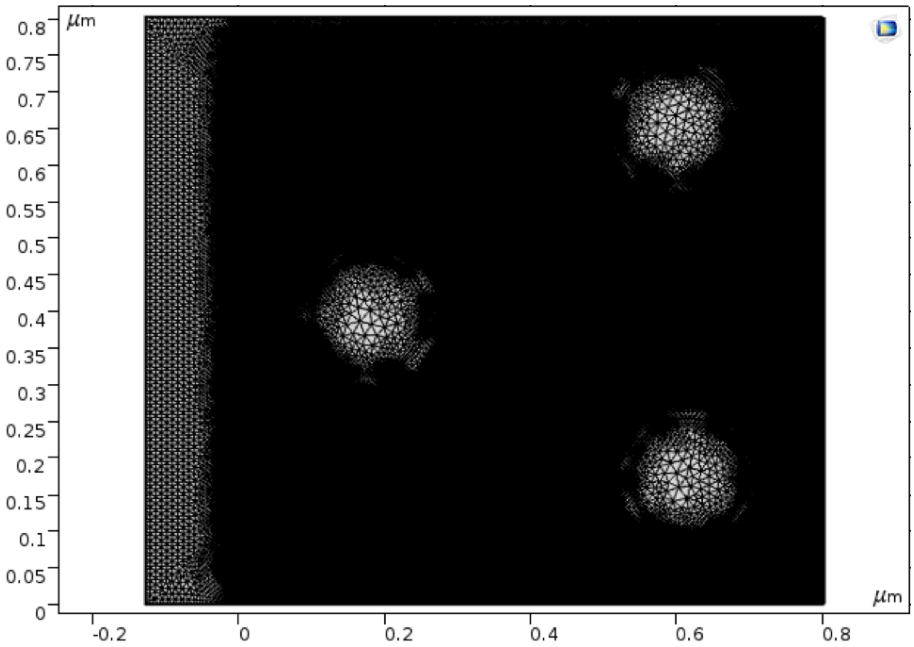

Figure 6.7. Mesh of a characteristic square (l=0-8 μm) with perflubron concentration equal to 2% and Hb concentration equal to 5%. On the leftmost side there is a rectangle representing the tissue portion.

Creating mesh plot (Figure 6.8) in the model is useful to understand the location of low-quality elements that sometimes are created if no correspondence is found between elements of different domains. These plots are also helpful to display the range of elements size inside the geometry. This information is really important when comparing results related to characteristic squares with same size but different molecules concentration. So, in those cases, the elements size range is kept equal among various models.

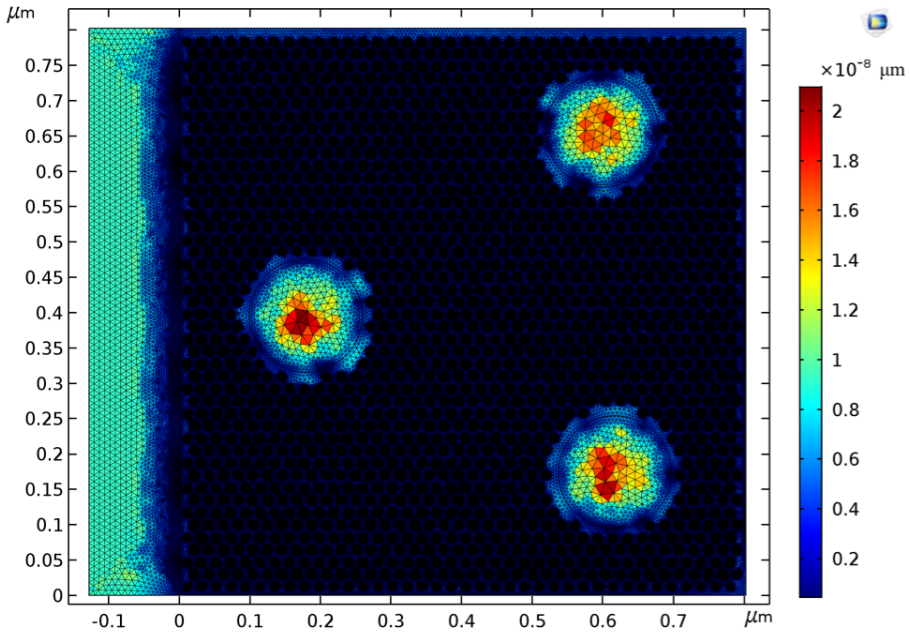

Figure 6.8. Mesh plot of a characteristic square (l=0-8 μm) with perflubron concentration equal to 2% and Hb concentration equal to 5% and its relative myocardium portion. It shows the range of mesh element size.

Chapter 7

Results and discussion

The model of our oxygen-releasing hydrogel described in Chapter 6 is analyzed in Comsol Multiphysics through a time-dependent study in order to focus on the oxygen concentration behavior inside the different domains during time.
At first, a study is carried out to define the best combination between hemoglobin and perflubron concentrations to guarantee efficient oxygenation of the myocardial damaged portion together with reduced side-effects. Once concentrations are set, the influence of hydrogel bulk is analyzed. Finally, an upscaling of the model geometry is performed in order to understand if the results obtained for the characteristic squares can be eventually generalized to the entire gel area.
It is worth noticing that those simulations are based on a two-dimensional approximation of the problem. Hence, the influence of the hydrogel thickness is not considered.
In addition, in all the simulations, a null initial oxygen concentration inside the myocardium is considered. This represents the worst case because the infarcted myocardial portion reaches 0% O_2 in ischemic conditions or when the infarct scar is forming. Otherwise, oxygen levels inside that region are $\sim$1%.

7.1 Influence of different concentrations on the oxygen-delivering system behavior

As detailed in previous chapters, the oxygen-delivering system presented in this work is made up of hemoglobin and perfluorocarbon molecules, in particular perflubron emulsion. So, it is relevant to analyze the impact of their concentrations on the release kinetics of the system as well as on its efficacy.
To do so, a characteristic square of side equal to 0.8 μm is considered. This dimension is chosen according to the processing power of the machine employed to run Comsol Multiphysics: at the same concentration, a greater number of molecules is drawn in larger squares and this may limit the mesh quality and increase the simulation complexity. On one side of this characteristic square, a rectangular tissue portion is drawn (A=1.024e-13 m^2).

According to the model, hemoglobin and perflubron molecules release their oxygen payload in the gel before its diffusion into the myocardial portion. In the studies

presented in the followings, gel and tissue oxygen concentrations follow exactly the same trend because the oxygen diffusion coefficients of those two domains are highly comparable (see Table 6.1).

At the beginning, three different concentration pairs are studied: 2% PFC-5% Hb, 2% PFC-0% Hb and 0% PFC-5% Hb. This is done to understand the importance of considering hemoglobin and PFC together as oxygen sources inside the gel.

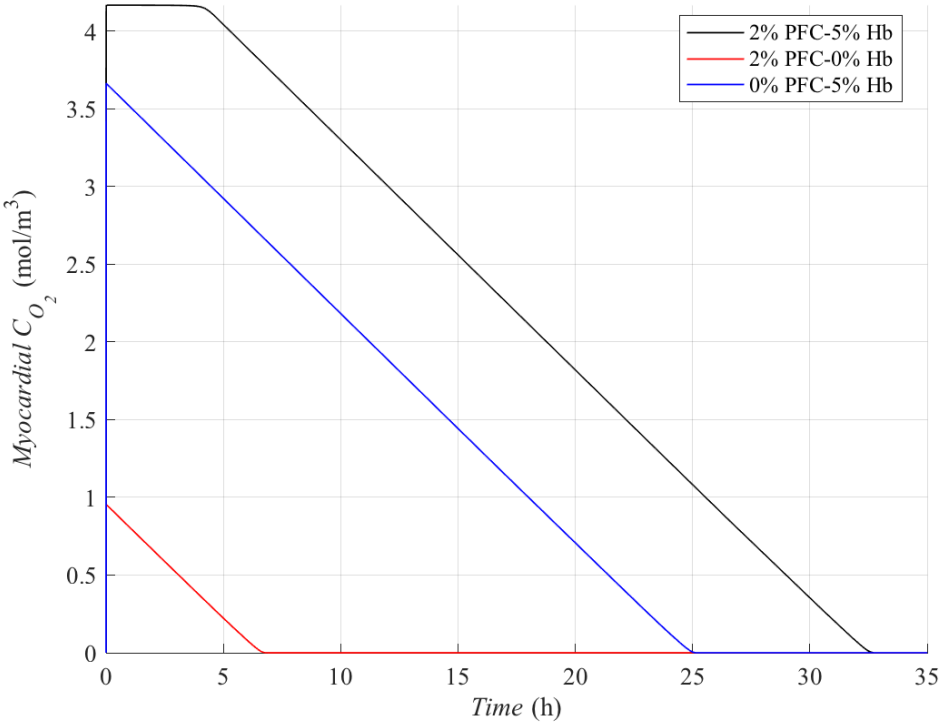

Figure 7.1. Myocardial oxygen concentration (C_{O_2}) versus time for different Hb-perflubron concentration pairs.

Figure 7.1 shows how the oxygen concentration (C_{O_2}) inside the myocardium varies in time when changing hemoglobin and perflubron concentrations. At the beginning, all three cases produce an abrupt increase in myocardial C_{O_2}.

If no PFC is present (blue curve), this increase stops when hemoglobin molecules use up their payload. Nevertheless, cardiomyocytes keeps consuming oxygen, therefore contributing to the downward trend of the curve. Here, the oxygen release lasts few tens of seconds (see Figure A.1) but the myocardium takes 25 hours to consume its oxygen following Michaelis-Menten kinetics. It can be concluded that, keeping

hemoglobin concentration fixed, the presence of perflubron emulsion contributes to guarantee optimal tissue oxygenation, making it reach physiological levels.
Similarly, if the hydrogel contains only perflubron emulsion (red curve), the initial myocardial C_{O_2} increase stops after ∼15 seconds (see Figure A.2) when PFC finishes its oxygen molecules and the downward trend of consumption begins. So, the presence of hemoglobin molecules is important for the outcome of this novel hydrogel because it helps extending the duration of myocardial oxygenation.

On the other hand, in presence of both hemoglobin and PFC, the expected behavior results. When the oxygen partial pressure in the tissue domain is high enough (∼100 mmHg) to guarantee efficient oxygenation, the myocardial C_{O_2} increase stops because the oxygen-releasing system slows or ceases its activity. After that, the curves exhibit a plateau because the oxygen slowly released by the hydrogel is immediately consumed by cardiomyocytes and equilbrium happens. The downward trend begins when there is no more O_2 inside hemoglobin and PFC and cardiomyocytes consume O_2 molecules for metabolic activities.

The release behavior of hemoglobin and perflubron in the examples with 0% PFC and 5% Hb and with 2% PFC and 0% Hb inside the hydrogel are presented in Appendix A.

Now, keeping hemoglobin concentration fixed to 5%, perflubron's one is increased to 3% and 4%.

Figure 7.2A shows the trend of myocardial oxygen concentration versus time for hydrogels with fixed hemoglobin concentration and varying perflubron concentration. The expected behavior is obtained since the initial increase is followed by an equilibrium condition and then by a downward trend referred to the consumption of oxygen at the hands of cardiomyocytes.

This behavior in myocardial C_{O_2} is reflected in the plots of oxygen concentration versus time for hemoglobin and perflubron molecules (respectively Figure 7.3 and 7.4). Regarding hemoglobin (Figure 7.3), its oxygen concentration has a trend that follows the pO_2 levels inside the tissue, as expected from the design stages. This can be also deduced from Figure 7.8A where hemoglobin C_{O_2} is plotted against the oxygen partial pressure inside myocardium (just for the case study with 2% PFC and 5% Hb).
According to the trend in Figure 7.3, at the very beginning, hemoglobin C_{O_2} rapidly decreases causing the rapid increase in myocardial C_{O_2}. Then, as soon as this latter reaches physiological levels, hemoglobin starts reducing its release rate (blue and red curves) or even cancelling it in the case of higher Hb concentrations (plateau in the black curve). The downward trend reflects the delivery recovery caused by the drop of myocardial oxygen concentration below the minimum physiological value triggered by metabolic consumption.
In addition, it is worth noticing that increasing perflubron concentration leads to a

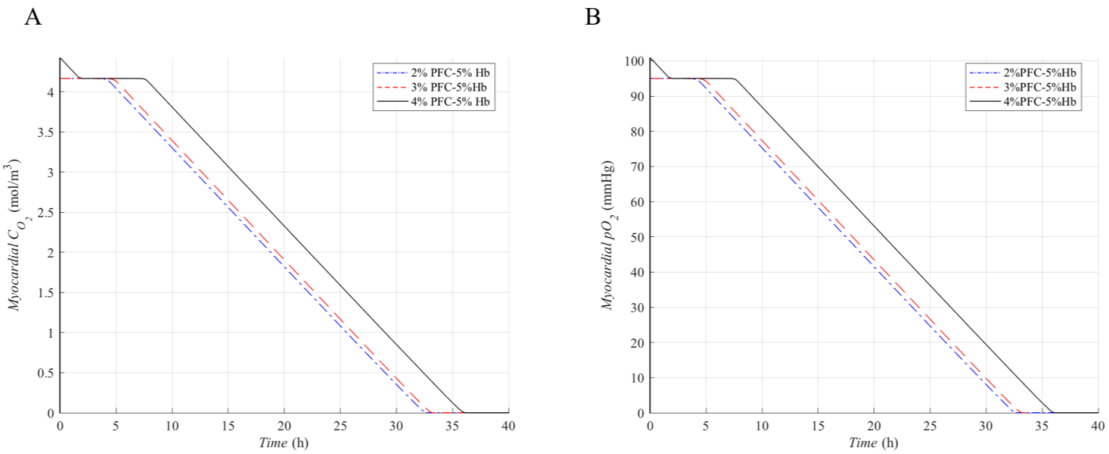

Figure 7.2. **A**. Myocardial oxygen concentration (C_{O_2}) versus time for different perflubron concentrations and fixed hemoglobin concentration. **B**. Myocardial oxygen partial pressure (pO_2) versus time for different perflubron concentrations and fixed hemoglobin concentration. Those curves follow the same trend of C_{O_2} ones because a proportionality relation has been established during the modeling stage (see Equation 6.8).

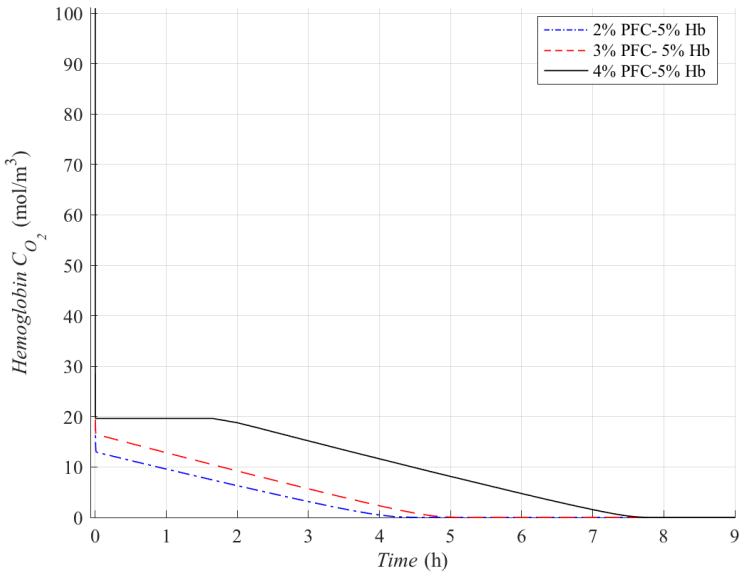

Figure 7.3. Oxygen concentration inside hemoglobin versus time for different perflubron concentrations and fixed hemoglobin concentration.

longer release time because, doing so, the PFC-based oxygen source is able to provide

a better initial oxygenation to the myocardium so that physiological levels are reached first and hemoglobin can start slowing its release earlier. Nevertheless, as it will be explained in the following, a compromise should be found between release duration and maximum oxygen levels inside the myocardium.

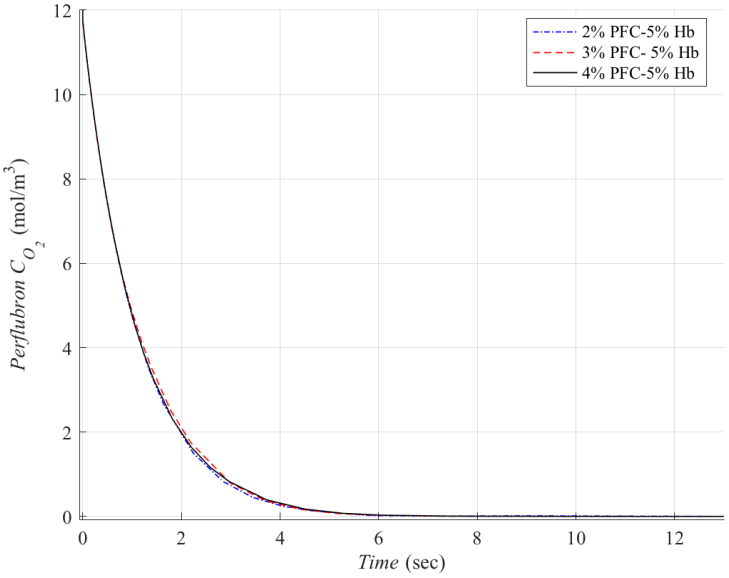

Figure 7.4. Oxygen concentration inside perflubron emulsion versus time for different perflubron concentrations and fixed hemoglobin concentration.

Differently from hemoglobin, as explained in Chapter 4, perfluorocarbon molecules do not bind oxygen in a cooperative way. Hence, their uptake and release kinetics are not sensitive to changes in environmental partial pressure (pO_2). This statement coming from experimental studies on PFC emulsions is mirrored in the model where emulsion droplets release their oxygen payload continuously, regardless of pO_2 levels in the myocardium. Indeed, the C_{O_2} trend of Figure 7.4 does not show any change when, around 5 seconds, myocardial pO_2 (FIgure 7.2B) has reached its maximum physiological level: the release keeps going anyway. Hence, after ∼11 seconds, emulsion payload is totally used up and immediately available for the myocardium.
Moreover, it is worth noticing that an increase in perflubron concentration produces an increase in the number of perflubron droplets inside a fixed hydrogel volume and, hence, in the total amount of oxygen carried by perflubron present in the hydrogel. As a consequence, even though PFC C_{O_2} decreases at the same velocity in all three cases of Figure 7.4, in the same time window, the hydrogel with 4% perflubron is able to release a greater amount of oxygen with respect to the 2%-perflubron hydrogel.
This phenomenon combined with the delivery kinetics typical of perfluorocarbon emulsions can produce adverse effects if there is no synergy with hemoglobin. This

happens when PFC concentration is increased (e.g. 3% and 4%). In those cases, the payload that perflubron keeps delivering linearly with respect to myocardial pO_2 (Figure 6.4) consists in an amount of oxygen that raises together with perflubron concentration inside the hydrogel. Hence, when hemoglobin stops its release, its saturation prevents it from storing other O_2 molecules coming from PFC and, hence, from delaying their diffusion towards the gel and the tissue. This phenomenon causes myocardial C_{O_2} to reach levels that are well above the physiological limits (see peaks in Figures 7.2A and B) and hence it can induce hyperoxia.
In addition, from Figure 7.4, it can be highlighted that no significant changes in the release speed are achieved when increasing PFC concentration, since its release kinetics is not influenced by its concentration.

Taking into account the duration of oxygenation and the importance of mantaining physiological oxygen levels inside the myocardium, the hydrogel with 3% perflubron and 5% hemoglobin seems to guarantee the best outcome.
At this point, keeping the concentration of perflubron fixed and equal to 3%, hemoglobin percentage inside the hydrogel is increased to 6% and 7% in order to find the most favorable combination.

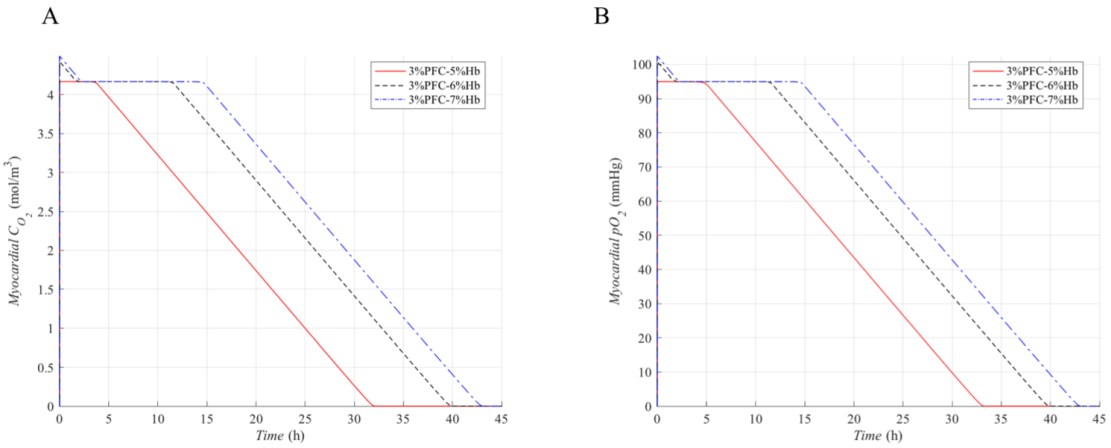

Figure 7.5. **A**. Myocardial oxygen concentration (C_{O_2}) versus time for different hemoglobin concentrations and fixed perflubron concentration. **B**. Myocardial oxygen partial pressure (pO_2) versus time for different hemoglobin concentrations and fixed perflubron concentration. Those curves follow the same trend of C_{O_2} ones because a proportionality relation has been established during the modeling stage (see Equation 6.8).

In this example, too, the trend of myocardial C_{O_2} in time (Figure 7.5A) results as expected. The same applies for hemoglobin (Figure 7.6A) and perflubron (Figure 7.6B) oxygen release behaviors.
It is worth noticing that, increasing hemoglobin concentration, the oxygenation

provided by this oxygen source is longer and, hence, its effects on the myocardium are extended in time, too. In fact, the hydrogels with more hemoglobin lasts ∼45 hours. On the contrary, this raise in hemoglobin percentage does not produce any consequence in the oxygen release kinetics of perflubron emulsion that uses up its O_2 payload after ∼11 seconds anyway.

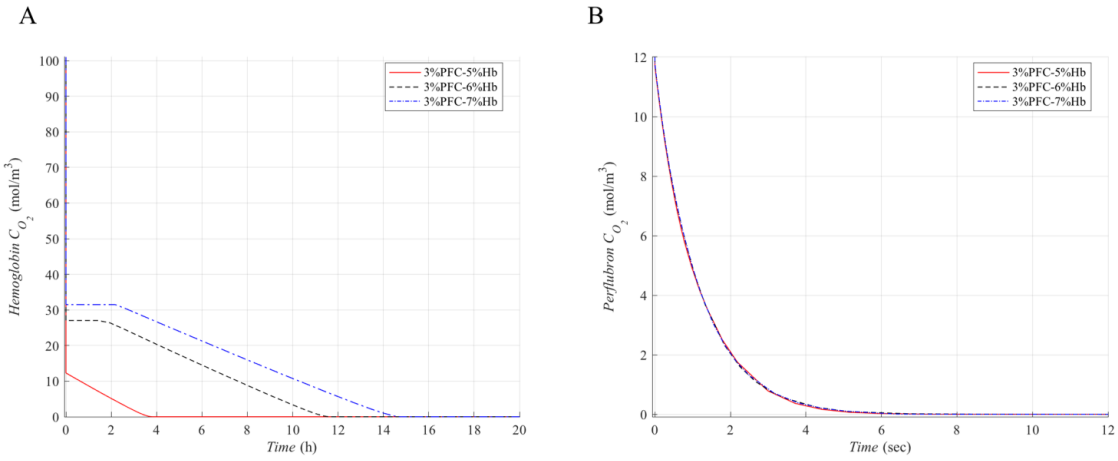

Figure 7.6. Hemoglobin (**A**) and perflubron (**B**) oxygen concentrations versus time for different hemoglobin concentrations and fixed perflubron concentration.

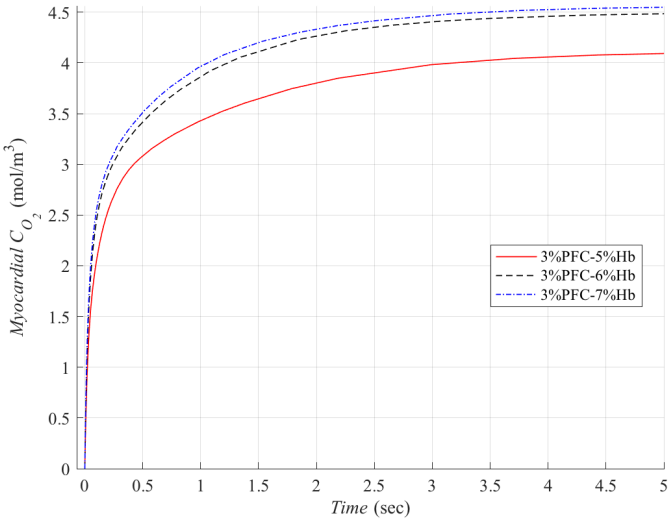

Figure 7.7. Myocardial oxygen concentration versus time for different hemoglobin concentrations and fixed perflubron concentration in a window time of 5 seconds.

In order to correctly choose the concentration of hemoglobin and perflubron for our hydrogel, oxygenation duration is not the only parameter that should be considered: attention should be paid also to the fast initial increase of oxygen concentration inside the myocardium. Indeed, abrupt reintroduction of oxygen in an infarcted region may favor ROS species formation and oxidative stress especially if this action leads to pO_2 values higher than the physiological limit (∼100 mmHg).
Figure 7.7 zooms on the vertical line that Figure 7.5A presents at time equal to zero. In the first 5 seconds, the speed at which the myocardial oxygen concentration grows depends on both hemoglobin concentration. Indeed, for higher Hb concentrations (e.g. 7%), myocardial C_{O_2} grows much faster than for smaller ones (e.g. 5%). This happens because hemoglobin, in that time frame, releases oxygen following the "sleepery slope" portion of the oxyhemoglobin dissociation curve, since, at the beginning, the tissue has a pO_2 lower than 60 mmHg. This can be noticed also in Figure 7.8A where C_{O_2} inside hemoglobin is plotted against myocardial pO_2. This curve appears to be interrupted because, approaching the physiological limit of ∼100 mmHg, hemoglobin blocks its oxygen release until myocardial pO_2 drops again.
Perflubron emulsion droplets, too, contribute to initial myocardium oxygenation but in a different manner. Comparing Figure 7.8B, which plots C_{O_2} inside perflubron against myocardial pO_2, with Figure 7.8A, it is clear that, in the pO_2 range 0-60 mmHg, hemoglobin contribution dominates. Oxygen release from the emulsion starts prevailing when hemoglobin slows its kinetics. This feature has been just described in the previous lines, highlighting that it can cause adverse effects in the myocardium if perflubron concentration is too high and no synergy with hemoglobin is present.

In conclusion, methods to reduce potential risks for myocardium during oxygenation include tuning the hydrogel diffusion coefficient in order to slow down oxygen diffusion from O_2-carrying molecules to the tissue and choosing oxygen sources concentrations that ensure synergy between their release kinetics. Hence, among the alternatives that have been analyzed, the hydrogel containing 3% PFC and 5% Hb is chosen. Its oxygenation has effects lasting ∼32 hours.

Practical experiments may eventually confirm this risk of producing adverse effects inside the myocardium when its oxygen partial pressure grows beyond the physiological limits. In that case, the concentration of hemoglobin and perflubron in our hydrogel may be slightly increased (e.g. 4% perflubron and 7% hemoglobin) in order to provide infarcted area oxygenation for more than 40 hours.

7.2 Influence of hydrogel bulk

Once established the best hemoglobin and perflubron concentrations for this oxygen-releasing system, it is worth analyzing the dissipative effects that may occur inside the hydrogel.

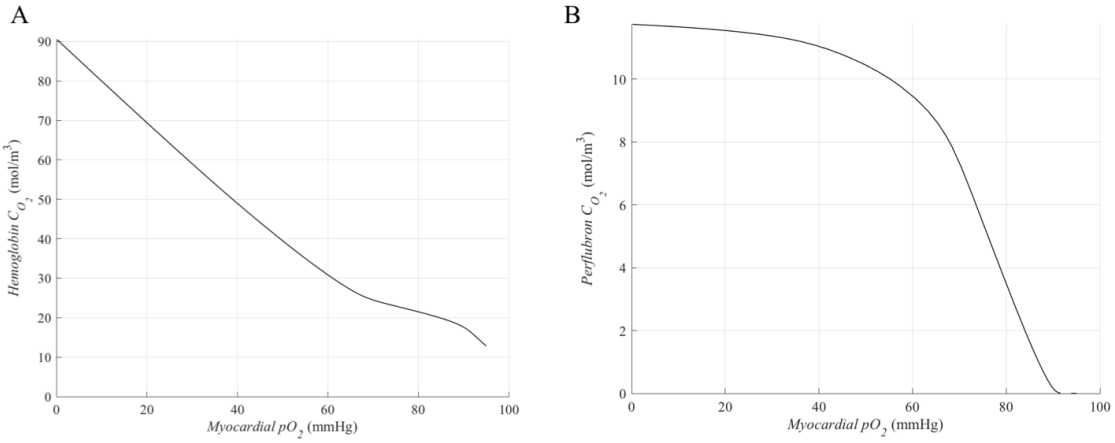

Figure 7.8. **A**. Hemoglobin oxygen concentration versus myocardial oxygen partial pressure. **B**. Perflubron oxygen concentration versus myocardial oxygen partial pressure. Both graphs refer to a hydrogel with 2% PFC and 5% Hb.

A 2D gel line made up of 4 characteristic squares (total length equal to 3.2 μm) is designed and studied (Figure 7.9). The rectangular tissue portion is kept in contact only with one of these squares. Hence, the hydrogel area is 25 times larger than the tissue area.
The kinetics of the model is the one described in Section 6.2.3 according to which every gel square contributes to the oxygenation according to its release kinetics. Regarding the mesh, the same reasoning presented in Section 6.3 is applied for the gel line, too, considering finer elements for hemoglobin and perflubron molecules and for the tissue. Unfortunately, due to a limited computing power, a longer gel line could not be meshed and simulated.

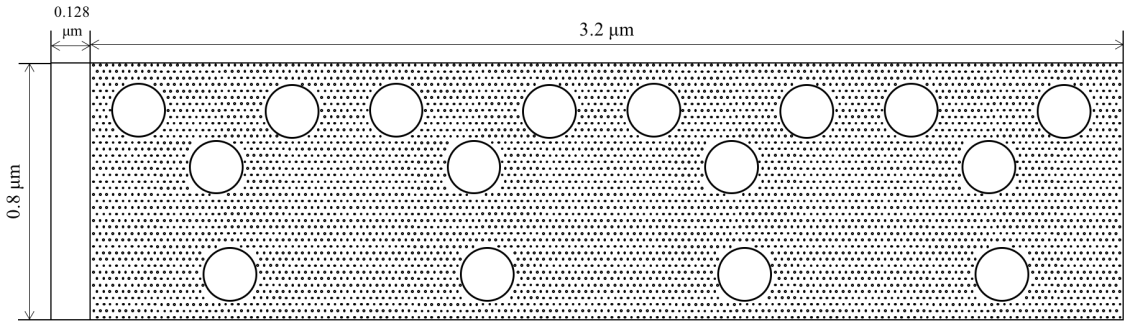

Figure 7.9. Model geometry of a gel line made up of 4 characteristic squares contemporarly oxygenating one tissue portion. Dimensions are expressed in μm.

What is expected from this simulation is to achieve a longer release duration

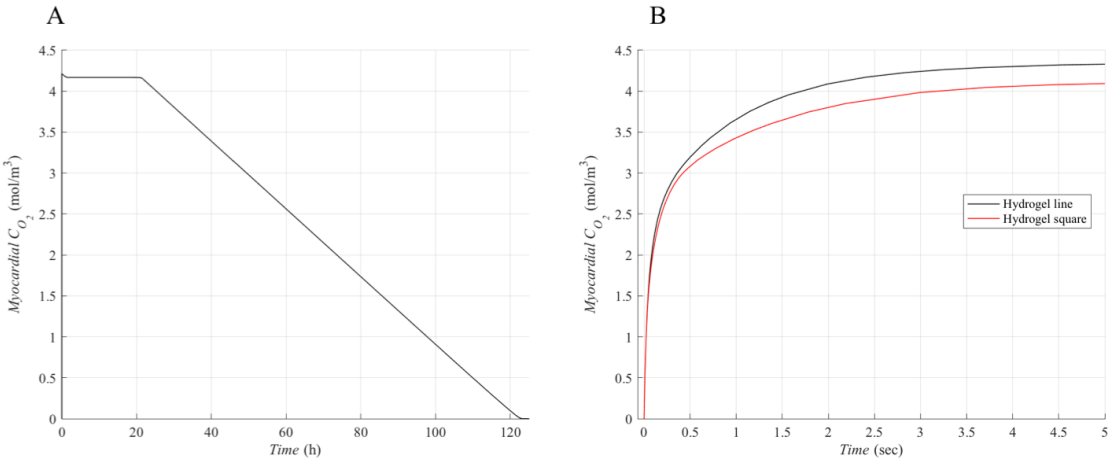

Figure 7.10. **A**. Myocardial oxygen concentration (C_{O_2}) versus time with oxygenation from a small hydrogel line. **B**. Myocardial oxygen concentration (C_{O_2}) in a time window of 5 seconds following oxygenation from a hydrogel line and from a hydrogel square.

with respect to the example of one gel square, if no losses are present during oxygen diffusion along the line, since a bigger hydrogel section is oxygenating the same tissue portion.
Figure 7.10A shows the trend of myocardial oxygen concentration in time. It resembles the results of Section 7.1 except for the duration of oxygenation effects which here is equal to 123 hours. In this example, too, myocardial pO_2 is kept below the physiological limit guaranteeing efficient and safe treatment of the damaged area. This goal is achieved even though, with respect to the model with one hydrogel square, the maximum value of myocardial C_{O_2} is slightly higher (Figure 7.10B).

This effect derives from the perflubron release which, being insensitive to environmental pO_2 variations, let myocardial C_{O_2} increase indefinetely. Indeed, Figure 7.11 shows how perflubron uses up its payload after 10 seconds exactly as occurs in the case of one hydrogel square. Nonetheless, the amount of oxygen carried by perflubron inside the hydrogel line is higher. Hence, during the same time frame, perflubron droplets release more oxygen with respect to the case in which there is only one hydrogel square.
Fortunately, the established concentrations of perflubron emulsion and hemoglobin guarantee synergy between them and this limits the potential adverse effects of this phenomenon.

Figure 7.12 depicts hemoglobin C_{O_2} versus time. The initial rapid decrease in oxygen concentration is needed to immediately re-estabilish physiological oxygen levels in the myocardium. Then, the release slows down to avoid tissue hyperoxia

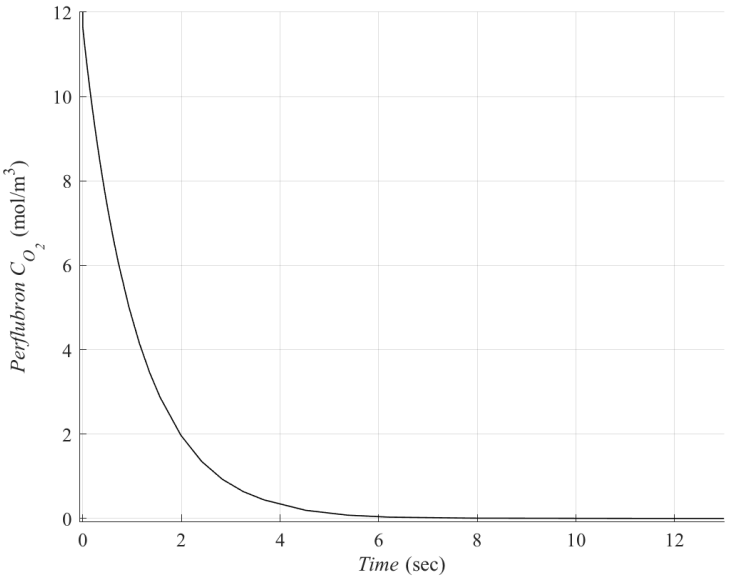

Figure 7.11. Perflubron oxygen concentration versus time in the model simulation of a hydrogel line.

and limit the potential damages triggered by perflubron O_2 release. Oxygen reservoir inside hemoglobin is used up after ∼22 hours, exactly when the plateau of Figure 7.10A stops. Hence, no dissipation is present during diffusion from Hb molecules to the hydrogel and finally to the tissue.

7.3 Model dimensions upscaling

Thus far, results show a hydrogel that is able to oxygenate a portion of infarcted myocardium for a reasonable period of time. Nevertheless, they refer to a characteristic 2D micrometric piece of the entire gel area. Hence, it may be worth upscaling the dimensions of the geometry considered so far to analyze the accuracy of this model also on a larger size scale similar to the real one.

For this purpose, three scaling factors have been chosen for the system model geometry: 500, 1041, 2082. An isotropic upscaling is performed. Concentrations of hemoglobin and perflubron molecules are kept equal to 5% and 3% respectively, during the scaling procedure. During this procedure, the diameter of oxygen releasing molecules, too, is upscaled. Hence, clusters are created, each containing a number of molecules approximately equal to the scaling factor. Doing so, the area occupied by hemoglobin and perflubron droplets remains the same but the perimeter across which

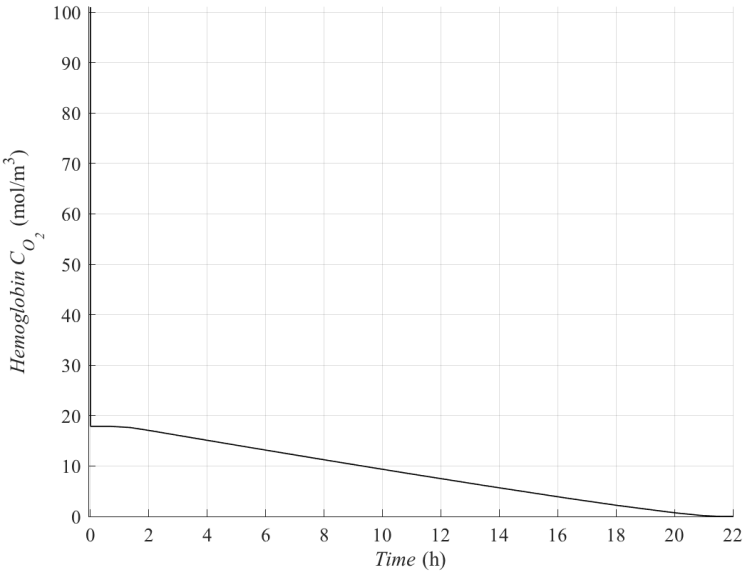

Figure 7.12. Hemoglobin oxygen concentration versus time in the model simulation of a hydrogel line.

they exchange oxygen in 2D is slightly reduced.

In Figures 7.13 and 7.15, oxygen concentrations trends of the upscaled model accurately resemble the ones related to the micrometric hydrogel geometry. The duration of oxygenation provided by hemoglobin and perflubron molecules is exactly the same ($\sim$ 33 hours) and slight variations in the curves' slope only depend on the mesh.
An evident difference that emerges from this upscaling refers to the diffusion of oxygen inside the hydrogel and the myocardium. Actually, the O_2 diffusion coefficients of those two domains (respectively, 1.5 e-9 and 2e-9 $m^2\,s^{-1}$) appear to be comparable when the model is applied at the micro scale. On the other hand, upscaling geometry dimensions, the difference between those two coefficients emerges and let oxygen diffusion inside the myocardium be slower than in the gel. This is shown in Figure 7.14 where plot B refers to a hydrogel geometry upscaled by a factor equal to 1041. This phenomenon has a positive effect on the efficiency of our hydrogel because the abrupt initial increase inside the myocardium is delayed during the first minutes, rather than seconds, of release when the geometry dimensions are increased.

In conclusion, results demonstrate how the model designed for this novel oxygen-releasing hydrogel returns the same behaviors in oxygen uptake, for the tissue, and release, for hemoglobin and perflubron molecules, at micrometer and millimeter scale. Hence, our hydrogel is able to efficiently oxygenate its relative myocardial infarcted

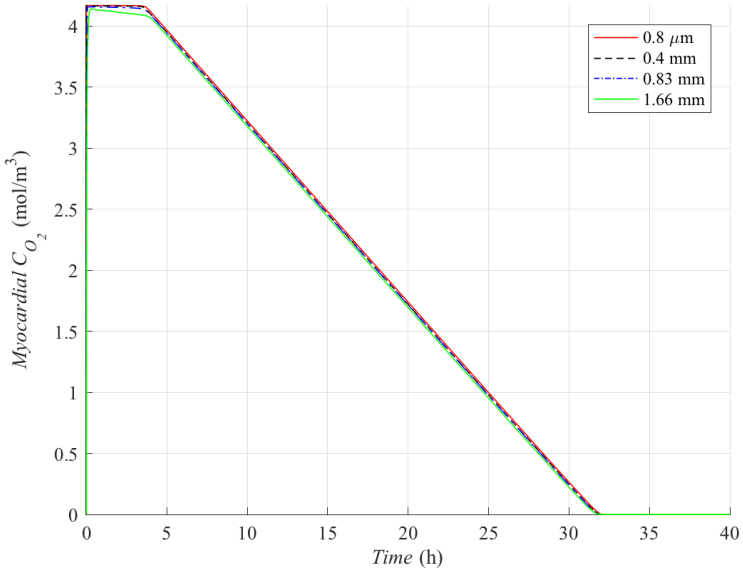

Figure 7.13. Myocardial oxygen concentration versus time in the micrometric hydrogel square and in its upscaled versions.

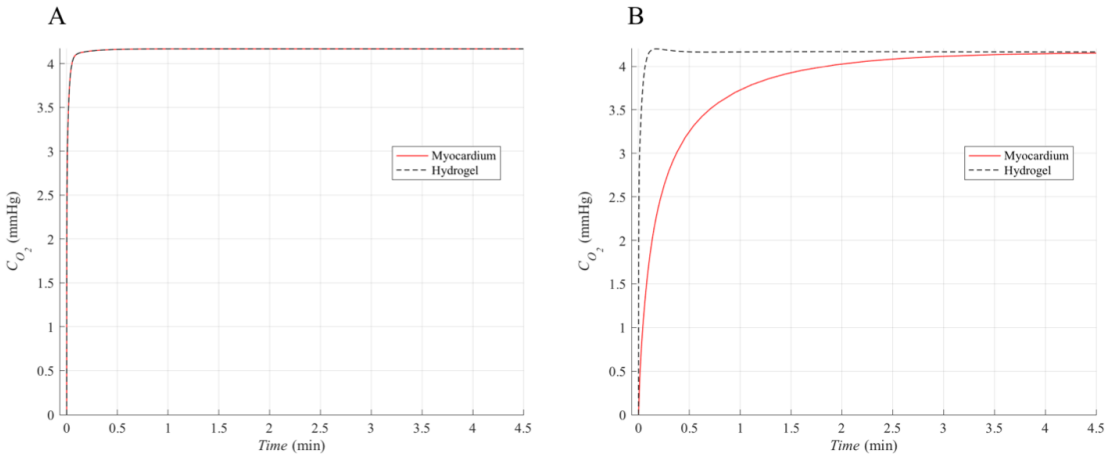

Figure 7.14. Initial increase in hydrogel and myocardial oxygen concentrations in (**A**) a micrometric geometry (l=0.8 μm) and (**B**) in one of its upscaled versions (l=0.83 mm).

portion during a period of approximately 1 day and a half.

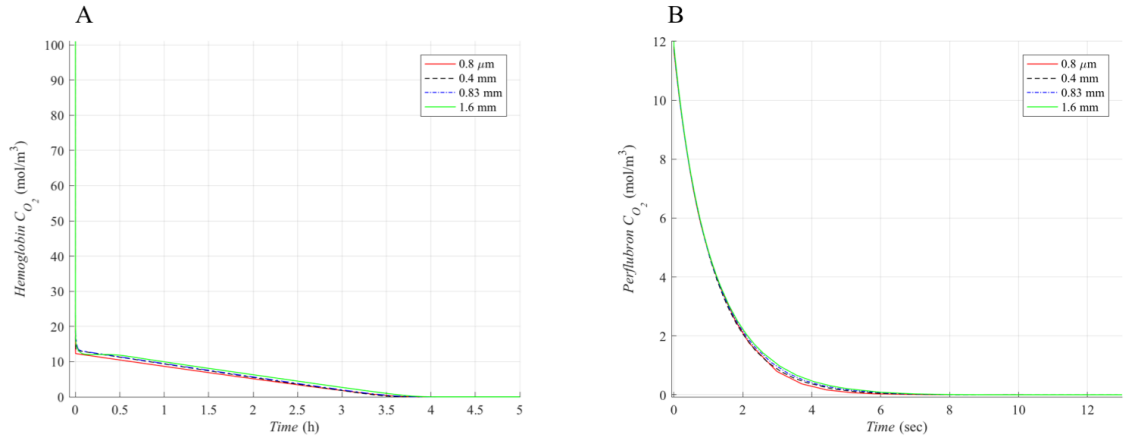

Figure 7.15. Hemoglobin (**A**) and perflubron (**B**) oxygen concentrations versus time in the micrometric hydrogel square and in its upscaled versions.

Chapter 8

Conclusions

Oxygen represents the fuel of life. It is essential for the survival of the entire human organism, from the small cellular compartments to the wide organs. Hence, if absent, it can undermine the physiological behavior of the body.
One of the districts that is mainly affected by lack of oxygen is the cardiovascular one where the heart muscle, without O_2 supplied by the coronary arteries, hardly contracts and pumps blood that feeds the organism. This alteration can occur as a consequence of a myocardial infarction (MI), during which the blood flow headed to the heart is stopped by the occlusion of a coronary vessel. This may modify cardiomyocytes functions and eventually leading to their necrosis.

The project presented so far provides a novel treatment for myocardial areas affected by infarction, following a topical approach. This treatment relies on the delivery of oxygen directly into the damaged tissue portion thanks to an oxygen-releasing system embedded inside an adhesive hydrogel, printed in a conformal way onto the target. Oxygen topical distribution has the goal of reducing the surface of the damaged area that is likely to become necrotic if medical action is not timely efficient. Particular attention should be paid to avoid inducing the opposite effects restoring oxygen levels in a non-gradual manner. Indeed, when the oxygen partial pressure inside the myocardium exceeds the phyisiological limits ($\sim$100 mmHg), hyperoxia may occur, producing ROS and oxidative stress.

After a careful analysis of the needs of the myocardium and of its cellular metabolism, a review of state-of-the-art oxygen-releasing biomaterials has been carried out. From this, it has emerged that the best known oxygen carriers for intravenous injection are hemoglobin and perfluorocarbon molecules thanks to their peculiar release kinetics. In addition, some hydrogels for the treatment of myocardial infarction have been already presented in literature but they principally host solid peroxides as oxygen sources. Those compounds, when in contact with water, decompose and release O_2 molecules and, together with them, also some cytotoxic byproducts that accumulate in the tissue.

It is against such background that this work designs an oxygen-releasing system able to oxygenate the tissue in an efficient way, relying on the interplay of hemoglobin and perflubron molecules with their complementary release kinetics. Also the biomaterials

selected for fabrication, GelMA and skin secretion of *Andrias davidianus*, comply with the parameters imposed by the tissue engineering application (biocompatibility, biodegradability, elasticity, etc) and by the bioprinting technique that requires enhanced versatility and printability.

After the design stages, a FEM model of this novel oxygen-releasing system has been described and analyzed. This model has been principally created, using Comsol Multiphyisics 4.2a, to resemble the biochemical properties of hemoglobin and perfluorocarbons and, in particular, their release kinetics, accurately expressed by the oxyhemoglobin dissociation curve and the Henry's law respectively. The oxygen consumption rate of cardiomyocytes which follows Michaelis-Menten kinetics has been taken into account, too.
Results show how this system oxygenates a representative myocardial portion in a reasonable period of time, avoiding the risk of hyperoxia. This latter goal is achieved only if volume concentrations of hemoglobin and perflubron are accurately tuned. Indeed, it has been demonstrated that with 5% hemoglobin and 3% perflubron in the hydrogel it is possible to create no harm for the tissue because the two molecules act in synergy: PFC delivers oxygen to let myocardium carry out its metabolic functions as soon as possible and hemoglobin, which is more sensitive to myocardial pO_2 variations, prevent PFC-released oxygen to produce adverse metabolic effects and guarantee oxygenation for $\sim$5 hours.

Furthermore, it has been noticed that the diameter of perflubron emulsion droplets can influence the oxygenation that the hydrogel provides to the infarcted area. If those droplets have a small diameter (e.g. 0.1 μm), they occupy less space and, for the same perflubron concentration and inside the same hydrogel volume, a bigger number of droplets can be accomodated. This means that, in total, a larger amount of oxygen is carried by PFC which, consequently, can release more O_2 molecules in the same time frame with respect to emulsions with smaller droplets.

Finally, an isotropic upscaling has been applied to the starting micrometric geometry. Results demonstrate that the model designed for this novel oxygen-releasing hydrogel returns the same behaviors in oxygen uptake, for the tissue, and release, for hemoglobin and perflubron molecules, for both micrometric and upscaled geometries. This leads to conclude that our hydrogel is able to oxygenate for approximately one day at a half a myocardial portion whose area is in a ratio of 4:25 with the gel's area.

This outcome is promising because the needs of the myocardial tissue are respected and efficient oxygenation is provided to the infarcted area across a fair time window. Those oxygen-delivering biomaterials that in literature are said to provide longer oxygenation are larger or have their release kinetics tested only in DBPS [46] without considering the oxygen consumption rate of cardiomyocytes. Furthermore, no evidence of a similar biomaterial that involves hemoglobin and perflubron as oxygen-sources has been found in literature, so no direct comparison is possible.

These encouraging results propel this project towards future improvements. Firstly, the model should be validated on a 3D geometry in order to deal with the dissipative effects that may occur across the thickness, too. Then, from a fabrication point of view, the hydrogel should be synthesized with a degree of porosity able to slow down oxygen diffusion towards the tissue as much as possible. In this way, myocardial oxygenation would last more and an abrupt increase in oxygen levels could be avoided. In conclusion, modeling and experimental parts should be carried out simultaneously so that a virtuous circle can grow and improve them at their best. In fact, *in vitro* experiments of this novel oxygen releasing hydrogel may eventually confirm this risk of producing adverse effects inside the myocardium when its oxygen partial pressure grows beyond physiological limits. In that case, the concentration of hemoglobin and perflubron in our hydrogel may be slightly increased (e.g. 4% perflubron and 7% hemoglobin) in order to provide infarcted area oxygenation for more than 40 hours.

Appendix A

Oxygen release from hydrogels with only hemoglobin or only perflubron molecules.

In Section 7.1, various combinations of hemoglobin and perflubron concentrations have been analyzed. The particular case of perfluorocarbon absence has been taken into account, too. Figure A.1 shows oxygen release from hemoglobin molecules towards the gel and the tissue.
This release lasts approximately 30 seconds because hemoglobin is the only oxygen source inside the hydrogel. Since at the beginning myocardial pO_2 is below 60 mmHg, this carrier delivers its payload at a high rate and this payload ends before efficient tissue oxygenation is obtained.

Section 7.1 considered also the case of a hydrogel with only perflubron as an oxygen source. The release of O_2 molecules from perflubron emulsion in this specific situation is shown in Figure A.2 where oxygen is consumed after $\sim$14 seconds. This occurs because at the beginning myocardial pO_2 is below the levels of normoxia and perflubron aims at re-oxygenating the tissue.

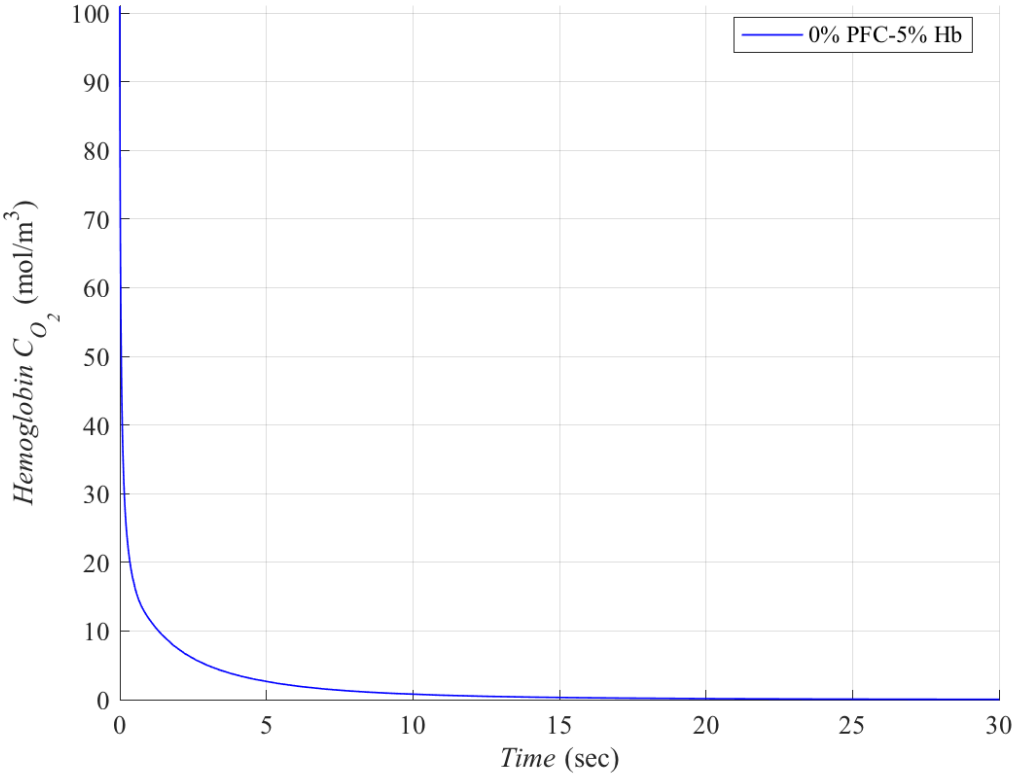

Figure A.1. Hemoglobin oxygen concentration versus time for hydrogel with only 5% Hb.

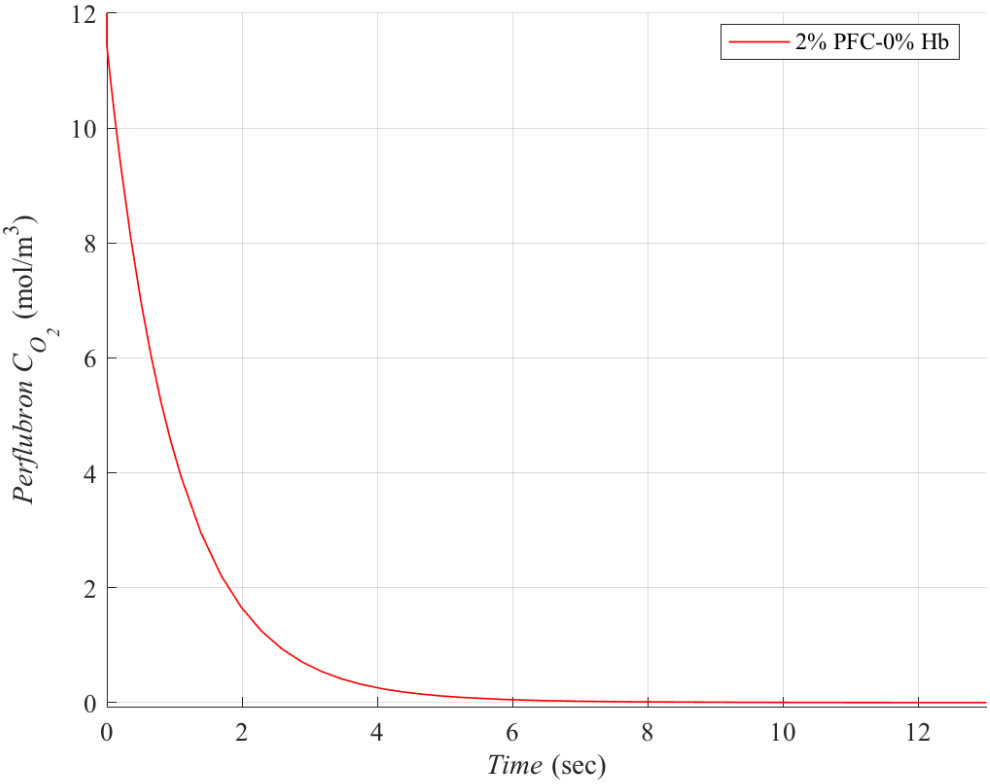

Figure A.2. Perflubron oxygen concentration versus time for hydrogel with only 2% perflubron.

Bibliography

[1] The WHO CVD Risk Chart Working Group, World Health Organization cardiovascular disease risk charts: revised models to estimate risk in 21 global regions., Lancet Global Health; 7: e1332–45; 2019.

[2] WHO Fact Sheet 2017 available **here**.

[3] Benjamin EJ, Muntner P, Alonso A, Bittencourt MS, Callaway CW, Carson AP, et al. Heart disease and stroke statistics—2019 update: a report from the American Heart Association. 2019;139(10):e56–528.

[4] MSD Manuals Ranya N. Sweis , MD, MS and Arif Jivan , MD, PhD, Northwestern University Feinberg School of Medicine.

[5] Stouffer, G. A., Runge, M. S., Patterson, C., Rossi, J. S., Netter, F. H., Netter's cardiology (3rd edition.). Philadelphia, PA: Elsevier, 2019.

[6] Buja L. M., Myocardial ischemia and reperfusion injury. Cardiovascular Pathology, 2005, 14(4), 170–175.

[7] DeVon H. A., Hogan N., Ochs A. L., Shapiro M., Time to Treatment for Acute Coronary Syndromes: The Cost of Indecision, J Cardiovasc Nurs., 2010, 25(2): 106–114.

[8] Schomig A., Ndrepepa G., Kastrati A., Late myocardial salvage: time to recognize its reality in the reperfusion therapy of acute myocardial infarction., European Heart Journal, 27, 1900–1907, 2006.

[9] Longo DL, Fauci AS, Kasper DL, Hauser SL, Jameson J, Loscalzo J. eds., Harrison's Principles of Internal Medicine, 19e. New York, NY: McGraw-Hill; 2015.

[10] Byrne, R. A., Stone, G. W., Ormiston, J., Kastrati, A., Coronary balloon angioplasty, stents, and scaffolds., The Lancet, 2017, 390(10096), 781–792.

[11] Araszkiewicz A., Grygier M., Lesiak M., Grajek S., The impact of ischemia-reperfusion injury on the effectiveness of primary angioplasty in ST-segment elevation myocardial infarction, Postep Kardiol Inter, 2013, 9, 3 (33), 275–281.

[12] Shuvy, M. et al., Oxygen therapy in acute coronary syndrome: are the benefits worth the risk? European heart journal 34, 2013, 1630–1635.

[13] Abuzaid A., Fabrizio C., et al., Oxygen Therapy in Patients with Acute Myocardial Infarction: A Systemic Review and Meta-Analysis, The American Journal of Medicine, Vol 131, No 6, June 2018.

[14] Wang F., Guan J., Cellular cardiomyoplasty and cardiac tissue engineering for myocardial therapy, Advanced Drug Delivery Reviews 62, 2010, 784–797.

[15] Cardiac stem cell therapy. Digital image. **Medgazzette24** by Shreyas Tanna.

[16] Stanley W. C., Changes in cardiac metabolism: a critical step from stable angina to ischaemic cardiomyopathy., European Heart Journal Supplements, 3 (Supplement O), O2–O7, 2001.

[17] Ortiz-Prado E., Dunn J.F., Vasconez J., Castillo D., Viscor G., Partial pressure of oxygen in the human body: a general review., Am J Blood Res, 9(1):1-14, 2019.

[18] Michiels Carine, Physiological and Pathological Responses to Hypoxia., American Journal of Pathology, Vol. 164, No. 6, June 2004.

[19] Mach W.J., Thimmesch A.R., Pierce J.T., Pierce J.D., Consequences of Hyperoxia and the Toxicity of Oxygen in the Lung., Nursing Research and Practice Volume 2011, Article ID 260482.

[20] O. Wichterle, D. Lim, Hydrophilic gels in biologic use., Nature 185, 117, 1960.

[21] Sutapa Biswas Majee, Emerging Concepts in Analysis and Applications of Hydrogels., Cahpter 2: An Introduction to Hydrogels and Some Recent Applications., August 2016.

[22] Shivani Nanda, Sood N., Reddy B.V.K., Markandeywar T.S., Preparation and Characterization of Poly(vinyl alcohol)-chondroitin Sulphate Hydrogel as Scaffolds for Articular Cartilage Regeneration., Indian Journal of Materials Science, Volume 2013, Article ID 516021.

[23] Yu Shrike Zhang, Ali Khademosseini, Advances in engineering hydrogels., Science, Vol. 356, Issue 6337, 2017.

[24] Hang Li, Asanka Wijekoon, Nic D. Leipzig, 3D Differentiation of Neural Stem Cells in Macroporous Photopolymerizable Hydrogel Scaffolds., PLoS ONE 7(11): e48824, 2012.

[25] Nasim Annabi, Nichol J.W., Xia Zhong, Chengdong Ji, Koshy S., Khademhosseini A., Dehghani F., Controlling the Porosity and Microarchitecture of Hydrogels for Tissue Engineering., Tissue Engineering: Part B, Volume 16, Number 4, 2010.

[26] E. Caló, V. V. Khutoryanskiy, Biomedical applications of hydrogels: A review of patents and commercial products., Eur. Polym. J. 65, 252–267, 2015.

[27] Ashammakhi N.,Darabi M.A., Kehr N.S., Erdem A., Hu S., Dokmeci M.R., Nasr A.S., Khademhosseini A., Advances in Controlled Oxygen Generating Biomaterials for Tissue Engineering and Regenerative Therapy., Biomacromolecules., 13;21(1):56-72, Jan 2020.

[28] Farris A.L., Rindone A.N., Grayson W.L., Oxygen delivering biomaterials for tissue engineering., J. Mater. Chem. B, 2016, 4, 3422.

[29] Suvarnapathaki S., Wu X., Lantigua D., Nguyen M.A., Camci-Unal G., Breathing life into engineered tissues using oxygen-releasing biomaterials., NPG Asia Materials, 11:65, 2019.

[30] Berg J., Tymoczko J. and Stryer L., Biochemistry. New York: W.H. Freeman, Chapter 10, 2002.

[31] Nelson David L., Cox Michael M., Principles of Biochemistry., New York: W.H: Freeman, 5th edition, Chapter 5 , 2010.

[32] CC Michel, Respiratory Physiology, Chapter 7, eds. AC Guyton, JG Widdicombe, Baltimore: University Park Press, pp. 67–104, 1974.

[33] Stowell C.P., Levin J., Spiess B.D., Winslow R.M., Progress in the development of RBC substitutes., TRANSFUSION;41:287-299, 2001.

[34] Jacques Creteur, William Sibbald, Jean-Louis Vincent, Hemoglobin solutions—Not just red blood cell substitutes., Crit Care Med, Vol. 28, No. 8, 2000.

[35] Aurelie Gaudard, Varlet-Marie E., Bressolle F., Audran M., Drugs for Increasing Oxygen Transport and Their Potential Use in Doping. A review., Sports Med; 33

(3): 187-212; 2003.
[36] William W. Muir and Maxey L. Wellman, Hemoglobin Solutions and Tissue Oxygenation., J Vet Intern Med; 17:127–135; 2003.
[37] Faivre B., Menu P., Labrude P., Vigneron C., Hemoglobin Autooxidation/Oxidation Mechanisms and Methemoglobin Prevention or Reduction Processes in the Bloodstream. Literature review and outline of autooxidation reaction., Artificial Cells, Blood Substitutes, and Biotechnology, 26:1, 17-26, 1998.
[38] Yi Jia, Li Duan, Junbai Li, Hemoglobin-Based Nanoarchitectonic Assemblies as Oxygen Carriers., Advanced Materials, 28, 1312–1318, 2016.
[39] Chang T.M.S., Nanobiotechnology for Hemoglobin-based Blood Substitutes., Crit Care Clin., 25(2): 373, April 2009.
[40] Merkel J.T., Desimone J.M. et al., Using mechanobiological mimicry of red blood cells to extend circulation times of hydrogel microparticles., PNAS, 108:2, 586–591, 2011.
[41] Spiess B.D., Perfluorocarbon emulsions as a promising technology: a review of tissue and vascular gas dynamics., J Appl Physiol 106: 1444-1452, 2009.
[42] Riess J.G., Understanding the Fundamentals of Perfluorocarbons and Perfluorocarbon Emulsions Relevant to In Vivo Oxygen Delivery., Artificial Cells, Blood Substitutes, and Biotechnology, 33:1, 47-63, 2005.
[43] White J.C., Godsey M.E., Bhatia S.R., Perfluorocarbons enhance oxygen transport in alginate-based hydrogels., J. Biomed. Mater. Res. A 101, 438–446, 2013.
[44] Akula S., Brosch I.K., Leipzig N.D., Fluorinated Methacrylamide Chitosan Hydrogels Enhance Cellular Wound Healing Processes., Annals of Biomedical Engineering., 45(11):2693-2702, 2017.
[45] Pedraza E., Coronel M. M., Fraker C. A., Ricordi C., Stabler C. L., Preventing hypoxia-induced cell death in beta cells and islets via hydrolytically activated, oxygen-generating biomaterials., Proc. Natl. Acad. Sci. U. S. A., 109 (11), 4245-4250, 2012.
[46] Zhaobo Fan, Zhaobin Xu, Hong Niu et al., An Injectable Oxygen Release System to Augment Cell Survival and Promote Cardiac Repair Following Myocardial Infarction., Scientific Reports, 8, 1371, 2018.
[47] Alemdar N., Leijten J., Camci Unal G., Hjortnaes J., Ribas J., Paul A., Mostafalu P., Gaharwar A. K., Qiu Y., Sonkusale S., Liao R., Khademhosseini A., Oxygen-generating photo-cross-linkable hydrogels support cardiac progenitor cell survival by reducing hypoxia-induced necrosis., ACS Biomater. Sci. Eng., 3 (9), 1964-1971, 2017.
[48] Perflubron properties available in **AlfaAesar catalogue**.
[49] Ronald W. Millard, Oxygen Solubility, Rheology and Hemodynamics of Perfluorocarbon Emulsion Blood Substitutes., Artificial Cells, Blood Substitutes, and Biotechnology, 22:2, 235-244, 1994.
[50] Kan Yue, Xiuyu Li, Schrobback K., Sheikhi A., Annabi N., Leijten J., Zhang W., Yu Shrike Zhang, Hutmacher D.W., Klein T.J., Khademhosseini A., Structural analysis of photocrosslinkable methacryloyl-modified protein derivatives., Biomaterials 139, 163-171, 2017.

[51] Van Den Bulcke A.I., Bogdanov B., De Rooze N., Schacht E.H., Cornelissen M., Berghmans H., Structural and Rheological Properties of Methacrylamide Modified Gelatin Hydrogels., Biomacromolecules 1, 31-38, 2000.

[52] Kan Yue, Trujillo-de Santiago G., Alvarez M.M., Tamayol A., Annabi N., Khademhosseini A.,Synthesis, properties, and biomedical applications of gelatin methacryloyl (GelMA) hydrogels., Biomaterials 73, 254-271, 2015.

[53] Jun Deng, Yingying Tang, Qing Zhang, Chao Wang, Yu Shrike Zhang et al., A Bioinspired Medical Adhesive Derived from Skin Secretion of Andrias davidianus for Wound Healing., Advanced Functional Materials, 1809110, 2019.

[54] Heinrich M.A., Wanjun Liu, Jimenez A., Jingzhou Yang, Akpek A., Xiao Liu, Qingmeng Pi, Xuan Mu, Ning Hu, Schiffelers R.M., Prakash J., Jingwei Xie, Yu Shrike Zhang, 3D Bioprinting: from Benches to Translational Applications., Small, 15, 1805510, 2019.

[55] Murphy S.V., Atala A., 3D bioprinting of tissues and organs., nature biotechnology, volume 32, number 8, 2014.

[56] Y. Zhang, K. Yue, J. Aleman, K. Moghaddam, S. Bakht, V. Dell'Erba, P. Assawes, S. Shin, M. Dokmeci, R. Oklu, A. Khademhosseini, 3D Bioprinting for Tissue and Organ Fabrication, Ann. Biomed. Eng., 45, 148, 2017.

[57] Ying G., Jiang N., Maharjan S., Yin Y., Chai R., Cao X., Yang J., Miri A.K., Hassan S., Yu Shrike Zhang, Aqueous Two-Phase Emulsion Bioink-Enabled 3D Bioprinting of Porous Hydrogels., Advanced Materials, 30, 1805460, 2018.

[58] G. Ying. J. Manríquez, D. Wu, J. Zhang, N. Jiang, S. Maharjan, D.H. Hernandez Medina and Yu Shrike Zhang, An open-source handheld extruder loaded with pore-forming bioink for in situ wound dressing., Materials Today Bio 8, 100074, 2020.

[59] Cheng R.Y., Eylert G., Gariepy J., He S., Ahmad H., Gao Y., Priore S., Hakimi N., Jeschke M.G. and Axel Günther, Handheld instrument for wound-conformal delivery of skin precursor sheets improves healing in full-thickness burns., Biofabrication 12, 025002, 2020.

[60] Olivier de Weck and Il Yong Kim, Lecture notes of the course "Engineering Design and Rapid Prototyping" available **here**.

[61] Harold P. Erickson, Size and Shape of Protein Molecules at the Nanometer Level Determined by Sedimentation, Gel Filtration, and Electron Microscopy., Shulin Li (ed.), Biological Procedures Online, Volume 11, Number 1, 2009.

[62] Jean G. Riess, Perfluorocarbon-based Oxygen Delivery., Artificial Cells, Blood Substitutes, and Biotechnology, 34: 567–580, 2006.

[63] Richard J. McMurtrey, Analytic Models of Oxygen and Nutrient Diffusion, Metabolism Dynamics, and Architecture Optimization in Three-Dimensional Tissue Constructs with Applications and Insights in Cerebral Organoids., Tissue Eng Part C Methods.; 22(3):221-49, 2016.

[64] Milica Radisic, William Deen, Robert Langer, Gordana Vunjak-Novakovic, Mathematical model of oxygen distribution in engineered cardiac tissue with parallel channel array perfused with culture medium containing oxygen carriers., Am J Physiol Heart Circ Physiol 288: H1278–H1289, 2005.

[65] Saikat Chakraborty, Vemuri Balakotaiah, Akhil Bidani., Diffusing capacity reexamined: relative roles of diffusion and chemical reaction in red cell uptake of O_2, CO, CO_2 and NO., J Appl Physiol 97: 2284–2302, 2004.

[66] Aude Carreau, Bouchra El Hafny-Rahbi, Matejuk A., Grillon C., KiedaC., Why is the partial oxygen pressure of human tissues a crucial parameter? Small molecules and hypoxia., J. Cell. Mol. Med. Vol 15, No 6, pp. 1239-1253, 2011.

[67] Chiara Magliaro, Mattei G., Iacoangeli F., Corti A., Piemonte V., Ahluwalia A., Oxygen Consumption Characteristics in 3D Constructs Depend on Cell Density., Frontiers in Bioengineering and Biotechnology, Volume 7, Article 251, 2019.